Alma Mater Studiorum – Università di Bologna

DOTTORATO DI RICERCA IN

Ingegneria Civile, Chimica, Ambientale e dei Materiali

Ciclo XXXII

**Settore Concorsuale: 09/D1**

**Settore Scientifico Disciplinare: ING-IND/22**

# DESIGN OF BIOBASED ADDITIVES FOR TUNING THE PROPERTIES OF BIOPOLYMERS

Presentata da: **Alessandro Sinisi**

**Coordinatore Dottorato** — **Prof. Luca Vittuari**

**Supervisore** — **Prof.ssa Paola Fabbri**

**Esame finale anno 2020**

# Summary

## ABSTRACT

This work mainly arises from the necessity to support the rapid introduction of different biobased polymers that the industrial sector has been facing lately. Indeed, while considerable efforts are being made to find environmentally and economically sustainable materials with specific properties, less attention is paid to their need to be properly compounded to fulfil increasingly rigorous technical and quality requirements. Although additives form a wide and significant part of the plastic industry, most of them is still not suitable for biobased polymers, especially when these are also biodegradable. Therefore, there is a strong demand for the development of a novel generation of additives able to tune the properties of biobased polymers while respecting sustainability and circular economy. Among the existing additives, plasticizers certainly play a crucial role from both an industrial and commercial point of view. However, serious health hazards posed by some of them, fossil-based origin together with end-use problems to be overcome, make research on greener and safer alternatives extremely important. With this in mind, a new class of biobased plasticizers is herein proposed as replacement of the currently used additives. Five different compounds were synthesized by a selective protecting-group-free route, which was developed in order to produce valuable asymmetrical ketal-diester from levulinic acid, a promising renewable chemical platform. The synthesis was intentionally designed not only to overcome chemoselectivity issues due to the competitive esterification and ketalization of this bifunctional building block, but also to avoid the use of unstable reagents as well as harsh reaction conditions. As a result, five molecules with different side chains were successfully obtained and fully characterized by means of nuclear magnetic resonance (NMR) and infrared (FT-IR) spectroscopies. These ketal-diesters additives were then added to poly(vinyl chloride) (PVC) as model polymer. Their compatibility and plasticizing effect were evaluated by scanning electron microscopy (SEM), differential scanning calorimetry (DSC), dynamic-mechanical thermal analysis (DMTA), and thermogravimetric analysis (TGA). The emerged trend showed a clear correlation between the structural features of the ketal-ester and the thermal and mechanical properties of the material. In particular, the best results in terms of glass transition temperature ($T_g$) reduction were achieved when the isobutyl- and benzyl-terminated additives were used. Leaching tests in both hydrophilic and hydrophobic

environments were also performed. No significant aqueous leaching was found, whereas despite of the aggressive treatment in hexane, the extraction for all additives was remarkably low. Importantly, when compared to commercial plasticizers such as di-2-ethylhexyl phthalate (DEHP), 1,2-cyclohexane dicarboxylic acid diisononyl ester (Hexamoll® DINCH), acetyl tributyl citrate (ATBC), and diethylhexyl adipate (DEHA), the proposed ketal-diester additives performed comparably and, in some cases, even better. In particular, it was observed that the plasticizing effect starts already at lower concentrations, permitting to use significantly less additive to obtain a similar effect to the one achieved with the nowadays available plasticizers.

The same asymmetric ketal-diester derivatives of levulinic acid were then added to bacterial poly(3-hydroxybutyrate) (PHB), a semi-crystalline polyester characterized by poor thermal and mechanical properties. Morphology assessments by SEM showed no phase separation and the plasticizing effectiveness of the proposed molecules was confirmed by DSC and DMTA. The resulting higher chain mobility was also found to affect the crystallization behavior of the material. Importantly, leaching tests in both water and hexane showed low plasticizer extraction values for all the samples.

With the aim to develop high value lignin-based UV-stabilizers, raw Kraft lignin was first refined by means of two different approaches. Readily usable lignin fractions with controlled structure and tailored properties were obtained, as confirmed by gel permeation chromatography (GPC), DSC and phosphorus ($^{31}$P) NMR. Acetylation and butyrylation reactions were successfully performed on selected lignin fractions and the products characterized by FT-IR and DSC. Both modified and unmodified fractions were then added to poly(vinyl alcohol) (PVA), with the idea to exploit its numerous hydroxyl groups as hydrogen-bonding sites to improve lignin-matrix interactions. Promising results in terms of compatibility were achieved with unmodified fractions. Indeed, DSC thermograms presented only one $T_g$ value for each composition, suggesting no phase separation.

In the end, levulinic acid was combined with glycerol, another versatile and valuable green chemical platform. A biobased glycerol-trilevulinate was successfully synthesized thanks to the development of a mild, solvent-free and industrially scalable synthetic route. The product was characterized by means of NMR and then

added to PVC as the model polymer. Its plasticizing effectiveness was preliminary evaluated by DSC, showing a significant decrease of the $T_g$ of the polymer matrix.

# 1. INTRODUCTION

Nowadays, the industrial sector related to plastic materials is facing the rapid introduction of different biobased polymers to replace the existing ones in a growing number of applications. The worldwide interest in biobased polymers has indeed rapidly accelerated to support sustainability.[1,2] Consequently, a lot of attention and efforts are dedicated to the study of the features and properties offered by these innovative polymers. However, industries have been experiencing difficulties mainly in scaling-up and adapting the above-mentioned new biomaterials to standard processing equipments and conditions.[3] Fortunately, hurdles such as manufacturing problems, performance limitations and restricted stability may be overcome through the use of proper substances called additives. Despite that, while the scope of bioplastics has been significantly increasing, the related range of additives has not been growing at the same pace. Therefore, further research has to be carried out in order to find new suitable additives able to improve the processability and tune the final properties of these promising biopolymers.[4]

## 1.1. Need for alternatives to conventional plastics

In recent years, bioplastics have been increasingly bursting into the global plastic market, mainly because of a growing environmental awareness. Indeed, concerns about fossil reserves depletion, greenhouse gas emissions and waste management have been dissuading consumers from using the so-called “traditional” plastics and companies from investing in them.[1] In particular, these plastics, other than being made up of non-renewable fossil raw materials, show several difficulties in both disposal and recycling. From this point of view, the major difficulty is to identify and sort all the plastic litter. Its heterogeneous composition together with the presence of several ingredients are indeed serious drawbacks.[5] Additionally, traditional plastic usually does not biodegrade, thus posing a threat to wildlife when it enters the natural environment due to incorrect disposal. The extensive presence of single-use items, their large dimensions, longevity and sometimes bright colors make them highly visible in the streets as well as in landfills, causing a negative emotional response, public opposition and bad press.[6] Even though these plastic wastes have

the potential to be burnt for energy production, uncontrolled incineration may result in hazardous emission.[7]

For all these reasons, it is easy to understand why biopolymers have emerged as potential alternatives.[8] The main purpose is indeed to protect the environment by not only using products made from renewable resources, but also that decompose into environmentally friendly constituents.[9] Before going into detail, it would be probably helpful to define some words which will be used often. Indeed, in literature and patents, terms such as *degradable*, *biodegradable*, *biobased*, and *biopolymer*, appear to have multiple and overlapping meanings.[10] *Degradable* is a broad term applied to polymers or plastics that disintegrate by a number of processes, including physical disintegration, chemical degradation, and biodegradation by biological mechanisms. As a result of this definition, a polymer may be degradable but not biodegradable. *Biodegradable* is instead applied to polymers that will degrade under the action of microorganisms such as molds, fungi, and bacteria within a specific period of time and environment. *Biobased* is a term focused on the raw materials basis, and it is applied to polymers derived from renewable resources. Raw materials are defined as renewable if they are replenished by natural procedures at rates comparable or faster than their rate of consumption. However, biodegradation depends on the structure and types of chemical bonds and it is not necessarily linked with any bio origin. In other words: while many biobased polymers are biodegradable, not all biodegradable polymers are biobased. Generally speaking, the term *biopolymer* refers to polymers that are derived from renewable resources. Therefore, it is possible to have three kinds of biopolymers:[8]

1) naturally occurring long-chain molecules such as starch, cellulose and hemicellulose;
2) polymers produced by bacteria such as polyhydroxyalkanoates;
3) synthetic polymers from biobased monomers obtained either by fermentation or conventional chemistry such as polylactic acid, polybutylene succinate and polyethylene.

Last but not least, *biopolymer* also refers to the biodegradability of the material. As a consequence, fossil-based but biodegradable polymers must be considered as well.

A biopolymer produced from renewable feedstock which will biodegrade at the end of its life leaving no waste products seems therefore to solve the major problems associated with plastic.[6] However, there is the need not only for environmentally friendly materials, but also for competitive performances compared to the conventional ones. Unfortunately, the generally poor mechanical properties, together with higher production costs, are what have been seriously hindering the transition toward these sustainable alternatives.[11] Indeed, especially in case of both natural occurring and bacterial polymers, it is almost impossible to control the polymer architecture, configuration and weight with either catalysis or reaction conditions. Consequently, biopolymers themselves are not enough, but with the help of external substances the trend may be reversed. These substances, which provides a cost-effective and flexible means to tune polymer properties (thus increasing their applications), are called additives.

## 1.2. Need for a new generation of additives

It can be firmly stated that polymer industry is impossible without additives. Indeed, since the early stages of its development, it was realized that relevant, useful and performing materials could not be obtained without incorporating certain additives into the polymer matrix.[12] Additives are essential ingredients of a manufactured polymeric article, providing it significant extensions of properties in one or more directions. In recent years, uninterrupted quest for easier processing, enhanced properties, better long-term performance and the need to respond to new environmental and health regulations, have made the role of additives crucial, in continuous evolution and diversification.[13] Research and development are therefore essential in this area. As a result, plastics additives now constitute a highly successful and key sector of the chemical industry. However, while the commercial availability of additives for fossil-based plastics is relevant and very well established at the global level, the vast majority of them is not suitable for biobased plastics, mainly in the case that they are also biodegradable.[14] Therefore, there is an urgent need to support research related not only to the tuning of the final properties of biobased polymers, but also to their processability during industrial transformations. This can only be made through the development of a new generation of additives.[4]

Among the several requirements these novel additives should fulfill, renewable origin associated to biodegradability certainly represent the best starting point.[15]

Additives used in plastics materials are normally classified according to their intended performance.[16] So, for instance, it is possible to find two main groups:

1) additives that modify the physical properties of plastics such as plasticizers, lubricants, impact modifiers, reinforcing fillers, colorants, blowing agents and antistatic agents;
2) additives that have a protecting effect against polymer aging and degradation such as heat stabilizers, antioxidants, UV absorbers, flame retardants and biocides.

It is important to highlight that the efficiency of a given additive (besides its own physical properties and its weight content in plastics) depends mainly on its degree of dispersion, which also affects the overall cost. In turn, the degree of dispersion of an additive in a polymer matrix depends mostly on the chemical natures of both additive and polymer, the additive physical state and the mixing process used. In other words, compatibility between additive and polymer as well as the efficiency of the homogenization process are of major significance.[16]
Considering what will be discussed in the next chapters, the focus will be now shifted on a widely used category of additives called plasticizers.

### 1.2.1. Plasticizers: background, technical challenges and new trends

Plasticizers are organic substances of low volatility and relatively low molecular weight (ranging from 300 to 600) that improve softness, flexibility and processability of polymers.[16–19] In particular, they are expected to decrease the melt viscosity, glass transition temperature ($T_g$), elasticity modulus, tensile strength and hardness of finished products, while at the same time increasing their elongation at break and toughness. Generally, plasticizers act by penetrating into the polymer matrix and inserting themselves into the intermolecular space between the chains.[17,20] In this way, they reduce the polymer-polymer secondary attractant forces (such as dipole-dipole interactions, hydrogen bonds), lowering the energy required for molecular

motion. Clearly, plasticizing effectiveness is largely dependent on structural features such as molecular geometry and polarity. While the first may affect plasticizer distribution throughout the polymer matrix, the latter are necessary for the plasticizer to properly interact with the chains.[21,22] As it will be discussed more in detail later, many mathematical models[23] and theories[20,24,25] have been proposed to explain plasticization. However, this phenomenon can be only partially clarified by these theories. Indeed, molecular weight, side-chain structure, bulkiness and length as well as the presence of polar functional groups are factors affecting all together the effectiveness of a plasticizer.[26,27]

Plasticizers are commonly classified as internal or external. Internal plasticizers are inherent parts of the polymer chemical structure, while external are not covalently bonded to the polymer chains. As a consequence, external plasticizers may be lost by evaporation, migration or extraction.[18] This aspect represents one of the main drawbacks of the use of any additive. Indeed, beyond shortening the usable lifetime of the material, the loss of an additive may also result in human and environmental exposure.[19] In case of toxic additives, this would involve a real risk to the health of living beings.

To date, esters of phthalic acid account for around 90% of plasticizers produced worldwide and, with more than 30 different phthalates on the market, diethylhexyl phthalate (DEHP) has been one of the most widely used.[17,19,28] Phthalates achieved considerable success because they combine most of the desirable properties of a plasticizer such as compatibility with many polymers, processing characteristics, high elasticity and flexibility in the final product even at low temperatures, almost no volatility at ambient conditions and low cost.[17,19,29,30] However, since the early ‘80s, there have been concerns regarding their potential carcinogenicity on a number of living organisms (proved first in rodents and then in mammals).[31,32] This aspect particularly affects phthalates used in critical applications such as children’s toys, infant care products as well as medical devices. In fact, they may leach out and be absorbed in small quantities by the body fluids with which they come into contact. Therefore, the use of phthalates has been increasingly regulated and restricted in different countries, including USA,[33] Canada,[34] and Europe.[35] Consequently, there have been a strong incentive to replace phthalates with many novel alternatives, especially characterized by either low migration or toxicity.[36–38] So, for instance, it is possible to find alkyl/aryl phosphates, aliphatic dicarboxylic acid esters (succinates,

adipates, azelates, sebacates), benzoates and cyclohexanecarboxylates.[28,39] Currently, a trend towards biobased plasticizers is clearly detectable, with citrates, epoxidized vegetable oils (from soybean, castor bean, linseed, sunflower seed) and fatty acid esters getting rapidly into the market.[18,40–42]

Plastic industry growth and plasticizer evolution go hand in hand. Indeed, the extensive use of plastics in a progressively wider range of specialty applications, increased quality requirements, new material challenges to be addressed, rigorous product specifications together with commercial aspects and strict food, health, safety and environmental regulations have led to the development of all the currently available plasticizers.[19] In addition, the increasing worldwide trend towards the use of biopolymers to replace petroleum-based conventional plastic goods has been pushing researchers and industries to develop novel biobased and preferably biodegradable plasticizers as a substitution for traditional ones.[43–45] The technical challenges that current plasticizer research must face mainly include leaching and migration issues, health and environmental effects, compatibility with new polymers, heath and light stability, biodegradability and improved material lifetime.[19] In order to develop economically and environmentally sustainable alternative plasticizers, natural resource known as biomass certainly represents the best starting raw material.

## 1.3. Lignocellulosic biomass derived chemical platforms

In recent years, biomass has been increasingly used as feedstock to produce precious building blocks for the synthesis of various value-added products.[46] Indeed, growing concerns regarding fossil resources depletion and their negative environmental effects (mainly global warming and littering problems) have started to threaten the future of plastic industry and enforce the demand for sustainable alternatives based on natural resources.[47,48] In this view, biomass is defined as organic matter generated from available atmospheric $CO_2$, water and sunlight through photosynthesis on a reasonable time basis. Consequently, biomass would allow fuels and chemicals to be produced with net zero carbon emission.[49] Generally, biomass includes energy crops and trees, agricultural food, aquatic plants, wood and wood residues, animal wastes, and other waste materials. Among these, lignocellulosic biomass has been drawing increasing attention as the most

abundant carbon-neutral renewable source. Mainly obtained from forestry and agricultural wastes, lignocellulosic biomass is indeed available worldwide in large quantities and, importantly, does not interfere with food supplies.[50] One of the most valuable molecules from lignocellulosic biomass is levulinic acid, which may branch to many valuable new compounds having novel applications.

### 1.3.1. Levulinic acid

Levulinic acid has been classified as one of the top-12 promising biomass derived building blocks by the United States Department of Energy.[51] Indeed, as a key intermediate for the synthesis of a wide range of chemicals with applications from fuel to plastic industries, levulinic acid has been assuming growing importance.[52–54] Recently, its large-scale production has also been achieved. For instance, it is worth mentioning the “Biofine Process”, which is based on acid catalyzed dehydration of lignocellulosic feedstocks in a two-stage process. Its levulinic acid yield is one of the highest reported in the literature (>60%, based on the hexose content of the carbohydrate-containing starting material), thus providing cost-competitive and high volume access to levulinics.[55] Consequently, the realization of levulinic acid as a giant commodity chemical can be achieved, with further reduction of its prices.

Levulinic acid chemical versatility derives from its bifunctional nature, since it bears both carboxylic and keto groups in its structure. As a result, it can undergo many chemical modifications, making it a significant precursor to many pharmaceuticals, fragrances and polymer additives.[54,56] In particular, ketal-ester derivatives of levulinic acid are increasingly standing out as plasticizers.[57] However, their synthesis represents a complex process mainly because the “Fischer” esterification and acetalization reactions employ the same type of protic acid catalysts in similar concentration. Consequently, the direct condensation of this keto-acid with diols often leads to a mixture of products in a non-selective manner particularly difficult to control (Scheme 1).[58]

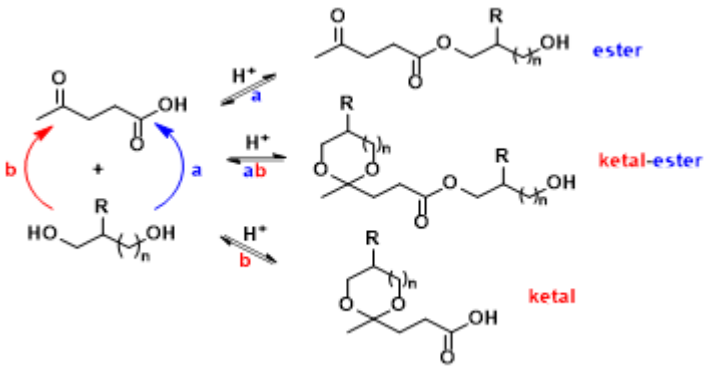


**Scheme 1.** Direct condensation of levulinic acid and a generic diol leading non-selectively to a mixture of products.

Different works have already dealt with the acid-catalyzed competitive esterification and ketalization of levulinic acid. Specifically, Mullen and co-workers reported the acid-catalyzed ketalization of ethyl levulinate without transesterification side-products.[58] Nevertheless, only ethyl levulinate was tested as the starting keto-ester partner, while the feasibility of the proposed process with different substrates has not been investigated. Consequently, modifications as well as the introduction of desired substituents in the final products are not possible, limiting the range of the final ketal-esters which can be prepared. On the other hand, Amarasekara and Animashaun studied the effect of various types of acid catalysts on the condensation of levulinic acid with glycerol to give ketal-ester oligomers[59] and with 1,2 and 1,3-diols to give a mixture of ketal, ester and ketal-ester derivatives.[60] However, the harsh reaction conditions applied in the previous work and the use of carcinogenic benzene in the latter, together with the complexity of the final mixtures make these protocols difficult to be adopted. Therefore, the investigation of the ketalization-esterification reactions of levulinic acid with diols and the need for selective synthetic processes still represent an exciting challenge, in order to make these ketal-ester derivatives more easily accessible and to exploit their potential as new emerging polymer additives.

### 1.3.2. Lignin

Lignin is a natural polymer accounting for the 15-30% of the whole lignocellulosic biomass, where is mainly responsible for structural integrity and stiffness, as well as for water transport and protection from invading agents and insects.[61] Its resistance and robustness are due to its highly cross-linked and branched polymeric structure, partially grafted to hemicellulose chains. Chemically, lignin is built up of three

different phenylpropanolic monomers (called monolignols) linked by carbon-carbon and ether bonds, making it the only renewable feedstock consisting of aromatic units (Figure 1).[62] The most common functionalities which directly determine its chemical reactivity includes aliphatic and phenolic hydroxyls, carbonyl, carboxyl and methoxyl groups and sulfonic acids.[63,64]

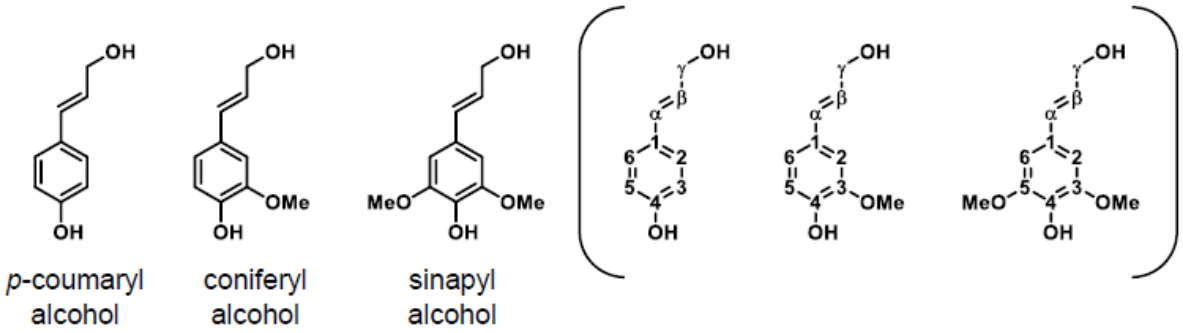


**Figure 1.** Three standard monolignol monomers (labeled according to the established literature).

Lignin is usually obtained in large quantity as waste byproduct in paper and biofuel productions but, notwithstanding its high availability, low price and potentially attractive applications, is mostly incinerated to generate energy.[65] This is due to its very complex, bulky and heterogeneous structure (Figure 2), which limits its industrial utilization. Indeed, the source and the isolation technology considerably affect lignin composition (monomer content, interunit linkages and functional groups), making the determination of the exact chemical structure of each lignin extremely difficult.[61]

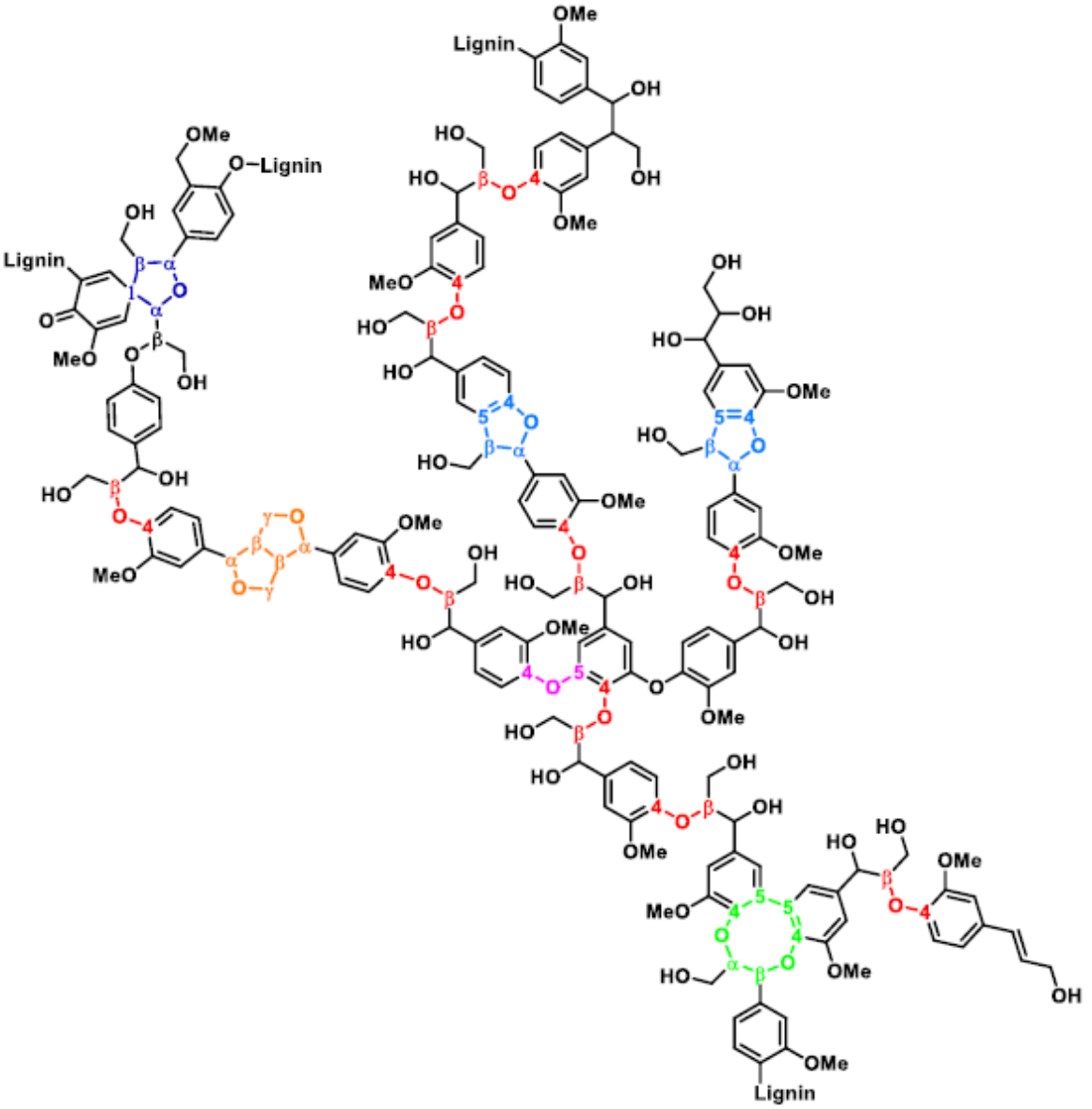


**Figure 2.** Generic structure of lignin and its common interunit linkages (red = aryl ether; orange = resinol; green = dibenzodioxin; light blue = phenylcoumaran; dark blue = spirodienone; purple = diaryl ether)

Currently, four industrial processes are used to obtain lignin (sulfite, Kraft, soda, organosolv).[66] However, since the lignin employed in the herein presented dissemination is a Kraft lignin, the focus will be put only on this one. Briefly, Kraft process depolymerizes lignin by adding it to a mixture of sodium hydroxide and sodium sulfides and heating between 150°C and 180°C. The consequent cleavage of ether bonds results in decreased molecular weight and increased phenolic hydroxyl content, thus enhancing the solubility of the fragments (with a small portion of them sulfated due to the presence of hydrosulfide anions). Isolation finally occurs through acidification and precipitation. In particular, the isolation of lignin from this

process has been improved by LignoBoost technology, which utilizes carbon dioxide as precipitating agent and a washing step with sulfuric acid to maximize the yield and purity.[67] However, as a result of these harsh conditions, Kraft lignin is a broad polydisperse mixture of heterogeneous structures. This aspect badly affects its utilization in material applications where constant molecular size, functionality and reactivity are instead required. Therefore, techniques to decrease lignin heterogeneity and polydispersity are almost always applied before using it as a reagent or additive.

### 1.3.3. Glycerol

Besides levulinic acid, also glycerol has been classified as one of the top-12 promising biomass derived building blocks by the United States Department of Energy.[51] This well-known three carbon triol has many applications including cosmetics, pharmaceuticals, food, plastics and resins. Although its microbial production by fermentation of sugars has been reported, the vast majority of glycerol is produced as a byproduct of soap and biodiesel making from animal fat and vegetable oils.[68] In particular, the glycerol overproduction due to the rapid growth in biodiesel industry has been pushing researchers to turn it into value added products, commodity chemicals and polymers.[69,70] Additionally, increasing use of biodiesel will lead not only to much greater glycerol availability, but also to lower its cost. Therefore, glycerol is considered a potential key chemical platform for the future biorefinery.[71]

## 1.4. Traditional and biobased tested materials

In this work, three different kinds of polymer were employed: fossil-based non-biodegradable polyvinyl chloride; biobased biodegradable polyhydroxybutyrate; fossil-based biodegradable polyvinyl alcohol.

### 1.4.1. Poly(vinyl chloride)

Poly(vinyl chloride) (PVC) is one of the largest thermoplastic commodities used for a wide range of industrial, construction and domestic sectors. The great spread of PVC is principally due to its stability, low cost, water resistance and recyclability. Indeed,

despite being petroleum-based and not biodegradable, PVC is the third most consumed polymer worldwide.[72] The reason is that PVC is very easily and effectively formulated with different additives, making it an extremely versatile material with a broad range of applications. Indeed, PVC is one of the most frequently plasticized polymers, accounting for about 80% of all plasticizers consumed.[19] As a consequence, PVC finds a wide variety of uses, from stiff to highly flexible materials.[73] For instance, some applications include piping, section bars, floor tiles, panels, window rolling shutters and awnings, tarps, cables, faux leather and also medical devices.[74] PVC inherent rigidity is mainly due to the dipole located on every C-Cl bond. Indeed, the resulting attractive dipole-dipole interactions considerably reduce the polymer chains mobility, thus making PVC a stiff material at room temperature.[75] That is why, in order to improve its processability and enhance its flexibility, extensibility and softness, a compatible plasticizer capable of interacting with the polymer chains and reducing the cohesive dipolar forces between them is usually added.[21,76] Consequently, these aspects makes PVC a perfect model-polymer for testing new biobased additives (especially plasticizers) and comparing them with the nowadays industrially used ones.[26]

### 1.4.2. Poly(3-hydroxybutyrate)

Polyhydroxyalkanoates (PHAs) are a class of fully biobased and biodegradable polymers (polyesters) used as intracellular energy storage in a wide range of bacterial species.[77] In particular, PHAs are synthesized and then intracellularly accumulated by most microorganisms under unfavorable growth conditions such as limited nutrients (phosphorus, sulphur, nitrogen, oxygen) but excess of carbon. The carbon sources may be carbohydrates, alcohols, alkanes, organic acids and lipids. PHAs are accumulated in the cells as granules, whose size and number vary depending on the different species. Around 250 bacteria have been found to produce PHAs and the reported PHA monomers are more than 100.[78] The most common method for PHAs recovery from biomass is solvent extraction, which allows highly purified PHAs to be obtained without any molecule degradation. The yield of PHAs may be as high as 80% of the microorganism dry weight.

Chemically, PHAs have the following general formula (Figure 3):

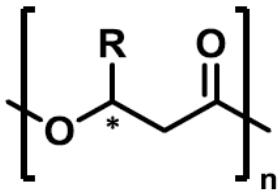


Poly-(R)-3-hydroxyalkanoate

**Figure 3.** General structure of polyhydroxyalkanoates.

They all bear an aliphatic chain in the β position. As a result, depending on the length of this segment, it is possible to identify three main groups: short-chain, medium-chain and long-chain PHAs. This aspect makes this family of biopolymers very versatile. Indeed, depending on the side-chain length, is it possible to range from stiff to elastomeric materials with different final properties (Figure 4).[79] In addition, the β carbon is chiral and always in R configuration, since enzymatic bacterial synthesis is highly stereospecific. This structural regularity gives the polymer a high degree of symmetry, thus allowing PHA chains to pack into crystals. In particular, a higher crystallinity degree will be observed in short-chain PHAs, where small pendant groups crystallize more readily than do PHAs with large, bulky pendant groups.

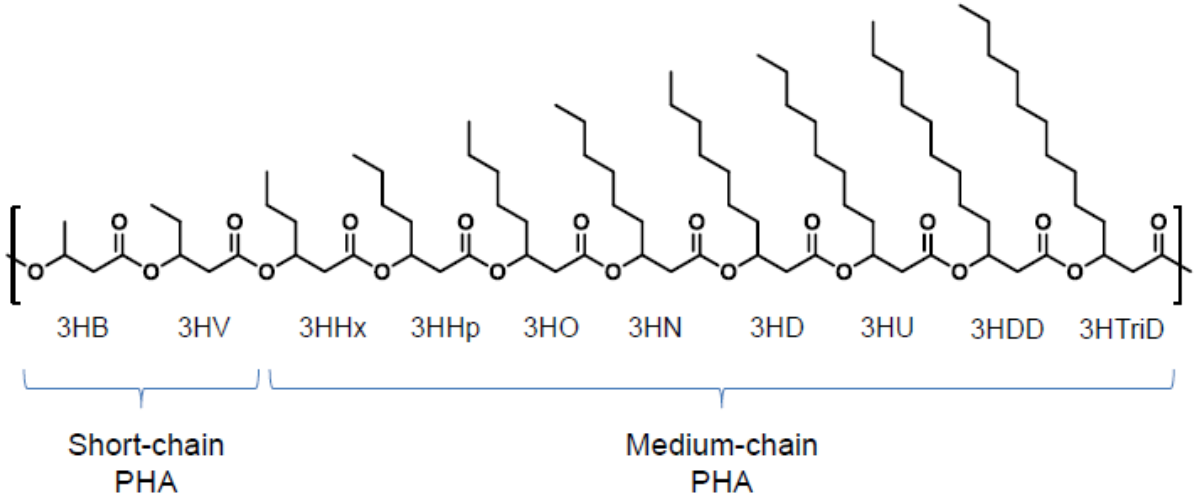


**Figure 4.** Common PHAs monomers (HB = hydroxybutyrate; HV = hydroxyvalerate; HHx = hydroxyhexanoate; HHp = hydroxyheptanoate; HO = hydroxyoctanoate; HN = hydroxynonanoate; HD = hydroxydecanoate; HU = hydroxyundecanoate; HDD = Hydroxydodecanoate; HTriD = hydroxytridecanoate)

PHAs with different chemical compositions may be produced by changing bacteria culture conditions such as type of microorganism, carbon sources supplied, temperature and moisture values.[80] General characteristics of PHAs include insolubility in water, relative resistance to hydrolytic degradation, high resistance to oils and fats (but low to acids and bases), high UV resistance, biocompatibility (and therefore suitable for medical applications) and good printability. Last but not least, PHAs are degraded upon exposure to soil, compost or marine sediment. Importantly, they can be biodegraded in both aerobic and anaerobic environments, without producing any toxic products.[81] Therefore, it is not surprising that PHAs have been gaining attention among biodegradable polymers due to their promising properties. For instance, some applications include (food) packaging, moulded goods, biomedical devices, films, bags and personal care tools.

The focus will be now shifted to poly-3-hydroxybutyrate (PHB), the most widespread member of the PHA family. Historically, PHB was first discovered in bacteria by Lemoigne in 1925.[82,83] Bacterially produced PHB is a semicrystalline isotactic stereoregular polyester with 100% R configuration.[84] As a result, it shows a high amount of crystal phase (up to 80%) characterized by large and perfect spherulites with inter-spherulitic cracks. This happens because natural PHB is free of heterogeneities (such as catalyst residues or other impurities which may act as heterogeneous nuclei) and has a low nucleation density. Consequently, only homogeneous nucleation occurs, leading to a very brittle material with low deformation at break.[85] Another drawback is that PHB thermally decomposes at temperatures just above its melting point, strongly limiting its processing. Indeed, the ester bond is quite labile, especially at high temperatures and in the presence of water/moisture. This means that a short exposure to more than 180°C could start inducing a severe degradation.[86] For these reasons, efforts in compounding PHB are mainly focused on the search of either nucleating agents or plasticizers able to reduce the crystal phase and the spherulite dimensions. This would considerably improve PHB mechanical properties, thus increasing its range of applications. In addition, plasticization may also result in a greater thermal stability, shifting degradation to higher temperatures.

### 1.4.3. Poly(vinyl alcohol)

Polyvinyl alcohol (PVA) is a fossil-based biodegradable polymer. PVA cannot be synthesized from its monomer (vinyl alcohol) because the latter would immediately form its more stable (thus unreactive) tautomer. Consequently, PVA is made from polyvinyl acetate (PVAc), which is treated with methanol and aqueous sodium hydroxide. Depending on the extent of the reaction, polymers with a certain degree of hydrolysis can be obtained. Therefore, the resulting material is always a copolymer of PVA and PVAc, even if commercial grade polymers are available with hydrolysis degrees as high as 98.5%. Although PVAc is completely amorphous, PVA is semicrystalline. Indeed, despite the irregular steric arrangement of its -OH groups along the chains, the volume taken up by them is so small that the polymer can crystallize. The remaining acetate units have an overall effect on the PVA chemical properties, solubility and crystallization behavior.[87] For instance, acetate hydrophobicity may weaken the intra- and intermolecular hydrogen bonding of the OH groups, thus decreasing the polymer melting temperature. On the other hand, glass transition temperature, melting temperature and crystallinity increase with increasing hydrolysis degree (less residual acetate groups, more attractive interactions between the OHs).[88] PVA use is very widespread, mainly for its low price and excellent film forming, emulsifying and adhesive properties. It is also resistant to oil, grease and solvents. PVA has practical applications in textiles wrap sizing, as binder for pigments and fibres, as additive in the production of detergents and cleansing agents, and for the manufacture of water-soluble films. Moreover, PVA is the only vinyl polymer that can be degraded by microorganisms. In particular, high levels of biodegradation can be achieved in water rather than in soil and compost.[89] However, thermal degradation characteristics of PVA limit its ability to be used as a conventional thermoplastic. Indeed, neat PVA thermally degrades at around 180°C. Since its melting point ranges from 180°C to 240°C depending on hydrolysis degree, it may start degrading while melting thus affecting its processing.[90] In addition, widely used PVA transparent films for packaging may need UV-stabilizers to protect both the polymer and the content from potentially degrading radiations.[91] Therefore, proper compounding is fundamental to either improve PVA existing properties or provide new ones, increasing its range of applications.

# 2. AIM

As mentioned above, the rapid introduction of biopolymers as sustainable alternatives to traditional petroleum-based commodities is not closely followed by the additive industry. Indeed, most of the commercially available additives are not suitable for biobased plastics, especially when the latter are also biodegradable. However, the need for biopolymers to show competitive and long-lasting performances together with continually revised international regulations to be observed, resulted in extensive efforts aimed at the creation of a new generation of additives. In particular, current research mainly focuses on different technical challenges, including migration and loss of additive, health and environmental effects, compatibility with new polymers, biodegradability and improved material properties and lifetime. Of course, biobased additives from renewable resources represent the best choice, in order to preserve the virtuous origin of the biomaterial.

With this in mind, the goal of this work was to develop innovative biobased additives for traditional and bioplastics. In particular, promising biomass derived chemical platforms such as levulinic acid, lignin and glycerol were selected as starting materials. Indeed, by exploiting the high chemical versatility of these compounds, it is possible to design accessible synthetic routes leading selectively to a wide variety of new additives. In particular, during my PhD research, ketal-diesters of levulinic acid, esters of refined lignin fractions and glycerol-levulinic acid triesters were synthesized. These molecules have been increasingly standing out as valuable additives, mainly plasticizers (levulinic acid-based compounds) and UV-stabilizers (lignin-derived compounds). Representative polymer matrices in which they have been tested in this work are fossil-based not biodegradable PVC, natural biodegradable PHB and fossil-based biodegradable PVA. These materials present indeed challenging drawbacks that may be overcome through the use of such kind of additives. Indeed, as described in the introduction, inherent rigidity of neat PVC, high crystallinity and resulting stiffness of PHB and transparency of PVA all affect and limit their applications. In addition, suspected carcinogenicity of phthalates in plasticized PVC together with leaching issues strongly stress the need for safer alternatives.

Therefore, in order to achieve the established goal, my research was arranged as follows:

1) Development and optimization of a selective synthesis leading to new asymmetric ketal-diester derivatives of levulinic acid
2) Structural characterization of the molecules
3) Preparation of plasticized PVC thin films with different additive content
4) Complete characterization of the materials
5) Leaching tests and comparison with nowadays most used commercially available plasticizers

The same asymmetric ketal-diester derivatives of levulinic acid were then tested in PHB:

6) Preparation of plasticized PHB thin films with different additive content
7) Complete characterization of the materials
8) Leaching tests

The focus was then shifted to glycerol-levulinic acid systems, with some good initial indications:

9) Optimization of a selective and easily scalable synthesis leading to glycerol-trilevulinate
10) Preliminary evaluation of its plasticizing effectiveness in PVC

Finally, during my six-months research period abroad at VITO (Mol, Belgium), I had the opportunity to work with lignin as starting raw material. The general aim of my research there consisted in the development of multifunctional lignin-based additives for plastics. In particular,

11) Refining of industrial Kraft lignin through different approaches to obtain readily usable lignin fractions
12) Structural and thermal characterization of the obtained fractions
13) Chemical modification of selected lignin fractions

14) Preparation of PVA thin films with different content of selected modified and unmodified lignins
15) Preliminary characterization of the materials

The compatibility and the effect of the synthesized additives on the properties of selected polymer matrices were fully evaluated by means of morphological, thermal and mechanical analyses. The emerged trends were discussed and rationalized, showing very interesting and promising results including structure-property relations.

# 3. EXPERIMENTAL SECTION

## 3.1. Ketal-diester derivatives of levulinic acid as plasticizer for PVC and PHB

### 3.1.2. Materials

Commercially available reagents and solvents were used as received without further purification. Levulinic acid (98.0%), ethylene glycol (anhydrous, 99.8%), 1,3-propanediol (98.0%), myristic acid (≥ 98.0%), stearic acid (95.0%), benzoic acid (99.5%), *p*-toluenesulfonic acid monohydrate (PTSA, ≥ 98.5%), sulfuric acid ($H_2SO_4$, 96%), sodium sulfate ($Na_2SO_4$, anhydrous, ≥ 99.0%), sodium chloride (NaCl, ≥ 99.5%), filter agent (Celite® 545), diethyl ether (≥ 99.0%), chloroform ($CHCl_3$, HPLC grade), deuterated chloroform ($CDCl_3$, 99.8 atom % D, contains 0.03% v/v TMS), dichloromethane (≥ 99.9%), ethyl acetate (≥ 99.5%), *n*-hexane (≥ 95.0%), water (HPLC grade), methanol (≥ 99.8%), tetrahydrofuran (THF, HPLC grade) and toluene (HPLC grade) were purchased from Sigma-Aldrich. Isopentanoic acid (99.0%), phenylacetic acid (99.0%) and sodium carbonate ($Na_2CO_3$, ≥ 99.0%) were supplied by Merck. Hexamoll® DINCH (1,2-cyclohexane dicarboxylic acid diisononyl ester) was purchased from BASF. Analytical thin layer chromatography (TLC) was performed using pre-coated aluminium-backed plates (Merck Kieselgel 60 F254) and visualized by a solution of potassium permanganate ($KMnO_4$, 0.06 M). For column chromatography, silica gel (MN Kieselgel 60, 0.063-0.2 mm, 70-230 mesh, Macherey-Nagel) was used.

PVC (industrial grade) was carefully purified by solubilization in THF (66.7 $mg \cdot mL^{-1}$), filtration and precipitation in a large excess of cold methanol, in order to completely remove all the possible present additives. Number average molecular weight ($M_n$) of 64900 $g \cdot mol^{-1}$ and weight average molecular weight ($M_w$) of 150300 $g \cdot mol^{-1}$ were determined, after the purification step, by gel permeation chromatography (GPC) with an Agilent 1260 Infinity instrument using a reflective index detector. The instrument was equipped with a PLgel MiniMIX-A column coupled with a Tosoh TSKgel SuperMultipore HZ-M column. The analysis was performed in THF (0.2 $mL \cdot min^{-1}$) and using toluene as flow marker, sample concentration of 1.5 $mg \cdot mL^{-1}$, calibration curve obtained with monodisperse polystyrene standards (EasiCal PS-2 Agilent kit).

Industrial grade PHB (kindly provided by Bio-on SpA (Bologna, Italy)) was carefully purified by solubilization in warm $CHCl_3$ (40 $mg \cdot mL^{-1}$), filtration through celite and precipitation in a large excess of cold methanol, in order to completely remove all the fermentation residues. Number average molecular weight ($M_n$) of 78000 $g \cdot mol^{-1}$ and weight average molecular weight ($M_w$) of 246400 $g \cdot mol^{-1}$ were determined, after the purification step, by gel permeation chromatography (GPC) with an Agilent 1260 Infinity instrument using a reflective index detector. The instrument was equipped with a PLgel MiniMIX-A column coupled with a Tosoh TSKgel SuperMultipore HZ-M column. The analysis was performed in $CHCl_3$ (0.2 $mL \cdot min^{-1}$) and using toluene as flow marker, sample concentration of 2.0 $mg \cdot mL^{-1}$, calibration curve obtained with monodisperse polystyrene standards (EasiCal PS-2 Agilent kit).

### 3.1.3. Synthesis of 2-hydroxyalkyl esters 2a-e (step 1)

In this first step of the proposed synthesis, a solvent-free reaction between ethylene glycol and carboxylic acids **1a-e** leads selectively to the corresponding 2-hydroxyethyl esters **2a-e**.

A general preparation procedure was as follows: in a round bottom flask equipped with a magnetic stirrer, the carboxylic acid **1a-e** (5 mmol) and *p*-toluenesulfonic acid monohydrate (0.25 mmol) were added to ethylene glycol (100 mmol). The progress of the reaction was monitored by TLC (*n*-hexane/ethyl acetate 2:1). After 18 h at 75°C, the mixture was allowed to cool down and then quenched with an aqueous solution of sodium carbonate (10 wt.%). The aqueous phase was extracted twice with diethyl ether and the combined organic phases were subsequently washed three times with water and once with brine (saturated aqueous solution of NaCl), respectively, in order to remove residual catalyst and unreacted reagents. After drying over anhydrous sodium sulphate, the solvent was evaporated under reduced pressure. Proton nuclear magnetic resonance ($^1$H-NMR) assignments, Fourier-transform infrared spectroscopy (FT-IR) assignments and yields of this reaction step are reported in detail in the Appendix. The corresponding products **2a-e** were used in the next step without further purifications.

### 3.1.4. Synthesis of levulinic acid diesters 3a-e (step 2)

During this second step of the proposed synthesis, hydroxyalkyl esters **2a-e** previously obtained are esterified with levulinic acid to give the corresponding diester derivatives **3a-e**.

A general preparation procedure was as follows: in a two-neck round bottom flask equipped with a water-collecting Dean-Stark trap connected to a reflux condenser, hydroxyethyl ester **2a-e** (3 mmol) and levulinic acid (9 mmol) were dissolved in toluene (0.15 M with respect to the limiting reagent) under stirring and a drop of sulfuric acid (96%) was added. The mixture was heated at 140°C and the reaction was monitored by TLC (*n*-hexane/ethyl acetate 2:1). After 7 h, the same work-up procedure described above for products **2a-e** led to the corresponding levulinic acid-derived diesters **3a-e**, which was used in the next step without further purifications. Proton nuclear magnetic resonance ($^{1}$H-NMR) assignments, Fourier-transform infrared spectroscopy (FT-IR) assignments and yields of this reaction step are reported in detail in the Appendix.

### 3.1.5. Ketalization of levulinic acid diesters (step 3)

In the last third step of the proposed synthesis, the reaction between the keto moiety of diesters **3a-e** and 1,3-propanediol brings to the corresponding ketal-diesters **4a-e**.

A general preparation procedure was as follows: in a round bottom two-neck flask equipped with a water-collecting Dean-Stark trap connected to a reflux condenser, the diester **3a-e** (1 mmol) and 1,3-propanediol (3 mmol) were dissolved in toluene (0.10 M with respect to the limiting reagent) under stirring and *p*-toluenesulfonic acid monohydrate (0.1 mmol) was added. The reaction, monitored by TLC (n-hexane/ethyl acetate 2:1), was heated at 140°C for 7 h. After the same work-up procedure described above for intermediates **2a-e**, the extracted residue was purified by column chromatography on silica gel (*n*-hexane/EtOAc 5:1). Proton and carbon nuclear magnetic resonance ($^{1}$H and $^{13}$C-NMR) assignments, Fourier-transform infrared spectroscopy (FT-IR) assignments and yields of this reaction step are reported in detail the Appendix.

### 3.1.6. Preparation of PVC thin films

In order to evaluate the plasticizing effect of compounds **4a-e**, homogeneous plasticized PVC thin films were prepared by solvent casting from PVC/THF solution (12.5 mg·mL$^{-1}$). Additives **4a-e** were added to the polymer solution at 10 and 20 parts by weight per hundred parts of resin (phr). The solutions were dried for 72 h at room temperature under an aspiration hood. Neat PVC and PVC-DINCH (20 phr) films were also prepared, using the same procedure. In particular, neat PVC was used as a reference in order to observe the properties variation due to the addition of the herein synthesized ketal-esters (such as thermal behavior and viscoelasticity), while PVC-DINCH (20 phr) films were used for comparison reasons in terms of $T_g$ lowering effect and extraction resistance. All additives and their content do not affect the aspect of the polymer, leading to approximately 100 μm thick transparent films.

### 3.1.7. Preparation of PHB thin films

In order to evaluate the plasticizing effect of compounds **4a-e**, homogeneous plasticized PHB thin films were prepared by solvent casting from PHB/$CHCl_3$ solution (12.5 mg·mL$^{-1}$). Additives **4a-e** were added to the polymer solution at 10 and 20 parts by weight per hundred parts of resin (phr). The solutions were dried for 72 h at room temperature under an aspiration hood. A neat PHB film was also prepared, using the same procedure. In particular, neat PHB was used as a reference in order to observe the properties variation due to the addition of the herein synthesized ketal-esters (such as thermal behavior, crystallinity degree and viscoelasticity). All additives and their content do not affect the aspect of the polymer, leading to approximately 70 μm thick white films.

### 3.1.8. Structural characterization of the synthesized molecules (2a-e, 3a-e, 4a-e)

In order to confirm the chemical structure of the intermediates (**2a-e**, **3a-e**) and of the final target molecules (**4a-e**), thus proving also the effectiveness of the developed synthetic procedure, 1D- and 2D- nuclear magnetic resonance (NMR) and infrared spectroscopy (FT-IR) experiments were carried out. $^{1}$H-NMR and $^{13}$C-NMR spectra were recorded at room temperature (25°C) on a Varian Mercury 400 spectrometer at

400 MHz (nominal frequency: 399.92 MHz) for $^{1}H$ and at 150 MHz (nominal frequency: 150.80 MHz) for $^{13}C$, while 2D-NMR experiments ($^{1}H$-$^{1}H$ gs-COSY, $^{1}H$-$^{13}C$ gs-HSQC and $^{1}H$-$^{13}C$ gs-HMBC sequences, where gs stands for gradient-selected) were recorded on an Inova 600 spectrometer at 600 MHz (nominal frequency: 599.73 MHz). Relaxation delays of 1 s and pulses at 45 degrees were employed. $^{13}C$-NMR were acquired in $^{1}H$ broad-band decoupled mode. $CDCl_3$ containing 0.03 vol.% of TMS as internal reference was used as solvent. Chemical shifts (δ) are reported in ppm relative to residual solvent signals ($CHCl_3$, 7.26 ppm for $^{1}H$-NMR; $CHCl_3$, 77.16 ppm for $^{13}C$-NMR). The following abbreviations are used to indicate the multiplicity in NMR spectra: s, singlet; d, doublet; t, triplet; m, multiplet; br s, broad signal. All the spectra were processed with VnmrJ software (Varian, Inc.).

The chemical structures of the synthesized molecules (**2a-e**, **3a-e**, **4a-e**) were further confirmed by FT-IR spectroscopy. Spectra were recorded on a PerkinElmer Spectrum Two spectrometer equipped with a diamond crystal in Attenuated Total Reflectance (ATR) mode. Measurements were performed in the range of 4000 to 400 $cm^{-1}$ at room temperature; the spectral resolution was 4 $cm^{-1}$ and the number of scans was 64 for each spectrum. Spectral data were processed with Spectrum 10 software (PerkinElmer).

### 3.1.9. Characterization of plasticized PVC thin films

Morphology of the samples and compatibility between PVC and the levulinic acid derivatives were evaluated on the cross-sections of neat and plasticized PVC films. The cross-sections were prepared by cryo-fracturing in liquid nitrogen and investigated by field emission scanning electron microscopy (FESEM) using a Nova NanoSEM 450 electron microscope (FEI Company-Bruker Corporation), applying an accelerating voltage of 15 kV. The cross-sections were previously coated with gold (thickness 10 nm) by an electrodeposition method to impart electrical conduction. The obtained images were analyzed by ImageJ open-source software.

Thermal behavior of the prepared films was evaluated by differential scanning calorimetry (DSC, Q10, TA Instruments), fitted with a standard DSC cell and equipped with a Discovery Refrigerated Cooling System (RCS90, TA Instruments). Samples of about 10 mg were placed into aluminum pans and subjected to two

heating cycles from −60°C to +180°C (hold for 1 min) with heating and cooling rates of 10°C·min$^{-1}$. The DSC cell was purged with dry nitrogen at 50 mL·min$^{-1}$. The system was calibrated both in temperature and enthalpy with Indium standard. Each sample was analyzed in triplicate. DCS curves were processed with TA Universal Analysis 2000 software (TA Instruments) in order to extrapolate the glass transition temperature ($T_{g,DSC}$) from the second heating scan.

Weight-loss decomposition profile and corresponding thermogravimetric derivative (DTG) curves were investigated by thermogravimetric analysis (TGA, Q50, TA Instrument) in order to determine the possible effect of the proposed additives on the thermal stability of the neat PVC. Measurements were performed under dry nitrogen flow (60 mL·min$^{-1}$) on samples of approximately 13 mg placed in a platinum pan. The samples were analyzed by applying a heating ramp from room temperature to 800°C with a heating rate of 10°C·min$^{-1}$. Peak temperatures of thermal degradation ($T_{p1}$ and $T_{p2}$) were determined as the temperature corresponding to the maximum of the DTG curves by using TA Universal Analysis 2000 software (TA Instruments). These temperatures were specifically referred to neat PVC in order to properly demonstrate and evaluate the effect on thermal stability due to the structure or content of the synthesized molecules.

Dynamic-mechanical thermal analysis (DMTA, Q800, TA Instrument) was carried out in triplicate in order to measure temperature-dependent viscoelastic properties of the material, including glass transition temperature ($T_{g,DMTA}$), elastic modulus *(E')* and loss factor (tanδ). Rectangular-shaped samples (15 x 10 x 0.1 mm) were tested in film tension mode at a constant frequency of 1 Hz under strain control fixed at 0.4% while heated from 20°C to 80°C at a rate of 3°C·min$^{-1}$ under nitrogen gas flow. DMTA thermograms were processed with TA Universal Analysis 2000 Version 4.5 A Build 4.5.0.5 software (TA Instruments).

The migration resistance of the plasticizers was evaluated by extraction tests in either deionized water or *n*-hexane, based on standard method ASTM D1239-14.[92] Samples of approximately 300 mg of both neat and plasticized PVC films (20 phr additive content) were placed in a closed vessel containing 20 mL of the given extracting solvent for 24 hours at room temperature under gentle magnetic stirring. Afterward the samples were dried for 24 hours at 40°C under vacuum and re-

weighed. The weight loss corresponds to the extracted addictive and it was calculated according to the following equation:

$$weight\ loss\ (\%) = (\frac{W_1 - W_2}{W_1}) \times 100 \quad \text{(Equation 1)}$$

where $W_1$ and $W_2$ represent the initial and the final weights of the samples, respectively.

### 3.1.10. Characterization of plasticized PHB thin films

Morphology of the samples and compatibility between PHB and the levulinic acid derivatives were evaluated on the cross-sections of neat and plasticized PHB films. The cross-sections were prepared by cryo-fracturing in liquid nitrogen and investigated by field emission scanning electron microscopy (FESEM) using a Nova NanoSEM 450 electron microscope (FEI Company-Bruker Corporation), applying an accelerating voltage of 5 kV. The cross-sections were previously coated with gold (thickness 10 nm) by an electrodeposition method to impart electrical conduction. The obtained images were analyzed by ImageJ open-source software.

Thermal behavior of the prepared films was evaluated by differential scanning calorimetry (DSC, Q10, TA Instruments), fitted with a standard DSC cell and equipped with a Discovery Refrigerated Cooling System (RCS90, TA Instruments). Samples of approx. 10 mg were placed into aluminum pans and subjected to three heating cycles from −60°C to +195°C (hold for 5 min) with a heating rate of 10°C·min$^{-1}$. On the other hand, the cooling rates were 10°C·min$^{-1}$ during the first cooling scan and as fast as possible (quenching) during the second cooling scan. The DSC cell was purged with dry nitrogen at 50 mL·min$^{-1}$. The system was calibrated both in temperature and enthalpy with Indium standard. DCS curves were processed with TA Universal Analysis 2000 software (TA Instruments) in order to extrapolate the peak melting temperature ($T_m$) and the enthalpy of fusion ($\Delta H_m$) from the second heating scans, in order to remove the influence of material processing. The degree of crystallinity (C) was calculated according to the following equation:

$$Degree\ of\ crystallinity\ (\%) = (\frac{\Delta H_m}{\Delta H_{m,0} w_{PHB}}) \times 100 \quad \text{(Equation 2)}$$

where $\Delta H_m$ and $\Delta H_{m,0}$ are the enthalpies of fusion of the sample and 100% crystalline PHB, respectively, and $w_{PHB}$ is the weight fraction of PHB in the sample. $\Delta H_{m,0}$ was taken as 146 J/g.[93] Finally, glass transition temperature ($T_g$) was evaluated from the third heating scan, as the mean value between onset-point and end-point of the transition range.

Dynamic-mechanical thermal analysis (DMTA, Q800, TA Instrument) was carried out in triplicate in order to measure temperature-dependent viscoelastic properties of the material, particularly storage modulus *(E')*. Rectangular-shaped samples (15 x 10 x 0.07 mm) were tested in film tension mode at a constant frequency of 1 Hz under strain control fixed at 0.4% while heated from -60°C to 60°C at a rate of 3°C·min$^{-1}$ under nitrogen gas flow. DMTA thermograms were processed with TA Universal Analysis 2000 Version 4.5 A Build 4.5.0.5 software (TA Instruments).

The migration resistance of the plasticizers was evaluated by extraction tests in either deionized water or *n*-hexane, based on standard method ASTM D1239-14.[92] Samples of approximately 300 mg of both neat and plasticized PHB films (20 phr additive content) were placed in a closed vessel containing 20 mL of the given extracting solvent for 24 hours at room temperature under gentle magnetic stirring. Afterward the samples were dried for 24 hours at 40°C under vacuum and re-weighed. The weight loss corresponds to the extracted addictive and it was calculated according to the following equation:

$$weight\ loss\ (\%) = \left(\frac{W_1 - W_2}{W_1}\right) \times 100 \qquad \text{(Equation 1)}$$

where $W_1$ and $W_2$ represent the initial and the final weights of the samples, respectively.

## 3.2. Lignin-based additives for polymeric materials

### 3.2.1. Materials

Dry Kraft Lignin (dry matter 95%) was kindly provided by VTT Technical Research Centre of Finland, involved in the BBI Horizon 2020 project “Smart Technologies for the Conversion of Industrial Lignins into Sustainable Materials (SmartLi)”. As regards commercially available reagents and solvents, they were used as received without

further purification. Poly(vinyl alcohol) (PVA, $M_w$ 89,000-98,000, 99+% hydrolyzed), triethylamine ($Et_3N$, ≥ 99.5%), 4-(dimethylamino)pyridine (DMAP, ≥ 99.0%), acetic anhydride (ReagentPlus, ≥ 99.0%), butyryl chloride (98.0%), tetrahydrofuran (THF, HPLC grade), tetrahydrofuran (THF, ≥ 99.0%), ethyl acetate (EtOAc, ≥ 99.5%), methanol (MeOH, ≥ 99.8%), ethanol (EtOH, 96.0%), acetone (≥ 99.5%) were purchased from Sigma Aldrich.

### 3.2.2. Lignin fractionation

Lignin fractionation by means of water-induced precipitation was carried out as follows: in an Erlenmeyer flask equipped with a magnetic stirrer, about 10 g of Kraft lignin were added to 100 mL of aqueous ethanol (80% $^v/_v$) or acetone (60% $^v/_v$). After stirring for 30 min at room temperature, the solution was centrifuged for 20 min at 25000 xg and the supernatant was then recovered. The insoluble lignin fraction was dried and weighed, while the supernatant from this first fractionation step was diluted with water to reach the next solvent concentration (70% $^v/_v$ for ethanol, 50% $^v/_v$ for acetone). When water was added, lignin precipitation was clearly visible. Again, this solution was stirred for 30 min at room temperature to allow lignin to precipitate and then centrifuged for 20 min at 25000 xg. The precipitate was then collected, dried and weighed whereas the supernatant was diluted by water addition to precipitate a new lignin fraction. These steps were repeated until solvent concentration of 10% $^v/_v$ was reached. The last lignin fraction was recovered from this solution by evaporating the solvent under reduced pressure. For ethanol-based method, once solvent concentration of 50% $^v/_v$ was reached, a new sequence was started by adding about 10 g of lignin to freshly prepared aqueous ethanol (50% $^v/_v$) and repeating the fractionation as explained above.

Lignin fractionation by means of sequential solvent extraction was carried out as follows: in a round bottom flask equipped with a magnetic stirrer, about 20 g of Kraft lignin were added to 200 mL of EtOAc. The resulting suspension was stirred at room temperature for 2 hours. Afterward, the insoluble lignin was removed from the mixture by Büchner filtration while the EtOAc solution was evaporated under reduced pressure to get the desired corresponding soluble fraction. The filtrated EtOAc-insoluble fraction was therefore subsequently extracted, according to the same

procedure, with EtOH, MeOH and acetone, respectively. Finally, the residue insoluble in any of the mentioned solvents was separated by Büchner filtration. All the so-obtained soluble fractions were dried and weighed in order to calculate the corresponding extraction yields.

### 3.2.3. Chemical modification of the ethanol soluble fraction ($LF_{EtOH}$)

A general preparation procedure for acetylation was as follows: in a glass reaction tube equipped with a magnetic stirrer, $LF_{EtOH}$ (1 mmol of total OHs) and triethylamine ($Et_3N$, 2 mmol) were dissolved in acetic anhydride (5 mmol) under stirring and then 4-dimethylaminopyridine (DMAP, 0.1 mmol) was added. After 18 h (overnight) at room temperature, the mixture was poured dropwise into a high excess of cold deionized water and the resulting precipitated product was recovered by Büchner filtration.

A general preparation procedure for butyrylation was as follows: in a glass reaction tube equipped with a magnetic stirrer, $LF_{EtOH}$ (1 mmol of total OHs), $Et_3N$ (2 mmol) and butyryl chloride (2 mmol) were dissolved in THF (0.4 M) under stirring and then 4-dimethylaminopyridine (DMAP, 0.1 mmol) was added. After 18 h (overnight) at room temperature, the mixture was poured dropwise into a high excess of cold deionized water and the resulting precipitated product was recovered by Büchner filtration.

### 3.2.4. Characterization of the lignin fractions

The number ($M_n$) and weight ($M_w$) average molecular weights and the polydispersity indexes (D) of the lignin fractions were determined by gel permeation chromatography (GPC) with a Shimadzu instrument using both a refractive index detector (Shimadzu RID-10A) and a UV-vis detector (Shimadzu SPD-20A) set at 254 nm. The instrument was equipped with a system of columns connected in series (Styragel Guard Column, Styragel HR1 and Styragel HR 0.5, Waters). 100 µL of the lignin sample in THF (2.0 $mg \cdot mL^{-1}$) were injected and the analysis was performed at a flow rate of 0.8 $mL \cdot min^{-1}$. The calibration curve was obtained by using monodisperse polystyrene standards (Polymer Standard Service).

The thermal behavior of all the lignin fractions was evaluated by differential scanning calorimetry (Discovery DSC 250), fitted with a Fusion DSC Cell™, a 54-position autosampler and equipped with a Discovery Refrigerated Cooling System (RCS90) (all TA Instruments). First of all, since lignin is known to give off volatiles, a hole was made in the lid of each aluminum pan to provide a means for the gaseous compounds to easily escape. Then, samples of about 2.5 mg were placed into the pans and subjected to two heating cycles from −50°C to +250°C (hold for 1 min) with heating and cooling rates of 10°C·min$^{-1}$. The DSC cell was purged with dry nitrogen at 50 mL·min$^{-1}$. DCS curves were processed with TA TRIOS software in order to extrapolate the glass transition temperature ($T_g$) from the second heating scan.

In order to investigate the chemical structure of the lignin fractions, NMR experiments were kindly carried out by University of Hasselt (Belgium). In particular, the number of hydroxyl groups (OH) in aliphatic, phenolic and carboxylic acid moieties was determined by means of $^{31}$P-NMR after derivatizing the hydroxyls in the lignin samples with phosphorus-containing reagent. The spectra were recorded at room temperature on a Varian Inova 400 spectrometer at 400 MHz. $^{31}$P-NMR samples were prepared and analyzed according to the procedure reported by S. Constant et al.[94]

### 3.2.5. Characterization of esterified ethanol soluble fraction ($LF_{EtOH}$)

In order to confirm the chemical structure of both acetylated and butyrylated lignin, thus proving also the effectiveness of the synthetic procedure, infrared spectroscopy (FT-IR) experiments were carried out. Spectra were recorded on a Nicolet iS10 spectrometer (Thermo Fisher Scientific) equipped with a Smart iTX diamond crystal in Attenuated Total Reflectance (ATR) mode. The scans were performed between 4000–500 cm$^{-1}$, with 4 cm$^{-1}$ scan resolution and 32 scans for each sample. Blank atmospheric scans were subtracted from the sample scans prior to their analysis. Spectral data were processed with Omnic software.

The thermal behavior of acetylated and butyrylated lignin was evaluated by differential scanning calorimetry (Discovery DSC 250), fitted with a Fusion DSC

Cell™, a 54-position autosampler and equipped with a Discovery Refrigerated Cooling System (RCS90) (all TA Instruments). First, since lignin is known to give off volatiles, a hole was made in the lid of each aluminum pan to provide a means for the gaseous compounds to easily escape. Then, samples of about 2.5 mg were placed into the pans and subjected to two heating cycles from −50°C to +250°C (hold for 1 min) with heating and cooling rates of 10°C·min$^{-1}$. The DSC cell was purged with dry nitrogen at 50 mL·min$^{-1}$. DCS curves were processed with TA TRIOS software in order to extrapolate the glass transition temperature ($T_g$) from the second heating scan.

### 3.2.6. Preparation of PVA thin films

In order to evaluate the compatibility and then the effect of modified and unmodified lignin fractions on the properties of polyvinyl alcohol (PVA), lignin-PVA thin films were prepared by solvent casting method. The procedure was as follows: 250 mg of PVA were added to 18 mL of deionized water and stirred at 90°C until complete dissolution. The polymer solution was allowed to cool down and then lignin (previously dissolved in 2 mL of THF) was added dropwise under stirring at a content of 1, 3, 5 and 10 parts by weight per hundred parts of resin (phr). Lastly, the solution was poured into a 5 cm Petri dish and dried 24 h in an oven set at 60°C. A neat PVA film was also prepared, using the same procedure, for comparison reasons.

### 3.2.7. Characterization of PVA/lignin thin films

The thermal behavior of PVA/lignin thin films was evaluated by differential scanning calorimetry (Discovery DSC 250), fitted with a Fusion DSC Cell™, a 54-position autosampler and equipped with a Discovery Refrigerated Cooling System (RCS90) (all TA Instruments). Once again, hole was made in the lid of each aluminum pan to provide a means for the gaseous compounds to easily escape. Then, samples of about 5-8 mg were placed into the pans and subjected to two heating cycles from −50°C to +250°C (hold for 1 min) with heating and cooling rates of 10°C·min$^{-1}$. The DSC cell was purged with dry nitrogen at 50 mL·min$^{-1}$. DCS curves were processed with TA TRIOS software in order to extrapolate the glass transition temperature ($T_g$) and the peak melting temperature ($T_m$) from the second heating scan.

## 3.3. Glycerol-levulinic acid-based plasticizer

### 3.3.1. Materials

Commercially available reagents and solvents were used as received without further purification. Levulinic acid (98.0%), glycerol (≥ 99.5%), *p*-toluenesulfonic acid monohydrate (PTSA, ≥ 98.5%), sodium sulfate ($Na_2SO_4$, anhydrous, ≥ 99.0%), sodium carbonate ($Na_2CO_3$, ≥ 99.0%), sodium chloride (NaCl, ≥ 99.5%), diethyl ether (≥ 99.0%), chloroform ($CHCl_3$, HPLC grade), deuterated chloroform ($CDCl_3$, 99.8 atom % D, contains 0.03% v/v TMS), dichloromethane (≥ 99.9%), ethyl acetate (≥ 99.5%), *n*-hexane (≥ 95.0%), water (HPLC grade), methanol (≥ 99.8%), tetrahydrofuran (THF, HPLC grade) and toluene (HPLC grade) were purchased from Sigma-Aldrich. Analytical thin layer chromatography (TLC) was performed using pre-coated aluminium-backed plates (Merck Kieselgel 60 F254) and visualized by a solution of potassium permanganate ($KMnO_4$, 0.06 M).

PVC (industrial grade) was carefully purified by solubilization in THF (66.7 $mg \cdot mL^{-1}$), filtration and precipitation in a large excess of cold methanol, in order to completely remove all the possible present additives. Number average molecular weight ($M_n$) of 64900 $g \cdot mol^{-1}$ and weight average molecular weight ($M_w$) of 150300 $g \cdot mol^{-1}$ were determined, after the purification step, by gel permeation chromatography (GPC) with an Agilent 1260 Infinity instrument using a reflective index detector. The instrument was equipped with a PLgel MiniMIX-A column coupled with a Tosoh TSKgel SuperMultipore HZ-M column. The analysis was performed in THF (0.2 $mL \cdot min^{-1}$) and using toluene as flow marker, sample concentration of 1.5 $mg \cdot mL^{-1}$, calibration curve obtained with monodisperse polystyrene standards (EasiCal PS-2 Agilent kit).

### 3.3.2. Synthesis of glycerol-trilevulinate

A general preparation procedure was as follows: in a round bottom flask equipped with a magnetic stirrer, glycerol (5 mmol) and *p*-toluenesulfonic acid monohydrate (0.5 mmol) were added to levulinic acid (45 mmol). The progress of the reaction was monitored by TLC (*n*-hexane/ethyl acetate 3:1). After 6 h at 110°C, the mixture was allowed to cool down and then quenched with an aqueous solution of sodium

carbonate (10 wt%). The aqueous phase was extracted twice with diethyl ether and the combined organic phases were subsequently washed three times with an aqueous solution of sodium carbonate (10 wt%) and once with brine (saturated aqueous solution of NaCl), respectively, in order to remove residual catalyst and unreacted reagents. After drying over anhydrous sodium sulphate, the solvent was evaporated under reduced pressure. The corresponding product was used without further purifications.

### 3.3.3. Preparation of PVC thin films

In order to evaluate the plasticizing effect of glycerol-trilevulinate, homogeneous plasticized PVC thin films were prepared by solvent casting from PVC/THF solution (12.5 $mg \cdot mL^{-1}$). Glycerol-trilevulinate was added to the polymer solution at 10 and 20 parts by weight per hundred parts of resin (phr). The solutions were dried for 72 h at room temperature under an aspiration hood. A neat PVC film was also prepared, using the same procedure, for comparison reasons. The additive and its content do not affect the aspect of the polymer, leading to approximately 100 μm thick transparent films.

### 3.3.4. Characterization of glycerol-trilevulinate

In order to confirm the chemical structure of glycerol-trilevulinate, thus proving also the effectiveness of the synthetic procedure, proton nuclear magnetic resonance ($^1$H-NMR) spectroscopy was carried out. In particular, $^1$H-NMR spectra were recorded at room temperature (25°C) on a Varian Mercury 400 spectrometer at 400 MHz (nominal frequency: 399.92 MHz). Relaxation delays of 1 s and pulses at 45 degrees were employed. $CDCl_3$ containing 0.03 vol.% of TMS as internal reference was used as solvent. Chemical shifts (δ) are reported in ppm relative to residual solvent signals ($CHCl_3$, 7.26 ppm). The following abbreviations are used to indicate the multiplicity in NMR spectra: s, singlet; d, doublet; t, triplet; m, multiplet; br s, broad signal. All the spectra were processed with VnmrJ software (Varian, Inc.).

### 3.3.5. Characterization of plasticized PVC thin films

Thermal behavior of the prepared films was evaluated by differential scanning calorimetry (DSC, Q10, TA Instruments), fitted with a standard DSC cell and

equipped with a Discovery Refrigerated Cooling System (RCS90, TA Instruments). Samples of about 10 mg were placed into aluminum pans and subjected to two heating cycles from −60°C to +180°C (hold for 1 min) with heating and cooling rates of 10°C·min$^{-1}$. The DSC cell was purged with dry nitrogen at 50 mL·min$^{-1}$. The system was calibrated both in temperature and enthalpy with Indium standard. Each sample was analyzed in triplicate. DCS curves were processed with TA Universal Analysis 2000 software (TA Instruments) in order to extrapolate the glass transition temperature ($T_g$) from the second heating scan.

# 4. RESULTS AND DISCUSSION

## 4.1. Optimization of the synthesis of ketal-diester derivatives

Levulinic acid reacting with diols in acidic conditions brings inevitably to a mixture of esters, ketals and ketal-esters. Indeed, as aforementioned in the introduction, protic acid catalysts promote both esterification and acetalization, thus resulting in low selectivity in the desired product.[58] Consequently, the design and development of a new versatile synthetic route is needed. In order to do that, a generic asymmetric ketal-diester of levulinic acid was firstly set as our target compound. Then, a retrosynthetic analysis was carried out. This technique, which is very useful in the planning of organic syntheses, mainly consists in transforming a target molecule into simpler precursor structures. Each precursor material is in turn examined using the same method and so on until simple or commercially available structures are reached. Therefore, by means of the retrosynthetic analysis showed in Scheme 2, it was possible to design a convenient and accessible synthetic route. In particular, three different disconnection steps were identified: formation of the ketal ring, esterification of levulinic acid, and synthesis of a hydroxyalkyl ester, respectively. It is worth highlighting that levulinic acid comes into play in the second step, where its carboxylic portion may react only with the hydroxyl of the hydroxyalkyl ester. In this way, selectivity issues (esterification vs acetalization) related to the direct condensation of levulinic acid with diols are avoided. Consequently, there is no need to introduce protecting groups into levulinic acid to increase the chemoselectivity of the reaction. This means less additional steps because no protecting groups have to be put on and then removed, resulting in higher atom efficiency and less costs and wastes. Moreover, another big advantage of this synthesis is certainly the possibility to obtain the desired length and degree of branching of the final product by simply varying either the carboxylic acid or the diol in the first step.

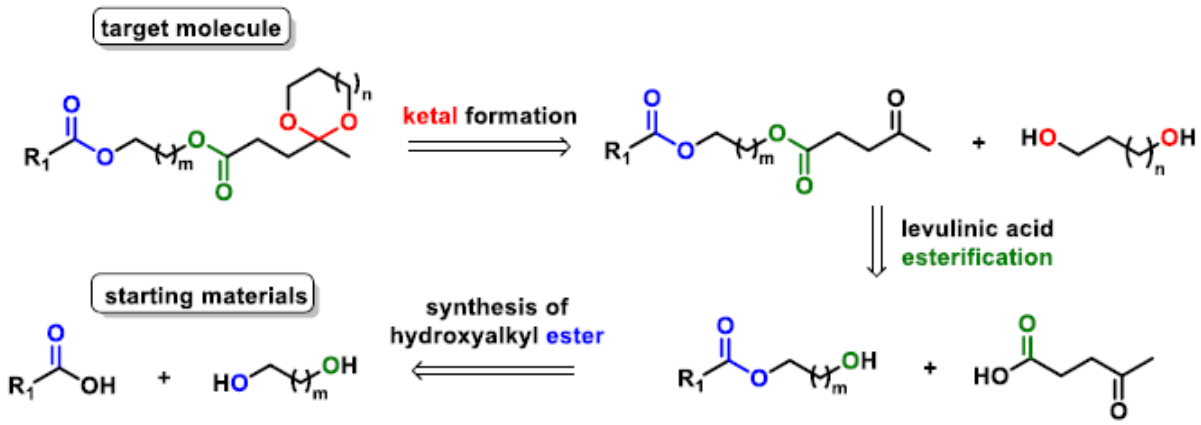


**Scheme 2.** Retrosynthetic analysis of our target molecule to design a proper route.

Before starting the optimization of the reaction conditions, the type of esterification to be employed was examined. Indeed, as can be seen in Scheme 2, the proposed route involves the synthesis of two esters. Esterifications are extremely common reactions in organic synthesis and many different protocols have therefore been developed. Among these, classic Fischer esterification[95] was selected mainly because of its simplicity and advantages. Generally, this reaction takes place between a carboxylic acid and an alcohol in presence of an acid catalyst in refluxing conditions. It is a condensation reaction; therefore, it proceeds in a stepwise fashion to produce the addition product and a water molecule as only byproduct. This leads to a high atom economy compared to other processes such as alcoholysis of acyl chlorides and acid anhydrides. In addition, these alternative protocols are more difficult to handle. For instance, acyl chlorides may result in the generation of hydrogen chloride gas upon contact with atmospheric moisture, are corrosive and react vigorously with water. Moreover, unlike other common methods including Steglich,[96] Yamaguchi,[97] and Mitsunobu esterifications,[98] no coupling reagents, acyl transfer catalysts or unstable and hazardous reagents are employed in Fischer route. This avoids harsh reaction conditions, additional steps and large and expensive amounts of reagents. Actually, also Fischer esterification suffers from some drawbacks, such as thermodynamic reversibility and relatively slow reaction rates. However, they can be easily overcome by using Le Chatelier's principle, which allows one to manipulate the outcomes of systems in chemical equilibrium by means of an externally induced change in one or more parameters.[99] In case of Fischer esterification, both the reaction rate and the product yield may be improved by using a large excess of one of the reagents and by physically removing water. Of course,

the aforementioned use of an acid catalyst and relatively high temperatures also increase the reaction rate and promote product formation.
Last but not least, an easy and potentially scalable workup has been designed to isolate the products without need for further purifications. In particular, it includes quenching with an aqueous base to deactivate the catalyst, extraction with diethyl ether and simple washing steps with water to get rid of unreacted reagents. As it will be explained later, only in the last step a purification of the crude product by means of column chromatography on silica gel is needed.

At this point, a first set of preliminary experiments was performed in order to assess the feasibility of the established process (Scheme 2) and to identify the best reaction conditions. As starting reactants, ethylene glycol was chosen as the alcohol, whereas myristic (**1a**) and stearic (**1b**) acids as the carboxylic acids. These molecules are saturated long-chain fatty acids with linear 14- and 18-carbon backbones, respectively. They were specifically selected because they are biobased (found naturally in vegetable oils and in milk fat) and because of their “size”. Indeed, as mentioned in the introduction, successful plasticization is a precarious balance between plasticizer molecular weight, geometry and kind of functional groups. So, while both ester and ketone groups of the target molecule are necessary to properly interact with the polymer, these nonpolar long-carbon segments are also necessary to break up some of the polymer chain-chain attractive interactions. The first step of the designed route, i.e. the synthesis of a hydroxyethyl ester, was therefore investigated (Scheme 3). The reaction was carried out solvent-free with *p*-toluenesulfonic (PTSA) acid as the catalyst. Considering both the boiling point of ethylene glycol (around 197°C) and the melting point of myristic acid (around 55°C), the temperature was set at 75°C and the reaction time at 16 h (overnight). In this way, the carboxylic acid was over its melting point, its solubility increased and consequently the system more homogeneous and reactive. On the other hand, ethylene glycol was below its boiling point, thus lowering its potential loss due to evaporation. Indeed, taking into consideration the previously discussion about chemical equilibrium, all the reactions were performed in a round-bottom flask without cap in order to allow water (byproduct) removal by simple evaporation. So, the catalyst amount and the concentration of the reactants were firstly investigated. Looking at Table 1, it is possible to see that decreasing the catalyst loading as well

as using a large excess of ethylene glycol (i.e., as a solvent), led selectively to the desired hydroxyethyl ester **2a** in high yield (95%, entry 3). Importantly, the large excess of glycol (20 equivalents in relation to the carboxylic acid) not only helped to shift the equilibrium towards right, but also avoided the formation of the undesired symmetric diester. This compound was instead found in the final mixture when either higher catalyst amount or stoichiometric ethylene glycol were used (entries 1 and 2). It was detected by means of NMR analysis as a singlet peak at about 4.25 ppm. Probably, the greater activation of the carbonyl group provided by the catalyst together with less available alcoholic OHs resulted in diesterification of ethylene glycol.

The reaction conditions of entry 3 were then applied to stearic acid, except for the temperature which was increased at 90°C (as a consequence of its melting point of about 70°C). The esterification occurred successfully, leading to the desired hydroxyethyl ester **2b** in high yield (80%, entry 4).

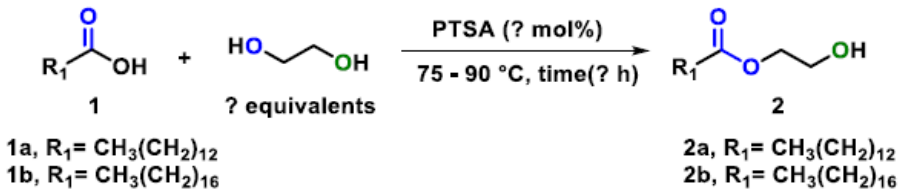


**Scheme 3.** Optimization of the hydroxyethyl ester synthesis (step 1).

**Table 1.** Optimization of the hydroxyethyl ester synthesis (step 1).

| Entry | **1** | Equivalents of Ethylene Glycol | PTSA (mol%) | Product (isolated yield %) |
|---|---|---|---|---|
| 1 | **1a** | 1 | 15 | dimer (not detected) |
| 2 | **1a** | 1 | 5 | dimer (not detected) |
| 3 | **1a** | 20 | 5 | **2a** (95) |
| 4 | **1b** | 20 | 5 | **2b** (80) |

Successively, step 2 was studied. In this step, the hydroxyethyl ester previously obtained reacts selectively with the carboxylic group of levulinic acid to give the corresponding asymmetric diester (Scheme 4). In this case, the tests were performed in toluene with a water-collecting Dean-Stark trap connected to a reflux

condenser. This equipment allows the water to be continuously removed by exploiting the water-toluene azeotropic mixture that distills out of the reaction. As already described, this helps to improve the yield of reversible Fischer esterification. For the same purpose, equivalents of levulinic acid, kind and amount of catalyst and solvent concentration (in relation to the limiting reagent) were then investigated (Table 2). Hydroxyethyl ester **2a** was used as starting substrate. A slight excess of levulinic acid and a dilute system resulted in low conversion (entry 1). Therefore, levulinic acid equivalents as well as solvent concentration were increased (entry 2). However, low conversion was again detected. That was probably due to the low solubility of PTSA in toluene. In order to get higher conversions and also speed up the reaction rate, the catalyst was replaced with sulfuric acid. Due to its extremely strong acidic nature, only a drop was added in the reaction mixture. In addition, the concentration was further increased to 0.15 M. These conditions led to the desired diester **3a** in very good yield (70%) and in shorter time (7h), as shown in entry 3. The same procedure was then applied to hydroxyethyl ester **2b**, leading successfully to the diester **3b** with an 87% yield (entry 4).

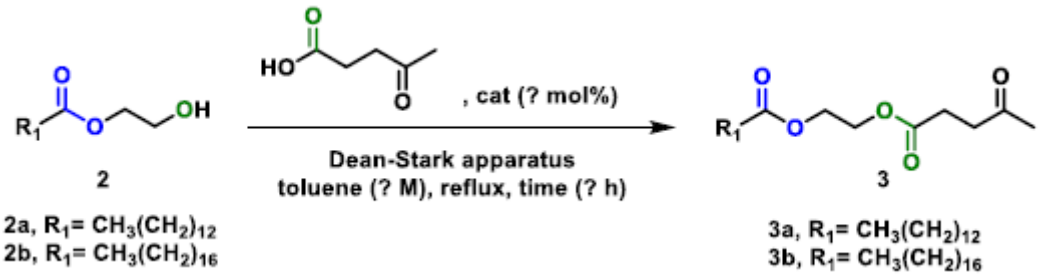


**Scheme 4.** Optimization of the esterification of levulinic acid (step 2).

**Table 2.** Optimization of the esterification of levulinic acid (step 2).

| Entry | **2** | Equivalents of levulinic acid | Cat (mol%) | Conc (M) | Time (h) | Product (isolated yield %) |
|---|---|---|---|---|---|---|
| 1 | **2a** | 1.5 | PTSA (5) | 0.05 | 16 | low conversion (not detected) |
| 2 | **2a** | 3 | PTSA (5) | 0.1 | 16 | low conversion (not detected) |
| 3 | **2a** | 3 | $H_2SO_4$ (1 drop) | 0.15 | 7 | **3a** (75) |
| 4 | **2b** | 3 | $H_2SO_4$ (1 drop) | 0.15 | 7 | **3b** (91) |

Finally, the formation of the cyclic ketal ring was studied (Scheme 5). Ethylene glycol and 1,3-propanediol were used as alcohols, while diester **3a** as substrate. PTSA was selected as catalyst because of its widespread use in these kinds of reactions. Amount of catalyst and solvent concentration were set equal to 10 mol% and 0.1 M, respectively. Also these tests were performed in toluene with a Dean-Stark trap connected to a reflux condenser for continuous removal of water from the reaction mixture. As shown in Table 3, the first attempt with only a slight excess of ethylene glycol resulted in low yield and long reaction time (entry 1). On the other hand, when 1,3-propanediol was employed, the yield was higher (entry 2). Indeed, as reported elsewhere,[100] the use of 1,3-diols instead of 1,2-diols gives more stable compounds because of the resulting six-membered acetal ring. 1,3-propanediol was therefore chosen as the suitable diol. A further increase of 1,3-propanediol equivalents (from 1.3 to 3) led to a higher yield of the desired ketal-diester in a shorter time (entry 3). These conditions were then applied to diester **3b**, giving the corresponding cyclic acetal with 60% yield (entry 4).

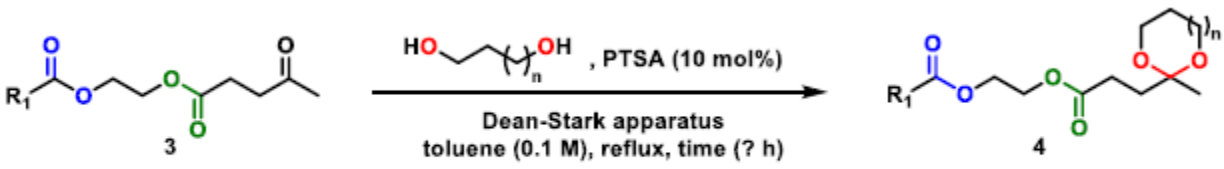


3a, $R_1$= $CH_3(CH_2)_{12}$
3b, $R_1$= $CH_3(CH_2)_{16}$

4a, $R_1$= $CH_3(CH_2)_{12}$ ; n= 1
4b, $R_1$= $CH_3(CH_2)_{16}$ ; n= 1

**Scheme 5.** Optimization of the ketalization reaction (step 3).

**Table 3.** Optimization of the ketalization reaction (step 3).

| Entry | **3** | Diol (equivalents) | Time (h) | Product (isolated yield %) |
|---|---|---|---|---|
| 1 | **3a** | ethylene glycol (1.3) | 16 | Not determined (low) |
| 2 | **3a** | 1,3-propanediol (1.3) | 16 | **4a** (45) |
| 3 | **3a** | 1,3-propanediol (3) | 7 | **4a** (55) |
| 4 | **3b** | 1,3-propanediol (3) | 7 | **4b** (60) |

It is worth considering that in this las third step of the synthesis, since acetalization conditions are the same of Fischer esterification, the diester substrates slightly undergo side-reactions such as transesterification and hydrolysis. For instance, 1,3-propanediol may react not only with the ketone group but also with the two ester moieties of **3**, thus breaking the diester. This is clearly visible in the TLC shown in Figure 5, where different spots (thus different molecules other than the product) are present. Consequently, purification of the final product by means of column chromatography on silica gel was necessary, slightly affecting the yield.

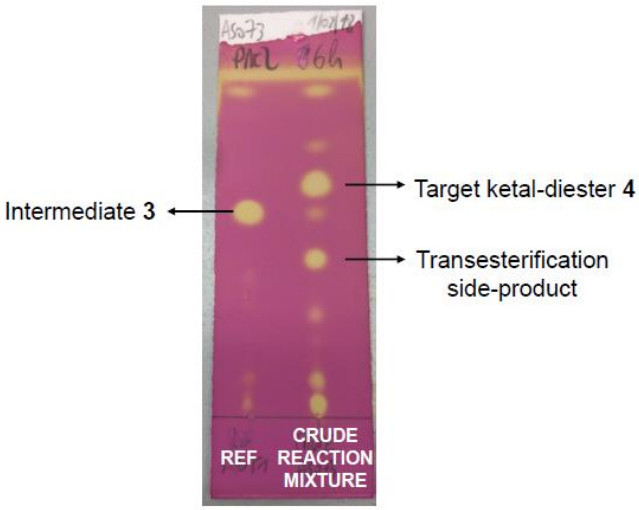


**Figure 5.** Representative TLC of the crude reaction mixture of step 3.

With the optimized conditions in hand, the scope of the reaction was then extended. Indeed, one of the main advantages of the developed route is certainly the possibility to obtain the desired length and degree of branching of the final product by simply varying the carboxylic acid **1** in the first reaction step. Therefore, besides the long straight myristic (**1a**) and stearic (**1b**) aliphatic segments already mentioned, three

additional different kinds of side chain were selected in order to evaluate their plasticizing effect toward PVC and PHB. In particular, branched aliphatic, aromatic and alkyl-aromatic moieties were introduced by means of isovaleric (**1c**), benzoic (**1d**), and phenylacetic (**1e**) acids, respectively. These carboxylic acids were intentionally selected because they can be obtained from renewable resources (as describes in the list reported in the Appendix), thus preserving the green origin of levulinic acid. It is worth stressing that the developed protocol (Scheme 6) readily tolerated the different starting carboxylic acids (**1a-e**), giving the corresponding intermediates **2a-e**, **3a-e** and the target ketal-diesters **4a-e** in good to excellent yields (Table 4).

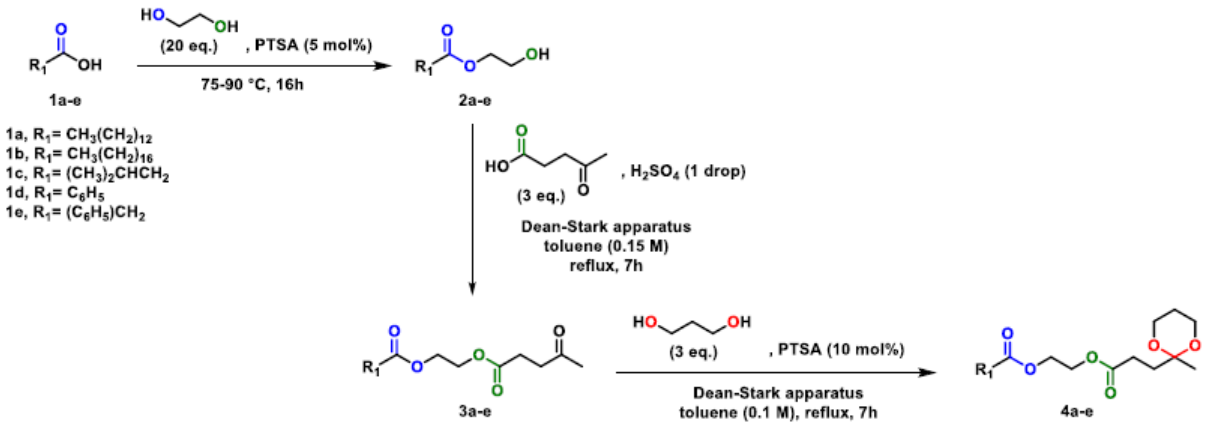


**Scheme 6.** Optimized synthetic route.

**Table 4.** Yields of the intermediates **1a-e**, **2a-e** and of the final ketal-diesters **4a-e**.

| Step | Product | Yield (%) | Step | Product | Yield (%) | Step | Product | Yield (%) |
|---|---|---|---|---|---|---|---|---|
| 1 | **2a** | 95 | 2 | **3a** | 75 | 3 | **4a** | 55 |
| | **2b** | 80 | | **3b** | 91 | | **4b** | 60 |
| | **2c** | 85 | | **3c** | 95 | | **4c** | 50 |
| | **2d** | 89 | | **3d** | 98 | | **4d** | 50 |
| | **2e** | 86 | | **3e** | 96 | | **4e** | 50 |

## 4.2. Characterization of the ketal-diester derivatives of levulinic acid

In order to confirm the chemical structures of the intermediates (**2a-e**, **3a-e**) and of the final target molecules (**4a-e**), thus proving also the effectiveness of the developed synthetic route, nuclear magnetic resonance (NMR) experiments were carried out. Therefore, at first, the chemical structures of the intermediates **2a-e** and **3a-e** were investigated by $^{1}$H-NMR (Figure 6 and Figure 7, respectively). As regards intermediates **2a-e**, the two multiplets centered at around 4.22 and 3.83 ppm were attributed to the methylene groups of the glycolic segment (K and J protons, respectively). These separated signals clearly indicate that desired mono-esterification of ethylene glycol occurred. Indeed, in case of di-esterification, these four protons would have led to a singlet in the ester region (about 4-4.5 ppm) due to the symmetry of the resulting undesired molecule. In each spectrum, the triplet in the range 1.80-2.20 ppm was instead attributed to the alcoholic proton (S), further proving that only one -OH group of the diol has been esterified while the other one is free to react in the next step. The presence of the aromatic ring was easily detectable: as regards **2d**, peaks at 8.05, 7.57 and 7.45 ppm clearly show the typical pattern of the benzoyl group (*ortho* (N), *para* (Q) and *meta* (P) protons, respectively), while the multiplet at 7.36-7.26 ppm and the singlet at 3.65 ppm were assigned to the protons (P,Q,R and M, respectively) of the benzylic moiety of **2e**. Coming back to aliphatic compounds **2a-b** (Figure 6a and 6b), their aliphatic myristic and stearic side chains were characterized as follows: signals at 2.32, 1.67-1.58, 1.34-1.21 and 0.88 ppm were assigned to methylene protons in α position (M), methylene protons in β (N), $C_{10}$ and $C_{14}$ linear methylene chain protons (P) and terminal methyl protons (Q), respectively. Finally, as regards the side-chain of **2c** (Figure 6c), signal at 2.22 ppm was assigned to the methylene protons in α (M), signal at 2.16-2.06 ppm to the isopropylic proton (N) whereas signal at 0.96 ppm to the six equivalent methyl protons (P).

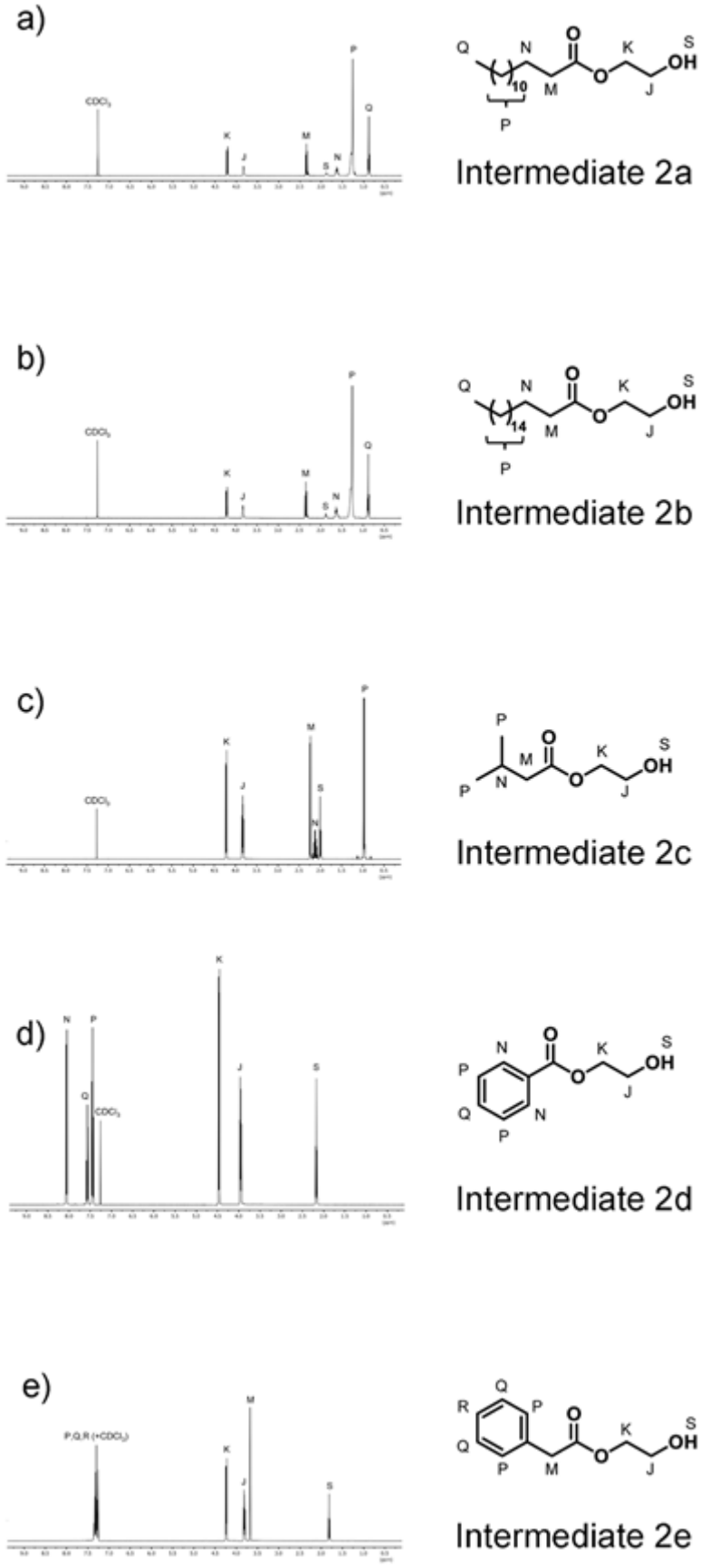


**Figure 6.** (a-e) $^{1}$H-NMR spectra of the intermediates **2a-e** with corresponding proton assignments.

Moving from hydroxyethyl esters **2a-e** to intermediates **3a-e** (Figure 7), it is possible to see not only the downfield shift of the two multiplets centered at about 4.22 and 3.83 ppm related to the four protons (K, J) of the ethylene glycol central moiety, but also the disappearance of the triplet of the alcoholic proton (S). In particular, for intermediates bearing aliphatic side-chains **3a-e**, J and K signals turned into a new single peak at 4.27 ppm. Its multiplicity (singlet) is due to the partial symmetry of the corresponding molecules. On the other hand, in aromatic intermediates **3d-e**, the same four J and K protons gave two separated multiplets because there is no such partial symmetry. Consequently, **3d** showed two separate multiplets at 4.54-4.51 (K) and 4.44-4.41 (J) ppm, while **3e** a single multiplet at 4.32-4.26 (K, J) ppm. Importantly, all these signals are in the ester region, thus confirming that esterification of the free -OH of **2a-e** with levulinic acid occurred.

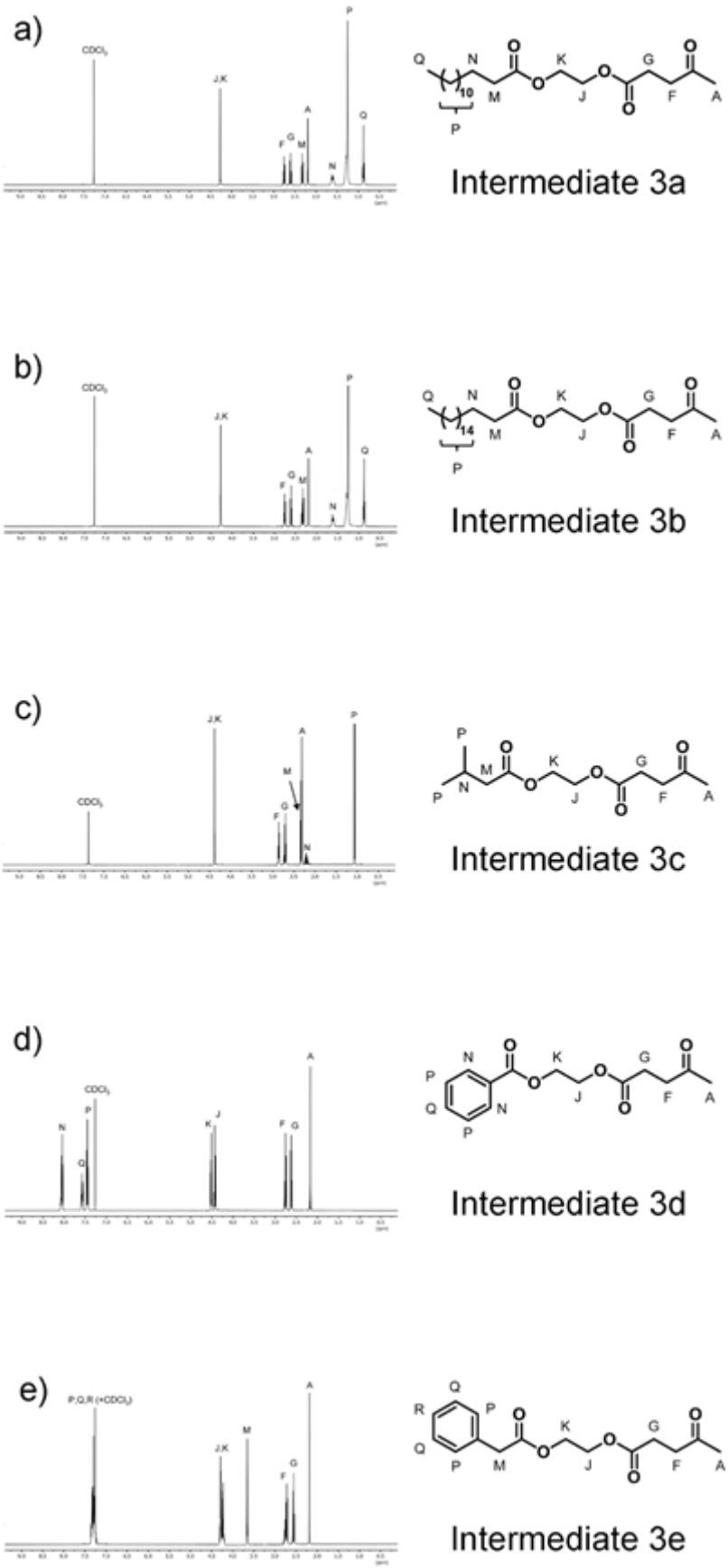


**Figure 7.** (a-e) $^{1}$H-NMR spectra of the intermediates **3a-e** with corresponding proton assignments.

Finally, $^{1}$H-, $^{13}$C- and 2D-NMR spectroscopies were used to fully characterize the final levulinic acid derivatives **4a-e**. Figures 8a-e and Figures 8f-l show $^{1}$H- and $^{13}$C-NMR spectra, respectively, of the final ketal-diesters **4a-e**; signal assignments were confirmed by means of bidimensional COSY, HSQC and HMBC correlation experiments (Figure 45, 46 and 47, reported in the Appendix). With respect to the ketal portion of the final derivatives **4a-e** (Figures 8a, 8b, 8c, 8d and 8e), three multiplets centered at about 3.90, 1.80 and 1.53 ppm can be observed in all the $^{1}$H-NMR spectra. These signals were assigned to the methylene protons (C, E) and to the diastereotopic protons (D) of the six-membered ketal ring, respectively. The disappearance of the electron-withdrawing keto group of diesters **3a-e** to form the cyclic ketal ring in **4a-e** is also supported by the observation of a shift to higher fields of the signals of the levulinate segment. In particular, triplets at approximately 2.50 and 2.00 ppm and singlet at 1.40 ppm were assigned to the four protons (G, F) and to the methyl protons (A) of the levulinate moiety, respectively. As expected, the side chains of compounds **4a-e** were detected without any shift in their positions in comparison to their synthetic intermediates.

These observations are in good agreement with the $^{13}$C-NMR results. Indeed, characteristic peaks of target molecules **4a-e** were also found in $^{13}$C spectra (Figures 8f, 8g, 8h, 8i and 8l). In particular, peak at about 98 ppm was assigned to the acetal carbon (B) and peak at about 59.9 ppm to the two equivalent alkoxy carbons in the ketal ring (C, E).

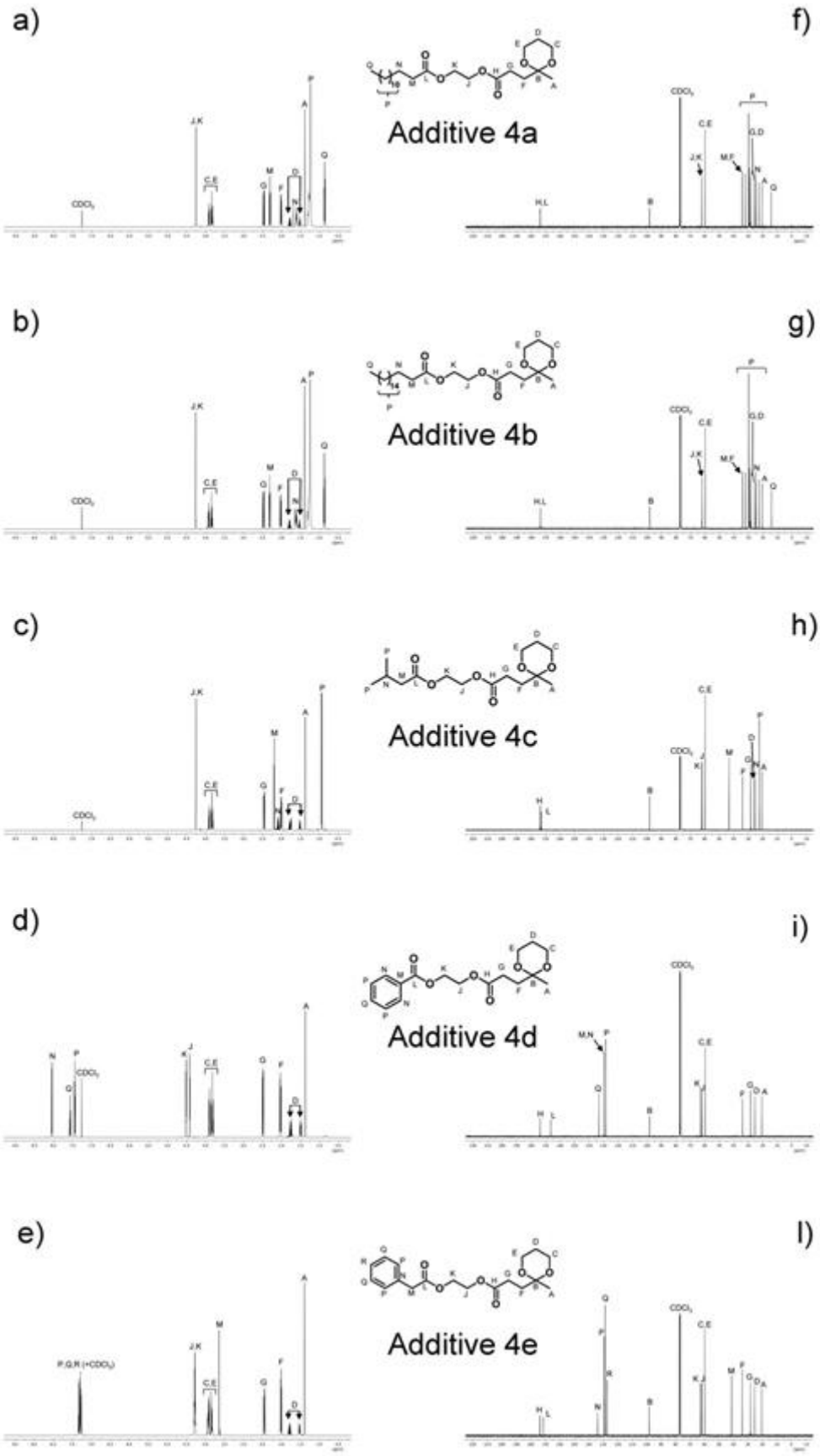


**Figure 8.** (a-e) $^{1}$H-NMR and (f-l) $^{13}$C-NMR spectra of the final ketal-diesters **4a-e** with corresponding proton and carbon assignments.

The structure of all the products were further assessed by FTIR investigations. The generic spectra of the intermediates (**2a-e**, **3a-e**) and final (**4a-e**) products are reported in Figure 9. As expected, moving from the 2-hydroxyalkyl esters **2a-e** to the keto-esters **3a-e**, the wide absorption peak between 3600 to 3200 $cm^{-1}$ of the O-H stretching vibration disappears due to the formation of the ester with levulinic acid. Moreover, beyond the characteristic peak at 1730 $cm^{-1}$ (ester C=O stretching), a peak at 1713 $cm^{-1}$ is observed, revealing the simultaneous presence of a keto group introduced with levulinic acid. This signal is not more detectable in the final molecules **4a-e** while new peaks appear at 1100, 1090 and 960 $cm^{-1}$ (alkoxy C-O stretching) confirming the reaction of the keto group with 1,3-propanediol and therefore the ketal formation.

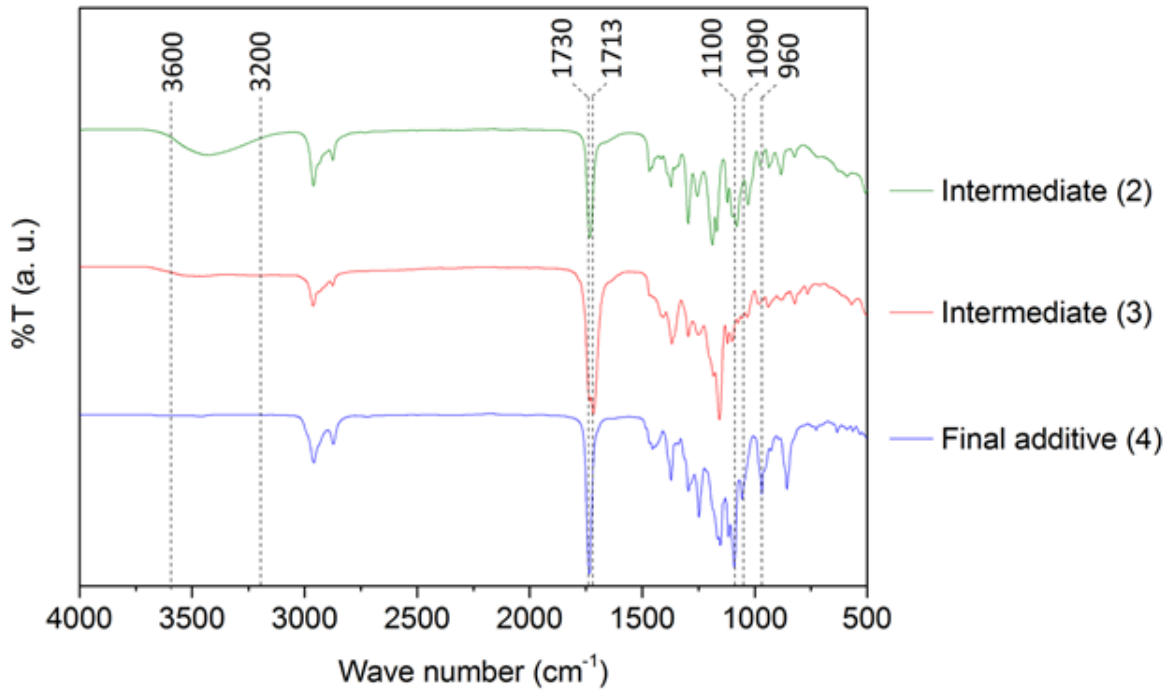


**Figure 9.** Representative FTIR spectra of intermediates **2**, **3** and final ketal-esters **4**. The dashed lines indicate the wave number of the characteristic absorption peaks, which appear and/or disappear during the synthesis of the target compounds.

Therefore, the combination of $^{1}H$- and $^{13}C$-NMR investigations with FT-IR results demonstrates that the proposed diesterification and further ketalization reactions occurred efficiently as desired.

## 4.3. Characterization of plasticized PVC thin films


**Figure 10.** Representative photograph of the prepared PVC films.

In order to evaluate the compatibility between PVC and additives (**4a-e**), the cross-sections of the plasticized PVC films were investigated by FESEM. Figure 11 shows the cross-sections of neat PVC (Figure 11a) and plasticized PVC films (Figure 11b-f) with 20 phr of additive. All the samples showed a homogeneous phase with no evidence of phase separation, confirming that the components are perfectly miscible. This is also an initial positive indication for having an effective plasticization, which requires an efficient chemical interaction between the phases. This good miscibility may be ascribed to non-covalent intermolecular attractive forces which bind together the polymer and the plasticizer.[21] In particular, our additives contain two polar carbonyl groups, in which oxygen is far more electronegative (partially negative, δ-) than carbon (partially positive, δ+) and so has a strong tendency to pull one of the two pairs of electrons that make up a carbon-oxygen double bond towards itself.[101] On the other hand, as mentioned in the introduction, every repeating unit of PVC contains a highly electronegative chlorine atom (δ-) that attracts electron charge and creates a permanent electric dipole.[21,27] As a result, the hydrogen (δ+) on the carbon atom bearing the chlorine is able to readily form a hydrogen bond with the carbonyl oxygen (δ-) of the plasticizing molecule.[102,103] In particular, thanks to these

interactions, polymer H–C–Cl and plasticizer C=O groups will be lined up, creating a sequential chain of ···Cl–C–H···O=C···Cl–C–H··· contacts which improve mutual attraction and therefore compatibility.[27,104,105] Such aspect not only leads to the desired plasticizing effect, but also avoided the self-coalesce of the additive into separated phases, which eventually could have leached out from the polymer surface.[21]

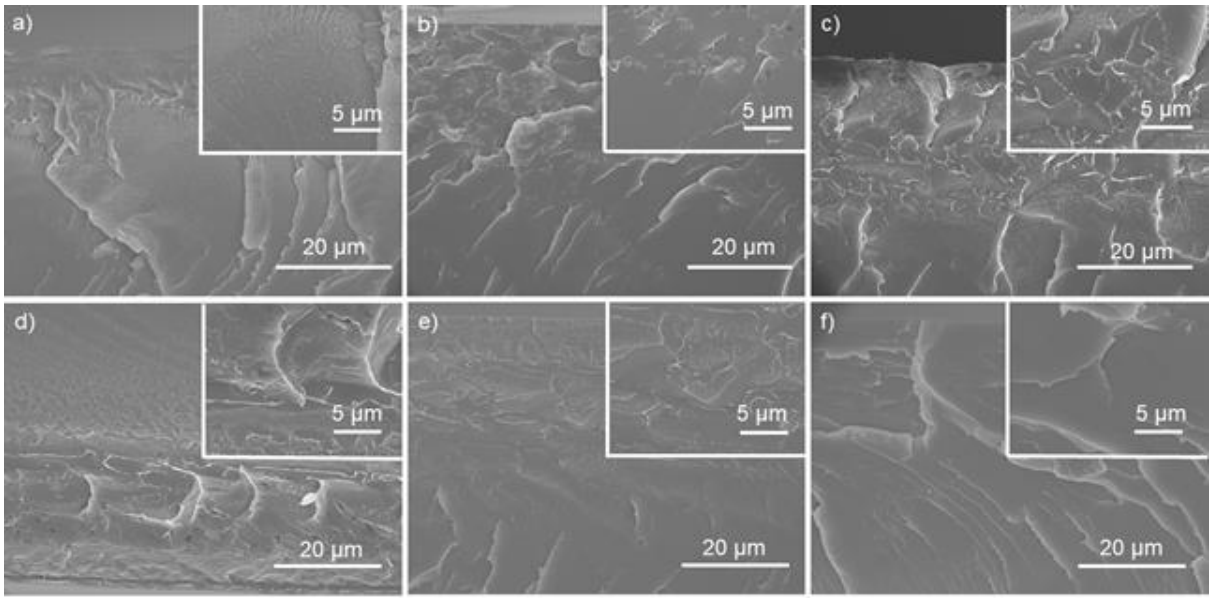


**Figure 11.** Cross-sections FESEM micrographs of (a) neat PVC, (b) 20 phr PVC-**4a**, (c) 20 phr PVC-**4b**, (d) 20 phr PVC-**4c**, (e) 20 phr PVC-**4d** and (f) 20 phr PVC-**4e**. Higher magnification images are reported in the insets.

Since $T_g$ reduction is the main indication of the efficiency of a plasticizer, DSC analysis was performed on neat and plasticized PVC and the resulting $T_{g,DSC}$ values are summarized in Figure 12 as a function of the additive content and in Table 5. A decrease of the $T_{g,DSC}$ can be observed for all the formulations with respect to the neat PVC ($T_{g,DSC}$ = 73°C). Interestingly, three main behaviors can be clearly observed. Specifically, at both 10 and 20 phr, the additive **4b** offered the poorest performance with a $T_{g,DSC}$ reduction of 24 and 41°C, respectively. Additives **4a**, **4c** and **4d** showed comparable plasticizing efficiency, with the $T_{g,DSC}$ that decreases approximately of 31-32°C and 46-50°C, increasing the additive content from 10 to 20 phr. On the other hand, the additive **4e** caused the largest decrease of the $T_{g,DSC}$, which reaches a value of 36 and 58°C for a plasticizer concentration of 10 and 20 phr, respectively.

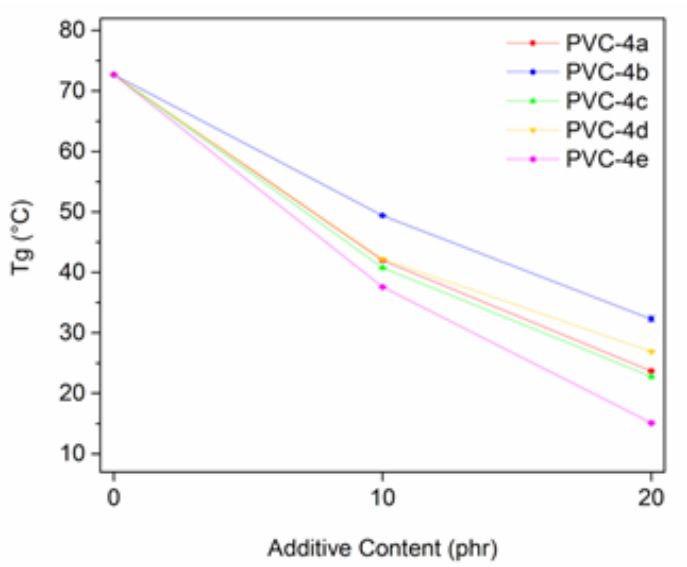


**Figure 12.** Average $T_{g,DSC}$ values of neat and plasticized PVC films as a function of the additive content.

**Table 5.** Average $T_g$ values of plasticized PVC films determined by DSC and corresponding standard deviations. * neat PVC average $T_g$ value: 72.7 ± 0.1°C.

| | **$T_{g,DSC}$ (°C)*** | |
|---|---|---|
| **PVC-Additive code** | **10 phr of additive** | **20 phr of additive** |
| PVC-**4a** | 42.0 ± 0.2 | 23.7 ± 0.1 |
| PVC-**4b** | 49.4 ± 0.1 | 32.3 ± 0.5 |
| PVC-**4c** | 40.8 ± 0.1 | 22.8 ± 0.2 |
| PVC-**4d** | 42.2 ± 0.1 | 26.9 ± 0.1 |
| PVC-**4e** | 37.6 ± 0.1 | 15.1 ± 0.2 |

In order to explain this trend, it can be useful to divide additives into two categories based on their side-chain chemical structure. Considering the aliphatic additives, it is possible to notice that decreasing the lateral chain length as well as increasing the steric hindrance by introducing a rotating substituent, the plasticizing effect becomes more evident. In fact, passing from a stearic (**4b**) to a shorter myristic chain (**4a**) and to a further shorter but branched 3-methylbutanoic one (**4c**), a gradual decrease of the $T_g$ values can be observed. Among the aromatic additives **4d** and **4e**, the

presence of both polar aromatic ring and ester group significantly enhances the interactions with the polarized C-Cl bond of PVC, resulting in a greater affinity and thus in an overall more important plasticizing effect if compared to the aliphatic additives. However, **4d** owns a rigid phenyl group whereas in **4e** the phenyl ring can freely move thanks to the $sp^3$-hybridized benzylic carbon atom. This results in a higher hindrance that reduces the polymer chain interactions, therefore making the ketal-ester **4e** the most effective plasticizer.

The relationship between the structural features of the additives and their plasticizing effects can be only partially explained by the plasticization mechanism reported by Mauritz *et al*.[23] Specifically, they showed that regardless the side chain structure, the plasticizing efficiency decreases with increasing molecular weight.

In order to better rationalize our findings, such idea has to be further expanded considering the lubricity theory,[24,30] which is based on the assumption that the stiffness of a polymer arises from intermolecular frictions that bind together the polymeric chains. Therefore, the plasticization effectiveness is strongly related to the ability of the additive to intercalate and split the polymer chains, thus weakening the frictional forces. Taking into account that the ketal-diester portion is equal for all the proposed molecules, the observed different plasticizing effect has to be associate to the structure of the side-chains. In accordance with the DSC curves (Figure 13), the aromatic ring of **4d** and **4e** prevent PVC chains interaction, thereby resulting in a sharp glass transition. In fact, as proposed by the free volume theory,[20,25,30] a plasticizer has to increase the free volume between the polymeric chains in order to reduce their dipolar interactions and lead to a reduction of $T_g$. This effect is particularly evident moving from derivatives **4a-c** to **4d-e**, when the aliphatic side chains are replaced with aromatic rings that are able to better separate the macromolecular chains thanks to their higher hindrance.

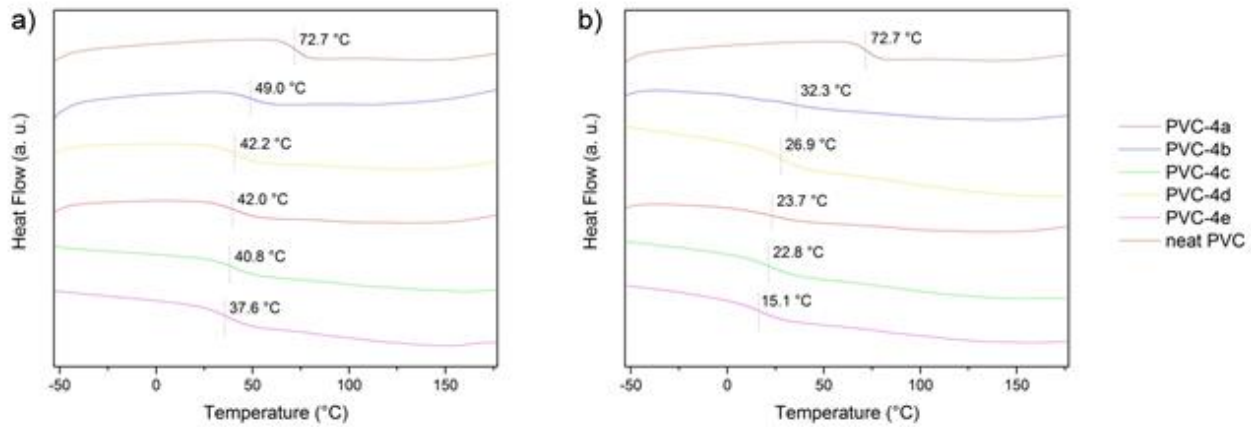


**Figure 13.** DSC second heating scans of neat and plasticized PVC films at (a) 10 phr and (b) 20 phr of additive content. The dashed lines represent the transition point, where $T_g$ was extrapolated.

For all these reasons, the detected trend is a direct consequence of the correlation between the structural features of ketal-ester additives and the observed final properties.[27]

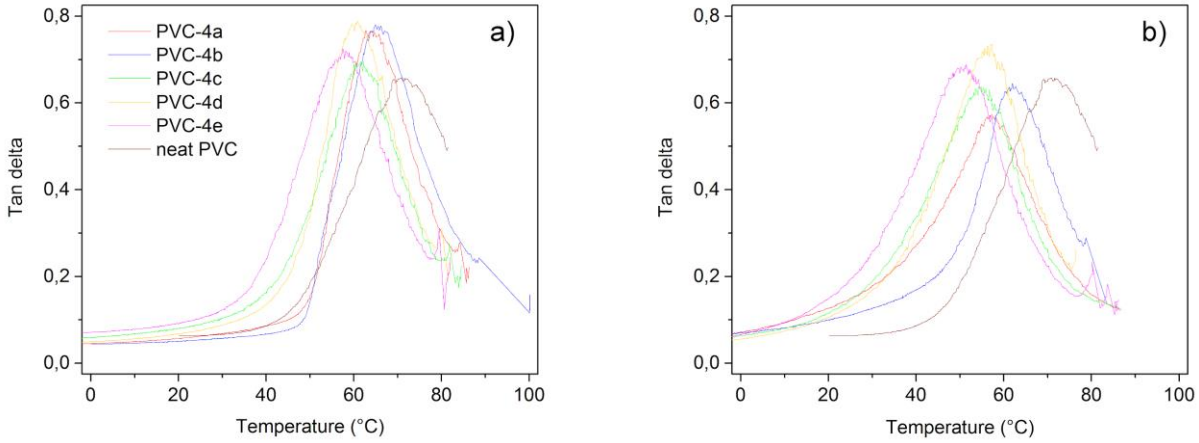


**Figure 14.** *Tanδ* curves of neat and plasticized PVC with (a) 10 phr and (b) 20 phr of additives as a function of the temperature.

The same trend was also observed when $T_g$ of neat and plasticized PVC samples was evaluated by DMTA measurements from tanδ curves, which are reported in Figure 14. As plotted in Figure 15 and summarized in Table 6, the $T_g$ of the material progressively decreased by increasing the content for all additives. Also in this case the derivative **4e** led to the best performance, shifting the $T_g$ of neat PVC from 68°C to 57°C and to 52°C for a plasticizer content of 10 phr and 20 phr, respectively. On the other hand, additive **4b** causes the slightest reduction of $T_g$ to 65°C for 10 phr and to 62°C for 20 phr. The plasticizers **4a**, **4c** and **4d** produced an intermediate effect on the $T_g$ (Figure 15) in good agreement with DSC results, thus further

confirming the previously observed correlation between additives chemical structure and final thermal properties of the material. It is noteworthy that the herein presented ketal-diesters have performances in terms of $T_g$ reduction comparable or even better of the commercial DEHP. In fact, a very recent study[41] has shown that 30 phr of DEHP reduce the $T_g$ of PVC up to 58.7°C (evaluated by DMTA performed in comparable conditions), while our additives display similar plasticizing effect already at 20 phr, except for the additive **4e** that is shown to be even more efficient at a concentration of 10 phr.

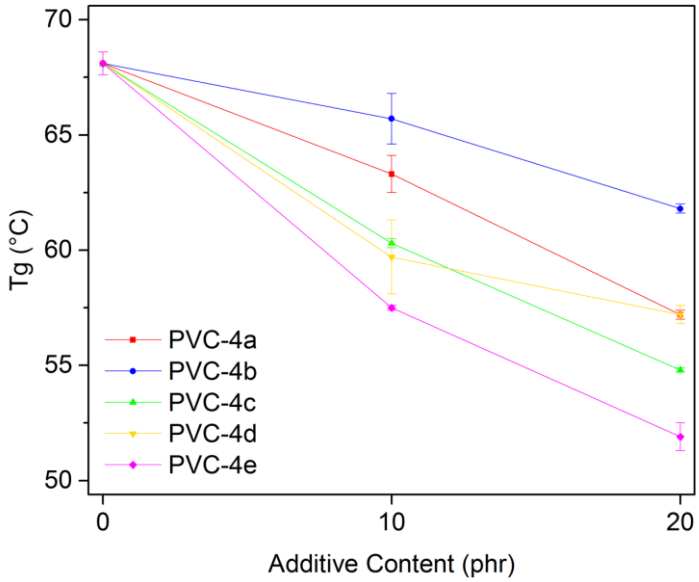


**Figure 15.** Average $T_{g,DMTA}$ of neat and plasticized PVC films as a function of the additive content.

**Table 6.** Average $T_g$ values of plasticized PVC films determined by DMTA and corresponding standard deviations. *neat PVC average $T_g$ value: 68.1 ± 0.5°C

| | $T_{g,DMTA}$ (°C)* | |
|---|---|---|
| **PVC-Additive code** | **10 phr of additive** | **20 phr of additive** |
| PVC-**4a** | 63.3 ± 0.8 | 57.2 ± 0.2 |
| PVC-**4b** | 65.7 ± 1.1 | 61.8 ± 0.2 |
| PVC-**4c** | 60.3 ± 0.2 | 54.8 ± 0.1 |
| PVC-**4d** | 59.7 ± 1.6 | 57.2 ± 0.4 |
| PVC-**4e** | 57.5 ± 0.1 | 51.9 ± 0.6 |

Moreover, tanδ curves can also provide an indication of the homogeneity of the investigated system. In particular, well-defined tanδ curves with no shoulder, as in this case (Figure 16a and 16b), suggest homogeneous additive dispersion and no phase separation, which are also in good agreement with the aforementioned SEM investigations (Figure 11).

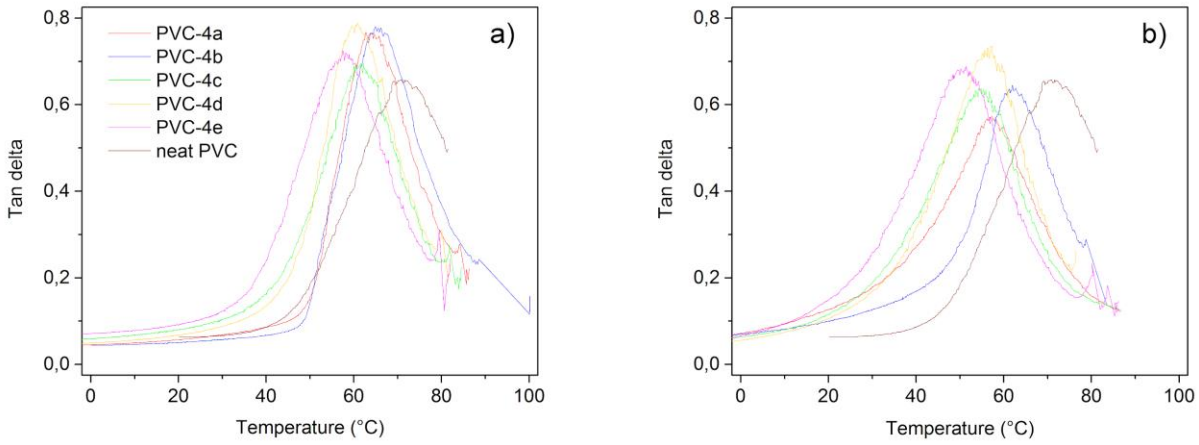


**Figure 16.** *Tanδ* curves of neat and plasticized PVC with (a) 10 phr and (b) 20 phr of additives as a function of the temperature.

DMTA was also performed to evaluate the possible variation of viscoelastic mechanical properties of studied materials. Specifically, storage modulus values *(E')* at room temperature (25°C) were extrapolated and reported in Table 7. Generally, as

shown in Figure 17, when the additive content is increased *E'* decreases, thus confirming the effectiveness of our molecules. Specifically, long side chain additives **4a** and **4b** (20 phr) cause the largest decrease of *E'* from 2900 MPa for the neat polymer to 1440 and 1570 MPa, respectively. In order to explain this behavior, DSC curves of the compounded PVC with 20 phr of **4a** and **4b** should be considered. In their thermograms (Figure 13) the transition from the glassy to the rubbery state is not very sharp, but it takes place over a broad temperature range. This makes quite tricky to identify a discreet $T_g$, being the midpoint of the jump not particularly evident as in the case of neat PVC, PVC-**4c**, PVC-**4d** and PVC-**4e**. Since $T_g$ can be defined as the temperature range over which segmental motion of atoms in the polymer backbone begins,[106] a wide transition temperature range means that the segmental PVC chains start moving at a temperature range close to room temperature. Consequently, material starts becoming more and more flexible with a viscosity decrease, which describes the lower values of *E'* observed at 25°C for PVC-**4a** and PVC-**4b**. Probably, at room temperature, the long aliphatic moieties of **4a** and **4b** are capable to break up the numerous chain-chain interactions, especially when the additive concentration is 20 phr, thus lowering the energy required for the transition and broadening the $T_g$ range.[107] On the other hand, the plasticizers **4d** and **4e** are characterized by a π-electrons system typical of aromatic rings. As reported from H. Akhina *et al.*,[108] such π-electrons lead to a stronger additive-polymer interaction and, consequently, to a restriction of PVC chains mobility. Macroscopically, in comparison with the effect of aliphatic chains of the molecules **4a**, **4b** and **4c**, it results in a stiffer mechanical behavior at room temperature.[109] For all the additives, no effect was detected in the rubbery state, where the modulus was found to be between 3 and 8 MPa for all the compositions (as shown in the storage modulus curves as a function of the temperature in Figure 18). This region above the $T_g$, also called rubbery plateau, is indeed mainly controlled by the molecular weight of the polymer, entanglements and/or physical and chemical crosslinks.[110]

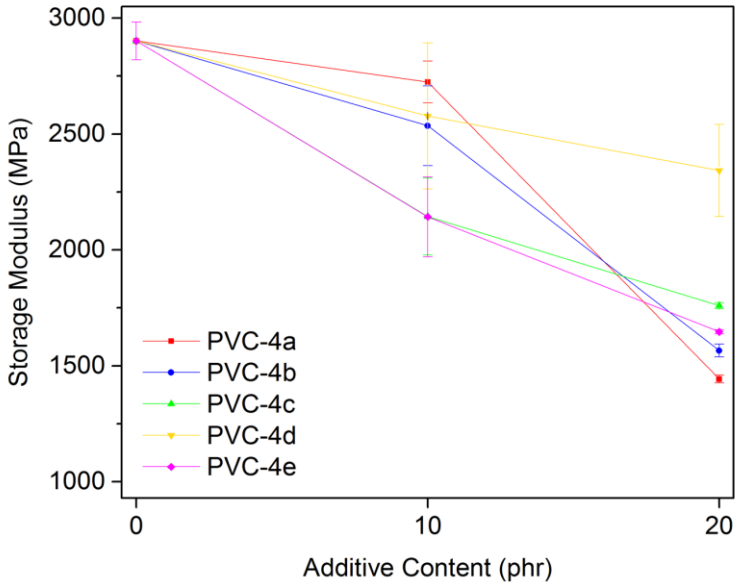


**Figure 17.** Average storage modulus values (at T= 25°C) of neat and plasticized PVC films as a function of the additive content.

**Table 7.** Average storage modulus (*E'*) of plasticized PVC films determined by DMA at 25°C and corresponding standard deviations. * neat PVC average *E'* value: 2902 ± 82 MPa

| | ***E'* (MPa)*** | |
|---|---|---|
| **PVC-Additive code** | **10 phr of additive** | **20 phr of additive** |
| PVC-**4a** | 2725 ± 90 | 1443 ± 17 |
| PVC-**4b** | 2536 ± 172 | 1566 ± 28 |
| PVC-**4c** | 2144 ± 166 | 1760 ± 13 |
| PVC-**4d** | 2578 ± 315 | 2343 ± 199 |
| PVC-**4e** | 2143 ± 172 | 1647 ± 9 |

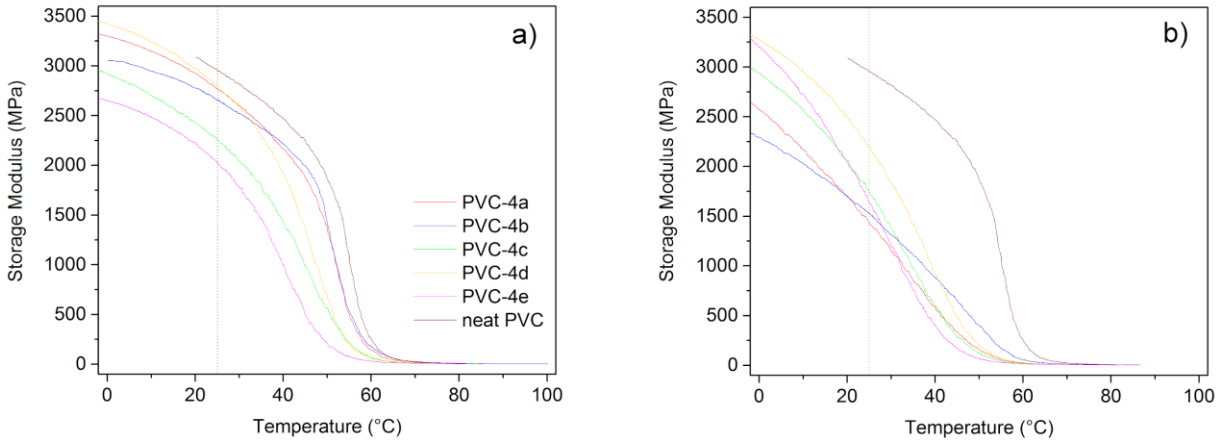


**Figure 18.** Storage modulus curves of neat and plasticized PVC with (a) 10 phr and (b) 20 phr of additives as a function of the temperature. The dashed line indicates room temperature (25°C), which is the temperature at which E' values were extrapolated.

The possibility to increase the temperature range at which thermal degradation takes place is an important aspect, which extends the processability window of the material. Typically, PVC thermal degradation consists of two stages: dehydrochlorination ($T_{p1}$) and cracking of the hydrocarbon chains ($T_{p2}$).[111] TGA measurements were performed to determine if the synthesized plasticizers have an effect on the thermal stability and weight-loss decomposition profile of PVC. Figure 19a and 19b display the DTG curves obtained from TGA measurements on 10 and 20 phr PVC formulations, respectively. As shown by Table 8, all additives can similarly shift both $T_{p1}$ and $T_{p2}$ toward higher temperatures with $T_{p1}$ that is increased up to 18°C and $T_{p2}$ up to 9°C. On the contrary, it was observed that the plasticizer content does not significantly affect the thermal stability of the polymer. These results clearly suggest the thermal stability of PVC is mainly affected by the moieties common to all the chemical structures of the additives (ketal and diester groups). Specifically, the most evident effect was observed on dehydrochlorination step, in which gaseous hydrochloric acid and small amounts of hydrocarbons are yielded.[112] The observed shift is due not only to the formation of hydrogen bonds between PVC and ester groups of derivatives, but also to the presence of the ketal ring. As reported elsewhere,[103,113,114] the presence of highly electronegative chlorine atoms allows the hydrogen on the same carbon atom to readily form a hydrogen bond with carbonylic oxygen of the plasticizer. These intermolecular forces enhance the additive-matrix compatibility, but also stabilize the C-Cl bond shifting dehydrochlorination degradation step toward higher temperatures. In addition, as similarly reported for oxirane rings,[42] the HCl released during the thermal

dehydrochlorination of PVC can be entrapped by the cyclic ketal of molecules **4a-e**, resulting in a deprotection of the carbonylic group and thus preventing that the yielded HCl further catalyzes the PVC degradation.[115]

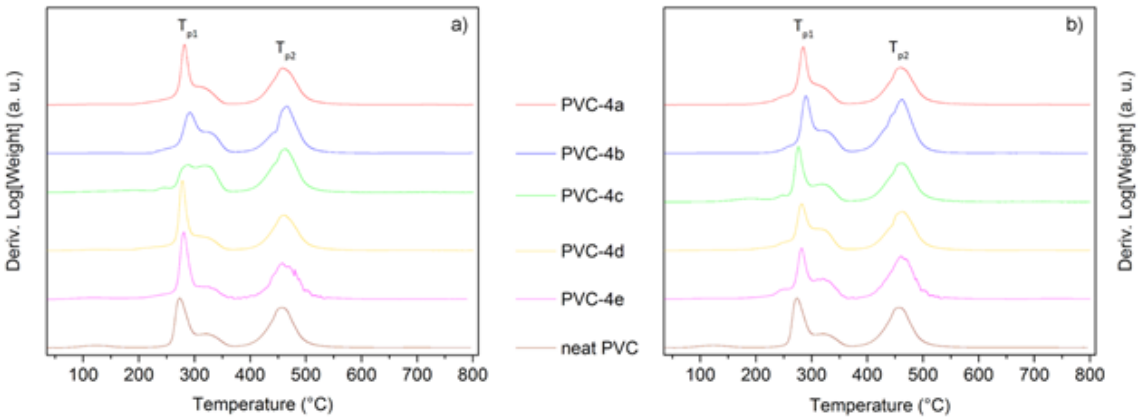


**Figure 19.** DTG curves of neat and plasticized PVC films with additive content of (a) 10 phr and (b) 20 phr.

**Table 8.** Peak degradation temperatures ($T_{p1}$ and $T_{p2}$) of plasticized PVC films extrapolated from the corresponding DTG curves (in Figure 19). *$T_{p1}$ and $T_{p2}$ values for neat PVC are 271°C and 449°C, respectively.

| | **$T_{p1}$ (°C)*** | | **$T_{p2}$ (°C)*** | |
|---|---|---|---|---|
| **Sample code** | **10 phr** | **20 phr** | **10 phr** | **20 phr** |
| PVC-**4a** | 281 | 283 | 454 | 453 |
| PVC-**4b** | 289 | 288 | 458 | 455 |
| PVC-**4c** | 285 | 275 | 456 | 454 |
| PVC-**4d** | 277 | 281 | 455 | 453 |
| PVC-**4e** | 280 | 281 | 453 | 456 |

The polymer additive requires a negligible leaching in order to ensure long-term and stable material properties. The efficiency with a given medium which can extract the plasticizer from the surface of a specimen represents a significant preliminary test.

Additionally, the ability of the medium to permeate into the polymer matrix can be an additional factor that influences the leaching rates of the plasticizer. Deionized water and *n*-hexane were selected as models for hydrophilic and hydrophobic simulated environments, respectively. As expected, due to the poor solubility of the plasticizers in water, all the additives showed very low leaching in this medium with values of approximately 0.1 %wt. of the initial plasticizer content in 24 h (Figure 20). On the other hand, when *n*-hexane was used as extracting solvent, the amounts of additives extracted from PVC were significantly higher (Figure 20), due to the good miscibility of the synthetized ketal-diesters in this solvent. In particular, neat PVC showed negligible leaching of approximately 0.5 %wt. that was associated with the release of very low $M_w$ PVC fractions. Taking into account weight loss of the neat PVC, the plasticized samples PVC-**4a** and PVC-**4b** showed values in the range of 1.5 and 2.5 %wt. The samples containing the other plasticizers (**4c**, **4d** and **4e**) showed even lower weight losses with values always below 1 %wt. PVC-DINCH film was then tested in the same conditions to compare the extraction resistance of our additives with a widely used commercial plasticizer. As expected, the leaching of DINCH in water was lower than in hexane due to the low solubility of the additive in aqueous environment (Figure 20). However, DINCH extraction values, in both solvents, are significantly higher than the ones observed by the synthesized ketal-esters. In particular, a quite high leaching value of approximately 3 %wt. was observed in water, while a loss of about 4% wt. was measured in hexane (Figure 20). Therefore, despite the very aggressive extraction conditions in order to force the migration of the additives, the preliminary indications are remarkable. It is noteworthy that the very low migration rate observed for the proposed additives is perfectly comparable with the one recently reported by Yuan *et al.*, specifically obtained for a non-migrating additive tested in similar conditions.[36]

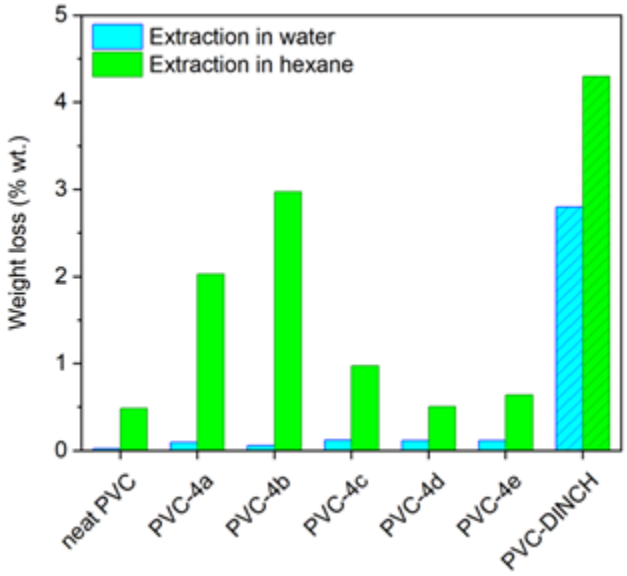


**Figure 20.** Weight loss percentages of neat and plasticized PVC films obtained by 24 h extraction in water (light blue) and n-hexane (green). PVC-DINCH leaching values are also reported for comparison reasons.

When an alternative plasticizer is proposed, at least comparable plasticizing properties with the conventional ones are required. The comparative study was based on the reduction of the $T_g$ evaluated by DSC as meaningful indicator of the plasticizing efficiency. Five well-known, widely used and commercially available plasticizers were selected to be compared with the derivatives **4c** and **4e,** the most effective molecules herein proposed. In particular, plasticizers such as didecyl phthalate (DDP), aliphatic Hexamoll® DINCH, and biobased acetyl tributyl citrate (ATBC) and diethylhexyl adipate (DEHA) and the very efficient fossil-based DEHP were taken as comparison. As clearly shown in Figure 21, the additives **4c** and **4e** in a concentration of 20 phr decreased the $T_g$ of the neat PVC from 73°C to 23°C and 15°C, respectively. Commercial ATBC, DDP and DEHP are less effective, showing higher $T_g$ values of 38°C[116] and 30°C,[15] respectively. Interestingly, also Hexamoll® DINCH in a concentration of 20 phr can lower the $T_g$ to about 25°C, thus less efficiently than our additives. Only DEHA performed slightly better than our molecules **4e**, with a $T_g$ of 13°C[15] (Figure 21). It is worth highlighting that the plasticizing effect of our additives is still comparable with the commercial ones even at a lower concentration. In fact, 10 phr of **4c** and **4e** were enough to decrease the $T_g$ of the neat PVC to 41°C and 38°C, similarly to the effect of ATBC used in double concentration (Figure 21). The reported comparison clearly shows that the proposed additives are valuable alternatives to the nowadays use products. Moreover, a very

remarkable effect on the $T_g$ can be also achieved by significantly reducing the content of additive, and therefore decreasing considerably the polymer production costs.

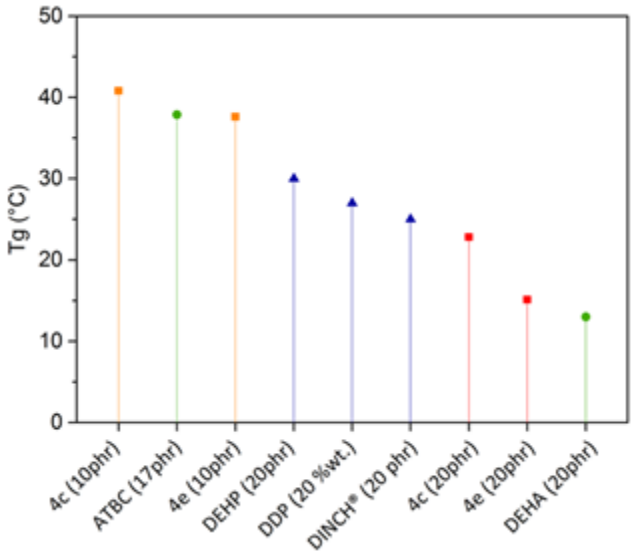


**Figure 21.** Comparison between the $T_{g,DSC}$ values of PVC films plasticized with ketal-ester additives **4c** and **4e** (10 phr in yellow and 20 phr in red) and the $T_{g,DSC}$ values of PVC films plasticized with commercial plasticizers at a content of approximately 20 phr.

The proposed ketal-diester derivatives of levulinic acid **4a-e** showed therefore to be very effective in a model polymer such as PVC. Indeed, they were able to lower both the $T_g$ and the storage modulus *E'* of the material as well as improve its thermal stability. Additionally, no significant leaching was found, neither in aqueous nor organic environments. Importantly, their performance was comparable (and, in some cases, even better) to the one of well-known commercially available plasticizers, also at lower concentrations.

Considering the results which have been obtained, some possible applications of PVC plasticized with the developed biobased additives **4a-e** can be suggested. In particular, taking into account that PVC possesses the largest share of the medical market and also the strong need to replace phthalates due to severe health risks,[73] the herein studied plasticized PVC systems might be used to make alternative medical devices. Depending on the amount of plasticizer added to the polymer, different flexible grades of PVC can be obtained, such as rigid, semirigid and flexible. For instance, rigid PVC, with a plasticizer content <10 %wt, may be used in

containers, connectors and syringes. On the other hand, semirigid PVC (10-30 %wt of plasticizer, as in the proposed study) may be used to make trays, blister packaging and hospital flooring. Finally, flexible PVC (up to 50 %wt of plasticizer) may find use as material for intravenous bags and blood bags.

The designed and synthesized asymmetric ketal-diester derivatives of levulinic acid **4a-e** proved therefore to be very effective as PVC plasticizer, successfully passing the test with this model polymer. In order to extend the range of polymers for which these plasticizers can be used, they were then added to PHB (representative polymer film in Figure 22) and their effect was investigated. As already mentioned in the introduction, PHB is a very challenging substrate completely different from PVC. Indeed, they differ in terms of starting source, chemical composition and structure, leading to specific properties. PVC is a fossil-based, synthetic and totally amorphous material while PHB is a semi-crystalline polyester naturally produced by bacteria. Consequently, their need for plasticization arises from different reasons as well. For instance, while PVC rigidity is mainly due to the C-Cl attractive dipole-dipole interactions between the chains, PHB pronounced brittleness is due to the high amount of crystalline phase and spherulite morphology. Therefore, notwithstanding PHB availability, natural origin, biodegradability and biocompatibility, its stiffness and low thermal stability have been seriously limiting its widespread use. In order to make PHB no more only a potential but also a real eco-friendly alternative to traditional fossil-based plastics, these drawbacks should be overcome or at least reduced by means of plasticization.

## 4.4. Characterization of plasticized PHB thin films

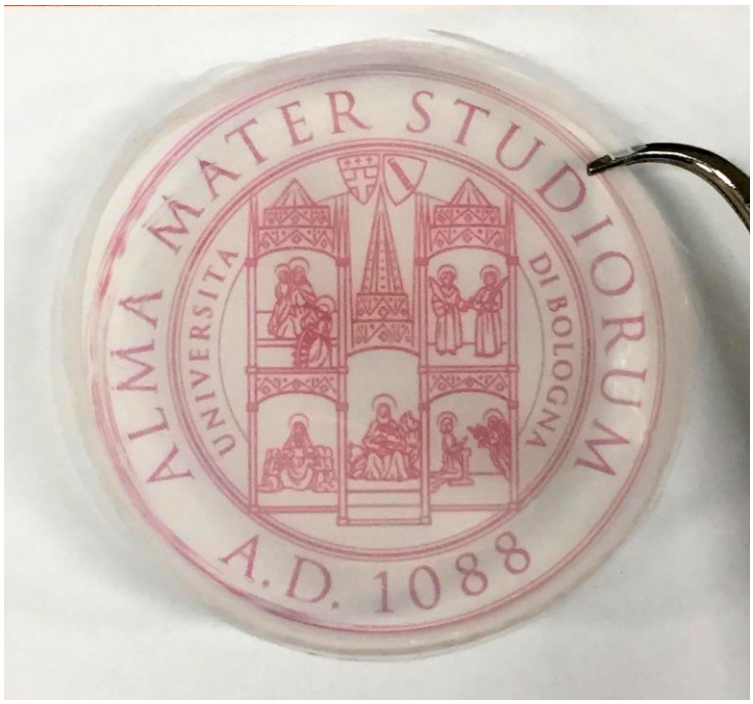


**Figure 22.** Representative photograph of the prepared PHB films.

In order to have an effective plasticization, the plasticizer must be highly miscible with the polymer matrix.[21] This aspect has been evaluated throughout FESEM morphological studies for ensuring the complete miscibility of the two components, which results in a homogeneous phase.[22] Therefore, at first, the cross sections of neat and plasticized PHB films with 20 phr of additive were investigated by FESEM. As clearly visible in the micrographs in Figure 23, no phase separation was observed, thus proving the mutual miscibility of the components. Generally, compatibility arises from the presence of intermolecular attractive forces between the additive and the polymer. This is the reason why, when designing a new plasticizer, polar moieties in its chemical structure are necessary.[20,27] Indeed, they allow the additive to interact with the matrix, enhancing compatibility. On the other hand, without such polar portions, a plasticizer would be too non-polar to be miscible with any polymer.[27] In the herein proposed work, good compatibility between PHB and our ketal-diesters is probably due to carbonyl-carbonyl (C═O···C═O) n→π* intermolecular noncovalent interactions, where one of the lone pairs (n) on the oxygen atom of a carbonyl group is delocalized over the antibonding π* orbital of a nearby carbonyl C═O bond.[117,118] Thanks to these interactions both polymer and plasticizer C═O bonds will be polarized, thus creating a sequential chain of O···C contacts which improve mutual attraction and miscibility. These kind of sequential n→π* interactions have already been reported to play a crucial role in other semicrystalline polyesters such as poly(lactic acid).[119]

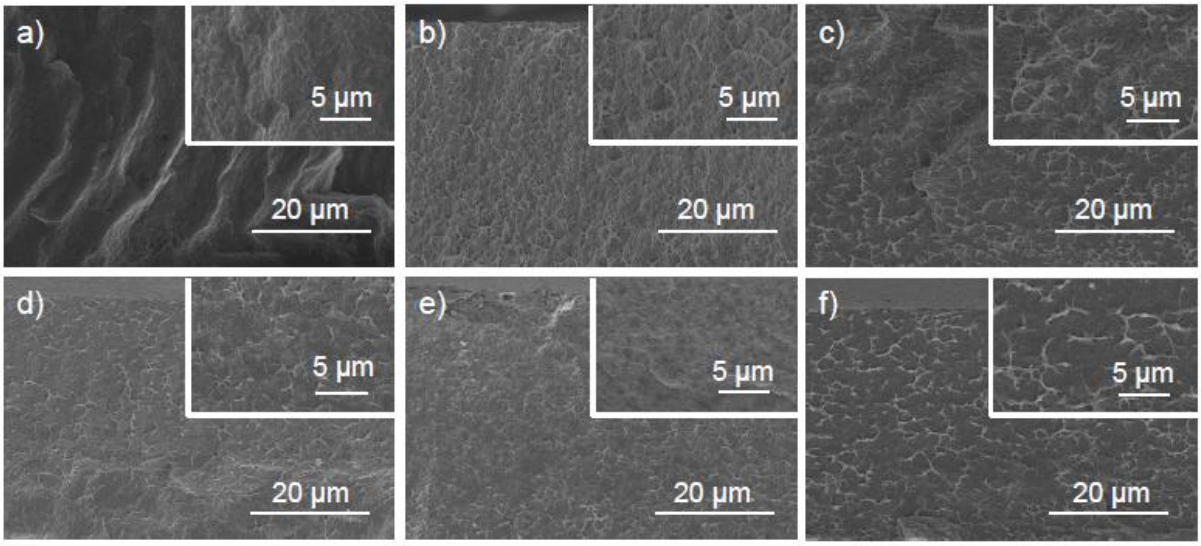


**Figure 23.** Cross-sections FESEM micrographs of (a) neat PHB, (b) 20 phr PHB-**4a**, (c) 20 phr PHB-**4b**, (d) 20 phr PHB-**4c**, (e) 20 phr PHB-**4d** and (f) 20 phr PHB-**4e**. Higher magnification images are reported in the insets.

Basically, the role of a plasticizer is to separate neighboring polymer chains by breaking up some of the attractive interactions between them. As a result, molecular mobility increases, since chains are no more bonded so closely and less constrained by cohesion points.[20,27,29] The main indication of this phenomenon is the decrease of the polymer $T_g$. Indeed, since $T_g$ is the temperature range over which the cooperative segmental motion of tens to a few hundreds of repeat units in the polymer backbone begins, the less the interchain forces, the less is the energy (and so, the lower the $T_g$) required to overcome them.[106,120] Therefore, DSC analysis was carried out to evaluate the plasticizing effectiveness of the proposed molecules in terms of $T_g$ reduction. The determined $T_g$ values of neat and plasticized PHB films are shown in Figure 24 as a function of the additive content and reported in Table 9. All plasticizers in both concentrations led to a significant decrease in $T_g$. In particular, additives **4b** and **4c** showed comparable $T_g$ decreasing effect from 0°C to -4°C and -5°C (at 10 phr) and to -6°C and -9°C (at 20 phr), respectively. Additives **4a**, **4d**, and **4e** led to a significant $T_g$ reduction of approximately 10°C and 17°C by increasing the additive content from 10 to 20 phr, respectively (Figure 24). According to the free volume theory, plasticizers penetrate and diffuse into the polymer, increasing the internal space between the macromolecules. This results in a higher molecular mobility which, in turn, lower both the $T_g$ and the elastic modulus of the material, making the polymer system more flexible.[29] The proposed ketal-diesters can be divided according to their chemical structure, with **4a-c** that bear an aliphatic chain as side group, while **4d-e** an aromatic ring. In particular, among the aliphatic-side group additives, **4a** and **4b** own long linear chains of 14 and 18 carbon atoms respectively, while **4c** bears a branched isopentyl group. The experimentally observed larger decrease in the $T_g$ induced by **4a** compared to **4b** may be ascribed to the smaller molecular weight of the former, resulting in a better diffusion through the matrix and, consequently, in a greater overall increment of the free volume. On the other hand, although a branched plasticizer is usually more efficient than the corresponding linear one,[20] additive **4c** showed slightly worse plasticizing effect than **4a**. However, in this case, the performance of **4c** could not be directly compared to the other aliphatic compounds because their molecular weights are significantly different. Moving to aromatic-side chain additives **4d** and **4e**, they largely affected the $T_g$ of PHB (Figure 24). These results may be explained considering the greater bulkiness of substituents such as aromatic rings, which, increasing the molecular

hindrance of the plasticizer, introduce more free volume among polymeric chains. Importantly, the plasticizing performance of our ketal-diesters is comparable to the one of different citrate esters, which represent a valuable and effective commercially available “green” alternative to phthalates for many biopolymers.[18,121] For instance, Ana Chaos and coworkers studied the plasticizing effect of tributyl citrate on PHB, observing a $T_g$ reduction to approximately -17°C with additive concentration of 20 %wt.[122] This value is basically the same obtained in this work for plasticizers **4a**, **4d**, and **4e** loaded at 20 phr (Figure 24), therefore confirming that this class of additives can actually compete with the commercially available products.

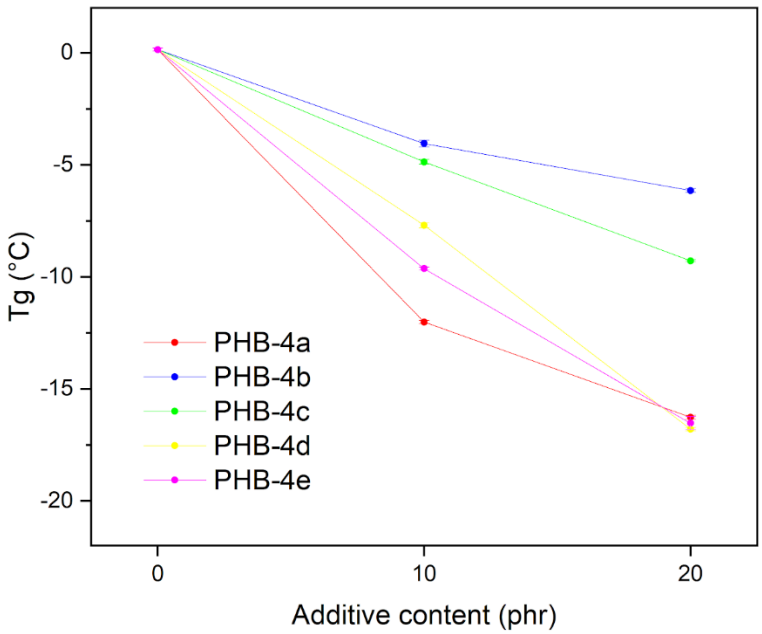


**Figure 24.** Average $T_g$ values of neat and plasticized PHB films as a function of the additive content.

**Table 9.** Average $T_g$ values of plasticized PVC films determined by DSC and corresponding standard deviations. * neat PHB Tg value: 0.14 ± 0.07°C.

| | **$T_g$ (°C)*** | |
|---|---|---|
| **PHB-Additive code** | **10 phr of additive** | **20 phr of additive** |
| PHB-**4a** | -12.02 ± 0.08 | -16.27 ± 0.09 |
| PHB-**4b** | -4.05 ± 0.15 | -6.15 ± 0.09 |
| PHB-**4c** | -4.87 ± 0.11 | -9.29 ± 0.05 |
| PHB-**4d** | -7.70 ± 0.12 | -16.80 ± 0.08 |
| PHB-**4e** | -9.63 ± 0.06 | -16.53 ± 0.29 |

It is worth considering that the $T_g$ trend (Figure 24) is not the same as the one detected in the previous work about plasticized PVC (Figure 12). In order to try to explain that, it would be better to take into consideration some aspects. For instance, the two matrices are completely different one another, starting from their origins: PVC is a synthetic polymer while PHB is produced by microorganisms. Importantly, PVC is totally amorphous while PHB is semicrystalline with a high content of crystalline phase. Therefore, plasticization mechanisms, which mainly rely on the amorphous portion,[20] may change dramatically between these two polymers. For instance, due to PHB typically high amount of crystal phase, its $T_g$ endothermic step is usually hardly detectable. This happens because the glass-transition, which is the gradual and reversible transition from a hard and relatively brittle state into a rubbery one as the temperature is increased, only concerns amorphous materials (or, as in this case, the amorphous regions within semicrystalline materials). For this reason, in this work $T_g$ values were extrapolated after a very fast cooling scan (quenching) from 195°C to -60°C, intentionally carried out in order to prevent PHB crystallization. In this way, the amount of amorphous phase is enhanced and, in the consecutive heating scan, the $T_g$ step is therefore more easily detectable (curves reported in Figure 25). In these heating scans it is also possible to see exothermic peaks due to PHB cold crystallization (Figure 25). This phenomenon occurs because, during

heating, the amorphous (but crystallizable) structure obtained from fast cooling becomes sufficiently mobile above the glass transition for reorganization and crystallization to occur.[123]

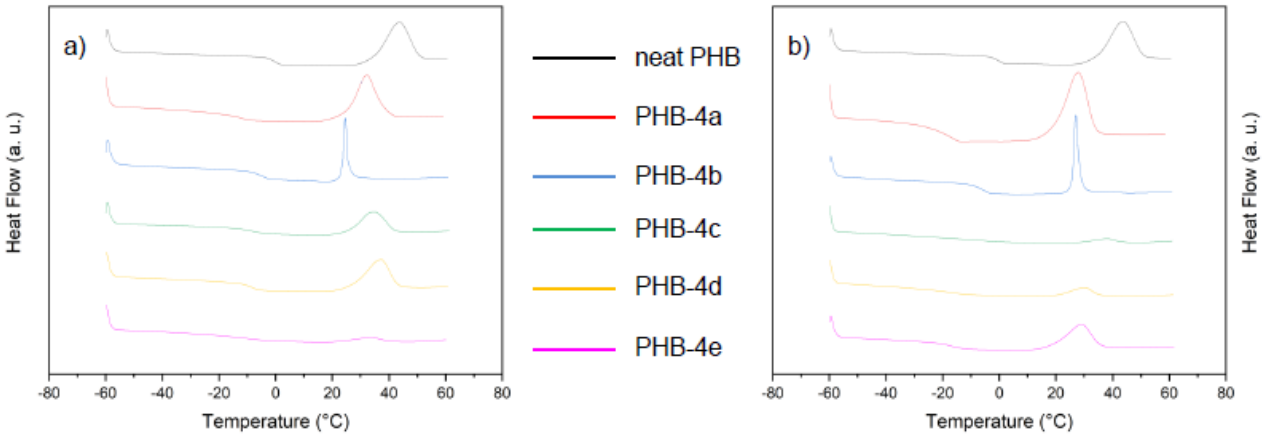


**Figure 25.** DSC third heating scans of neat and plasticized PHB films at (a) 10 phr and (b) 20 phr of additive content.

Therefore, the plasticizing effect takes primarily place in the amorphous region of the polymer. In particular, as described by A. Marcilla and M. Beltran,[20] when a plasticizer is added, the amorphous portion of the polymer swells, involving the addition of more free volume. Consequently, the mobility of the chains is considerably enhanced as well as the overall flexibility of the material. Storage modulus (*E'*) values at 25°C (listed in Table 10) were therefore extrapolated from DMTA curves (Figure 26) in order to evaluate the effect of the proposed plasticizers on the viscoelastic properties of PHB. As shown in Figure 27, the synthesized plasticizers led to an overall decrease of *E'* for both contents, confirming their plasticizing effectiveness on PHB.

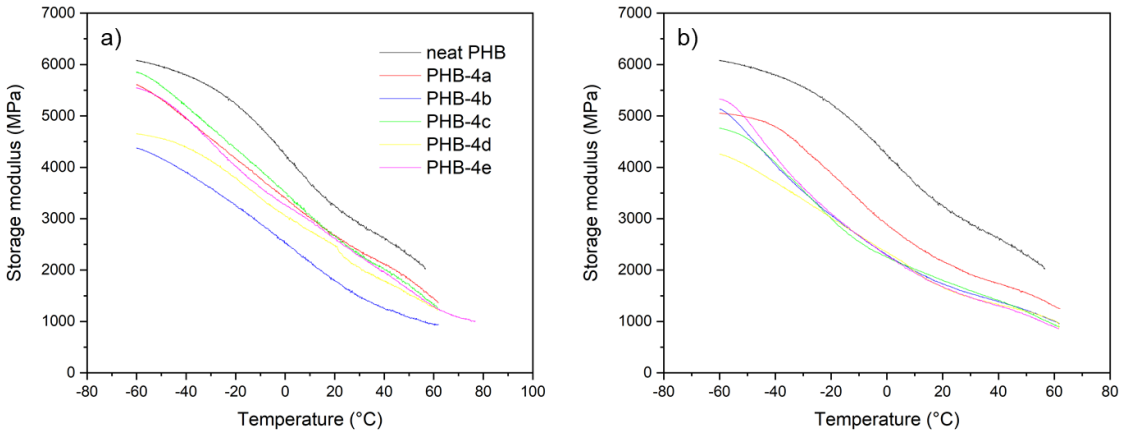


**Figure 26.** Storage modulus curves of neat and plasticized PHB with (a) 10 phr and (b) 20 phr of additives as a function of the temperature.

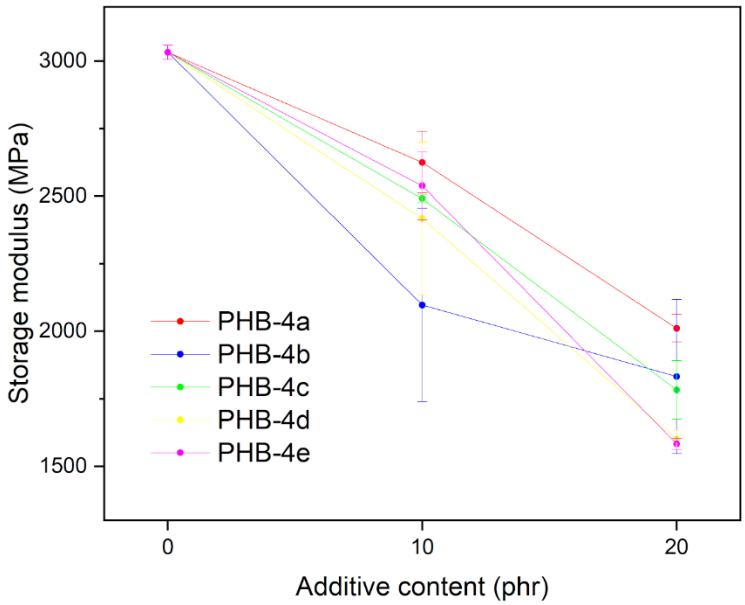


**Figure 27.** Average storage modulus (E') values at 25°C of neat and plasticized PHB films as a function of the additive content.

**Table 10.** Average storage modulus (E′) of plasticized PHB films determined by DMA at 25°C and corresponding standard deviations. * neat PHB average E′ value: 3032 ± 26 MPa

| | ***E′* (MPa)*** | |
|---|---|---|
| **PHB-Additive code** | **10 phr of additive** | **20 phr of additive** |
| PHB-**4a** | 2625 ± 114 | 2011 ± 51 |
| PHB-**4b** | 2097 ± 358 | 1832 ± 285 |
| PHB-**4c** | 2491 ± 15 | 1783 ± 108 |
| PHB-**4d** | 2417 ± 282 | 1600 ± 32 |
| PHB-**4e** | 2538 ± 126 | 1583 ± 21 |

Interestingly, among the plasticized samples, a correlation between *E′* and crystallinity can be noticed. Enthalpy of fusion ($\Delta H_m$) values obtained from DSC curves as area of the endothermic melting peak were used to calculate the degree of crystallinity of the samples as shown in Table 11. In particular, with an additive concentration of 10 phr, additives **4a** and **4e**, which induce the highest degrees of crystallinity (68% and 66%, respectively), also show the highest moduli compared to the other additives (2625 and 2538 MPa, respectively). On the other hand, **4b**, which at 10 phr is the only additive able to decrease PHB crystallinity degree, also results in the lowest value of *E′* (2097 MPa). Interestingly, **4d** and **4e** show different performances depending on their content. In fact, at 10 phr, they increase the crystallinity degree of PHB to 63% and 66%, while at 20 phr they decrease it to 60% and 58%, respectively. As a result, at 20 phr, they lead to the lowest observed *E′* values (1600 and 1583 MPa, respectively). Conversely, **4a** induces the highest degree of crystallinity, showing therefore the highest observed value of *E′* at 20 phr (2011 MPa).

**Table 11.** Enthalpies of fusion from the second heating scans ($\Delta H_m$) and corresponding crystallinity degree of plasticized PHB films. * $\Delta H_m$ and crystallinity degree values for neat PHB are 89.81 ± 0.33 and 61.51 ± 0.22, respectively.

| | **$\Delta H_m$ (J/g)*** | | **Crystallinity degree (%)*** | |
|---|---|---|---|---|
| **Sample code** | **10 phr** | **20 phr** | **10 phr** | **20 phr** |
| PHB-**4a** | 90.50 ± 0.53 | 87.05 ± 1.25 | 68.18 ± 0.40 | 71.55 ± 1.02 |
| PHB-**4b** | 78.25 ± 0.04 | 72.67 ± 0.69 | 58.95 ± 0.03 | 59.73 ± 0.57 |
| PHB-**4c** | 81.09 ± 0.44 | 78.57 ± 0.37 | 61.10 ± 0.33 | 64.58 ± 0.30 |
| PHB-**4d** | 83.86 ± 0.53 | 73.55 ± 0.48 | 63.18 ± 0.40 | 60.45 ± 0.40 |
| PHB-**4e** | 87.29 ± 0.60 | 70.84 ± 0.79 | 65.76 ± 0.45 | 58.23 ± 0.65 |

Generally, the increase in crystallinity is consistent with plasticization. In fact, the free volume added by a plasticizer increases molecular mobility, thus allowing the macromolecules to rearrange in new configurations resulting in a further nucleation.[20,124] However, the decrease in crystallinity caused by additives **4d** and **4e** at a higher concentration may be rationalized considering their chemical structure. Both additives are indeed characterized by polarizable aromatic rings, which form many points of mutual attraction along the polymer chains. However, this situation may prevent to some extent the chains from lining up together and compactly packing into crystals. On the other hand, additives **4a**, **4b**, and **4c** all bear aliphatic non-polar end groups which do not introduce additional cohesive links along the chains, allowing them to move and rearrange into ordered structures. This behavior may be explained taking into account the so called rigid amorphous fraction (RAF), which is a metastable nanophase structure at the interface between the crystallites and the surrounding phase typical of semicrystalline polymers.[125] This fraction is referred to as rigid because it is made up of amorphous chain portions whose mobility is hindered by the crystalline phase they are coupled with.[77] As reported by Di Lorenzo and co-workers,[125] full mobilization of the RAF of PHB takes place at

temperatures around 70°C. Therefore, at 25°C (temperature at which *E'* has been extrapolated), RAF is still vitrified, acting as a further tensed and rigid domain within the polymer.[126] Consequently, the higher values of *E'* found for the samples with higher degree of crystallinity may be due to the bigger amount of RAF related to the crystalline phase.

DSC measurements were also performed in order to investigate the effect of the synthesized ketal-diesters on the crystal phase of PHB. In particular, the melting temperatures ($T_m$) of neat and plasticized PHB were extrapolated from the second heating scans as peak temperature of the endothermic melting peak. As reported in Figure 28, all the additives lead to a decrease in the $T_m$ of PHB for both concentrations. In particular, it is possible to notice that, at 10 phr, additives **4a-b** are more effective than **4c-e**, lowering the $T_m$ from 171°C to approximately 168°C. Conversely, at higher contents, **4c-e** perform better than **4a-b**, resulting in further decreased $T_m$ values (164°C, 162°C, and 161°C, respectively). Interestingly, it is worth noting that plasticizers **4a-b** are very close in structure and size, both bearing long linear aliphatic end groups. This aspect may therefore be the reason why they perform so similarly, leading basically to the same $T_m$ value for each concentration.

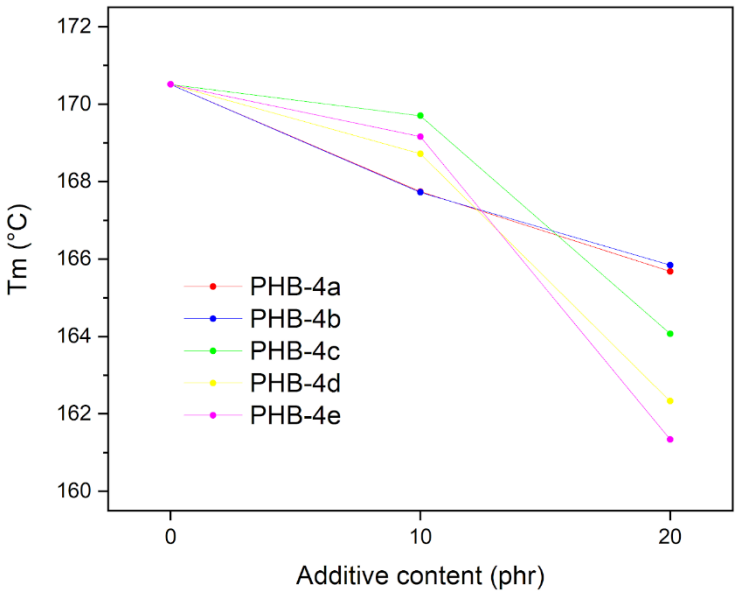


**Figure 28.** $T_m$ values of plasticized PHB films as a function of the additive content.

**Table 12.** $T_m$ values of plasticized PHB films determined by DSC. * neat PHB $T_m$ value: 170.51°C.

| | $T_m$ (°C)* | |
|---|---|---|
| **PHB-Additive code** | **10 phr of additive** | **20 phr of additive** |
| PHB-**4a** | 167.74 | 165.68 |
| PHB-**4b** | 167.72 | 165.84 |
| PHB-**4c** | 169.70 | 164.07 |
| PHB-**4d** | 168.72 | 162.33 |
| PHB-**4e** | 169.16 | 161.34 |

The melting of a polymer only concerns its crystalline phase, with the features of the crystallites (such as size, morphology and stability) mainly influencing the DSC endothermic peak shape as well as the $T_m$ value. For instance, neat PHB is characterized by a double melting peak, whose small shoulder has principally been attributed to lower molecular weight species, polymorphism, and different crystallites sizes.[127] Beyond crystallization conditions (as the cooling rate),[123,128] also plasticizers partially affect crystal nucleation and growth, typically leading to less perfect and stable crystallites and, therefore, to a lower $T_m$.[122,129,130] Considering the second heating scans of neat and plasticized samples reported in Figure 29, it is possible to see that all the plasticizers **4a-e** actually induce changes in the melting endotherm of PHB. In particular, it undergoes a widening effect toward lower temperatures for both additive contents (Figure 29). Therefore, the proposed plasticizers may produce a more convenient processing of the material by decreasing its melting temperature range.[131]

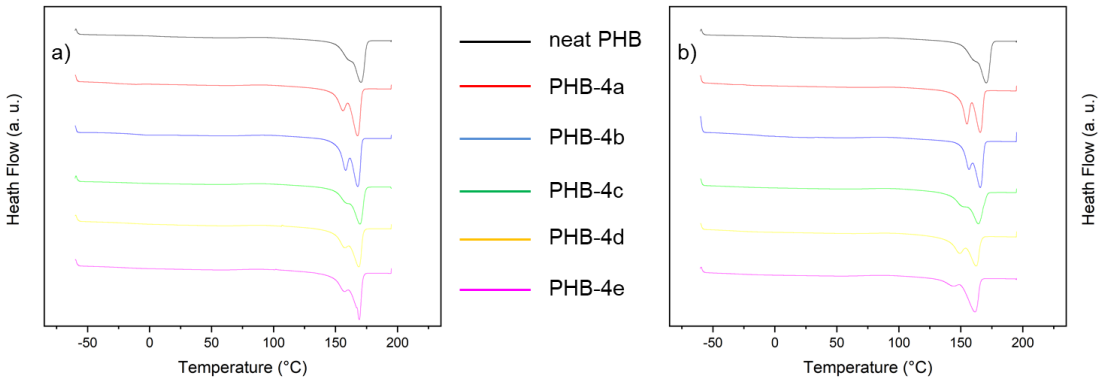


**Figure 29.** DSC second heating scans of neat and plasticized PHB films at (a) 10 phr and (b) 20 phr of additive content.

Even in this work with PHB, resistance to migration of our plasticizers **4a-e** was investigated by means of leaching tests. As mentioned in the introduction, issues concerning additive migration and leaching are one of the toughest challenges in current plasticizer research. Indeed, other than potential health and environmental risks, a plasticizer coming out of a polymer shortens the material usable lifetime, leaving it inappropriate for desired applications.[19] Once more, deionized water and *n*-hexane were selected as models for hydrophilic and hydrophobic environments, respectively (Figure 30). Neat PHB, tested as a reference, showed very low weight losses in both water and hexane (0.1 and 0.3% wt, respectively). This was probably due to low $M_w$ fractions as well as small residual impurities. As expected, weight losses in hexane were higher than water ones due to the good solubility of ketal-diesters **4a-e** in this organic solvent. In particular, additives **4a** and **4b** bearing long linear lipophilic carbon side-chains were preferentially extracted, with values (subtracting the loss of neat PHB) in the range 2.5 to 3.5% wt. The other samples (**4c**, **4d**, and **4e**) showed instead similar weight losses around 1.5% wt. On the other hand, water leaching was lower due to the hydrophobicity of both PHB and additives, with a maximum loss of 1.7% wt belonging to the PHB sample containing **4c**.

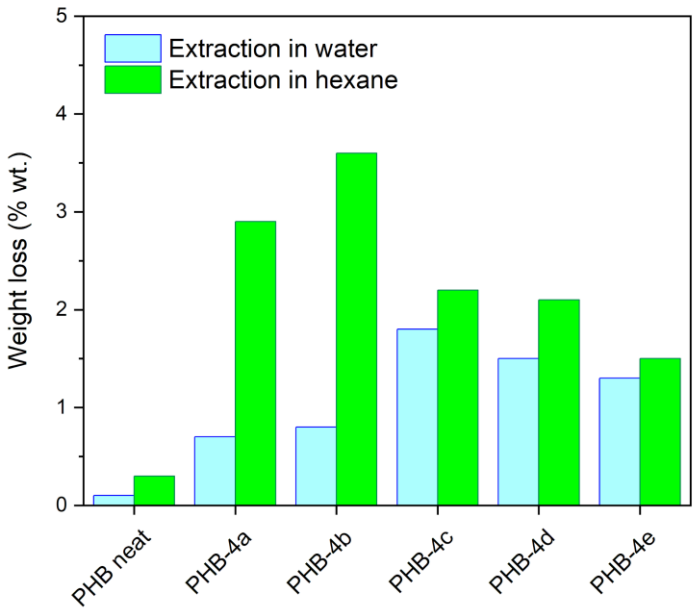


**Figure 30.** Weight loss percentages of neat and plasticized PVC films obtained by 24 h extraction in water (light blue) and n-hexane (green).

These preliminary indications by our ketal-esters are remarkable. Indeed, despite the aggressive treatment in hexane, leaching was very low.

### 4.4.1. Future works

As already mentioned in the introduction, PHAs have emerged as potential useful materials in the medical field for different applications owing to their unique properties.[132–134] In particular, the features that make them compatible to living systems are their biodegradability, non-toxicity of degradation products, ability to support cell adhesion and growth, and non-carcinogenicity.[135] Therefore, current research in plasticizers has also to take into serious consideration these precious inherent properties of biomaterials. Indeed, the new generation of additives must not badly affect the biocompatibility as well as the biodegradability of the biomaterial as such. For this purpose, cytocompatibility tests on plasticized PHB films with 20 phr of ketal-diester plasticizers are ongoing. In addition, biodegradability studies will be performed soon. Importantly, if the proposed plasticizers were found to be non-cytotoxic and biodegradable, fully biobased and biocompatible high value-added plasticized PHB formulations would be developed. In this case, scaffold for tissue engineering applications may be designed.[135] Furthermore, herein proposed plasticized PHB could find use as compostable packaging material as well as an

eco-friendly replacement for traditional disposable plastic items. Finally, plasticized PHB may also represent a sustainable alternative to semirigid PVC for medical applications.

## 4.5. Lignin-based additives for polymeric materials

As aforementioned in the introduction, lignin is an inherently highly heterogeneous polymer. Indeed, the relative content of the monolignols building up its structure as well as the many interunit linkages connecting them depend mostly on the plant species. In addition, this heterogeneity is even increased in Kraft pulping process, where strongly alkaline reagents and harsh reaction conditions allow cellulose to be extracted while lignin is first depolymerized and then isolated by means of LignoBoost technology. All of this to say that lignin, as a result, is a broad polydisperse mixture of different structures. This aspect badly affects its utilization in material applications where constant molecular size, functionality and reactivity are instead required. That is why techniques to decrease lignin heterogeneity and polydispersity are almost always applied before using it as either reagent or additive.

### 4.5.1. Lignin fractionation and characterization

Two methods were employed to obtain more homogeneous lignin fractions suitable for further applications: the one reported by A.-S. Jääskeläinen[136] and the one by A. Duval.[137] The first consists of dissolving lignin in aqueous solvent and then precipitating it due to addition of water, while the second is based on sequential solvent extractions to get soluble fractions. Importantly, both the methods utilize recommended green solvents and are easily controllable. All the lignins obtained were then characterized by means of GPC, DSC and NMR analyses in order to accurately define their structures.

#### 4.5.1.1. Aqueous solvent precipitation

The principle of aqueous solvent precipitation is to dissolve lignin in a solvent followed by addition of a nonsolvent to precipitate fractions with narrow molar mass distributions.[138] In particular, acetone and ethanol were selected as solvent while water as nonsolvent. This choice was made after previous investigations by the same authors, which screened different aqueous systems in order to find the most effective in dissolving and precipitating lignin.[136] Schematic descriptions of the employed aqueous solvent precipitation methods are shown in Scheme 7a and 7b. For ethanol-based route (Scheme 7b), fractionation was stopped when solvent

concentration of 50% $^{v}/_{v}$ was reached. Indeed, at this stage lignin concentration was so low that precipitation was not practical to continue further. Therefore, a new sequence was started by adding a new batch of lignin to freshly prepared aqueous ethanol (50% $^{v}/_{v}$).

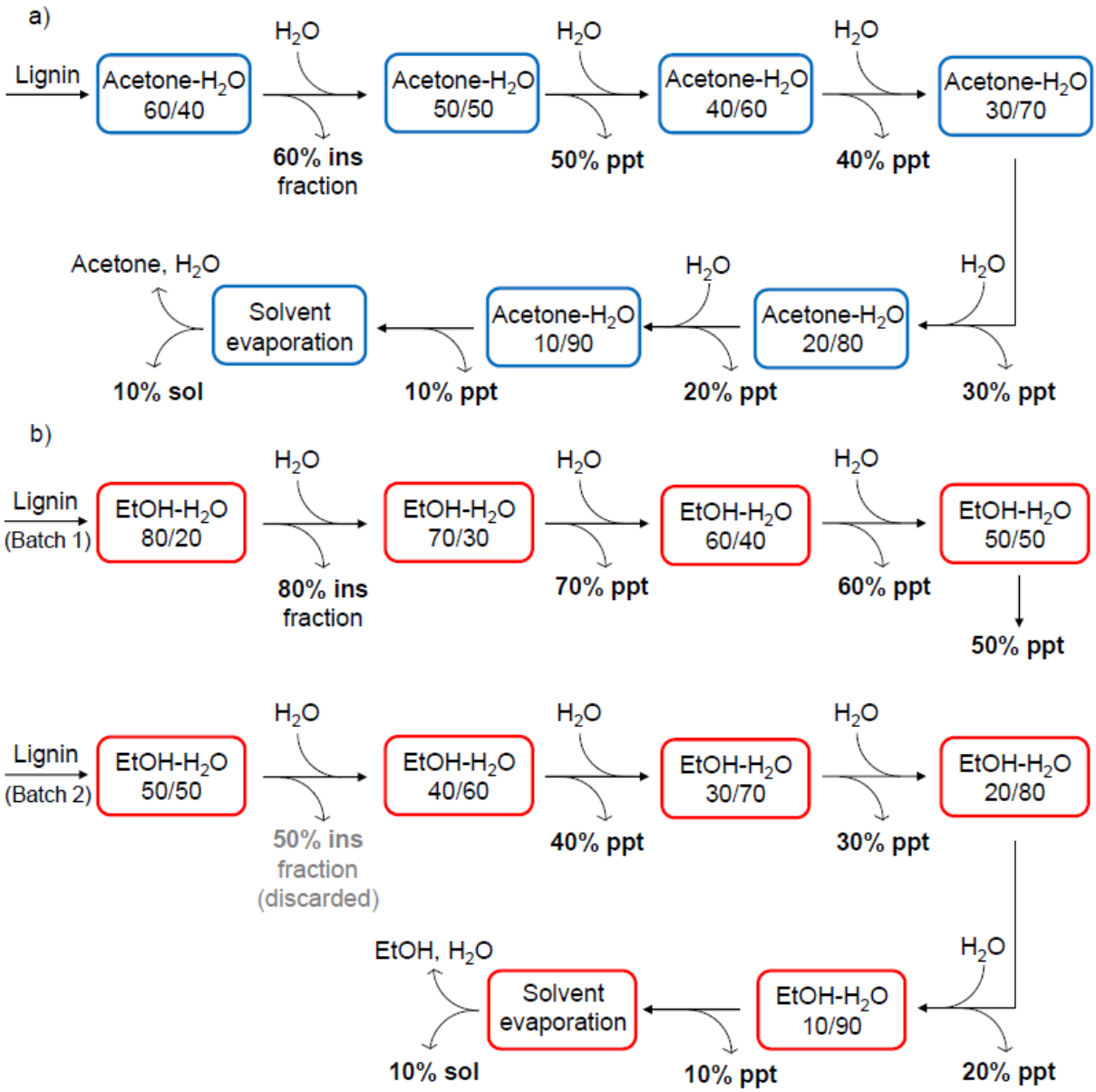


**Scheme 7.** Schematic description of aqueous (a) acetone and (b) ethanol fractionation methods.

The isolated average yields of the so obtained lignin fractions are reported in Figure 31 and summarized in Table 13 for both the aqueous acetone and ethanol fractionation methods. As it can be seen, the yields of the first insoluble fractions (60% ins and 80% ins) are quite high, especially when ethanol 80% $^{v}/_{v}$ was used as solvent (71% yield). The systematic decrease of solvent concentration due to water

addition resulted then in lignin precipitation, but relatively low amount of lignin fractions was collected in each step. Even in this case, the ethanol-based method turned out to be less effective in terms of precipitation yield, with the highest one represented by the 50% ppt fraction (10% yield). Instead, in the acetone-based process, the first two precipitated fractions (50% ppt and 40% ppt) were produced with good yields (45 and 13%, respectively). At solvent concentrations ranging from 30% to 10% for the acetone-based method and from 40% to 10% for the ethanol-based one, further water addition led to relatively low lignin precipitation (1 to 5% yields). Therefore, the last fractions (10% sol) were recovered by evaporating the aqueous solutions at reduced pressure (4 to 6% yields).

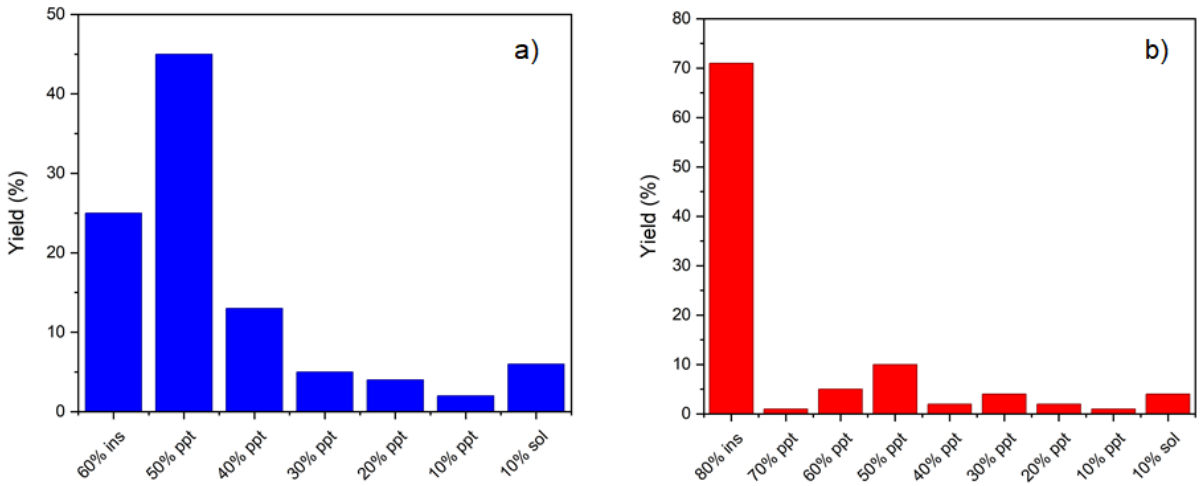


**Figure 31.** Average isolated yields of the fraction obtained from aqueous (a) acetone and (b) ethanol-based refining processes.

**Table 13.** Isolated yields of the fraction obtained from acetone and ethanol-based refining processes and corresponding standard deviations.

| Solvent | Fraction name | Yield (%) | Solvent | Fraction name | Yield (%) |
|---|---|---|---|---|---|
| Acetone | 60% ins | 25 ± 7.2 | Ethanol | 80% ins | 71 ± 9.2 |
| | 50% ppt | 45 ± 6.8 | | 70% ppt | 1 ± 0.3 |
| | 40% ppt | 13 ± 2.7 | | 60% ppt | 5 ± 1.2 |
| | 30% ppt | 5 ± 0.4 | | 50% ppt | 10 ± 1.9 |
| | 20% ppt | 4 ± 0.1 | | 40% ppt | 2 ± 0.9 |
| | 10% ppt | 2 ± 0.1 | | 30% ppt | 4 ± 2.4 |
| | 10% sol | 6 ± 1.5 | | 20% ppt | 2 ± 0.9 |
| | | | | 10% ppt | 1 ± 0.2 |
| | | | | 10% sol | 4 ± 0.8 |

As mentioned above, lignin refining is performed in order to obtain homogeneous fractions with controlled structure, molecular size and narrow distribution.[136,138] Therefore, GPC analysis was carried out to control these properties. The weight average ($M_w$) and number average ($M_n$) molecular weight and polydispersity (D) values of selected lignin fractions are reported in detail in Table 15. Importantly, as can be more easily noticed in Figure 32, the $M_w$ of the fractions gradually decreased during all the refining process. Indeed, a strong decreasing trend stood out, with the 10% ppt and 10% sol lignin fractions having a $M_w$ lower than 1000 Da. Moreover, the polydispersity of all the measured samples was lower than the one of both unfractionated lignin and insoluble fractions (Table 14). Therefore, since the dispersity is a measure of the heterogeneity of sizes of molecules in a polymer, the more its value approaches unity the higher the homogeneity.

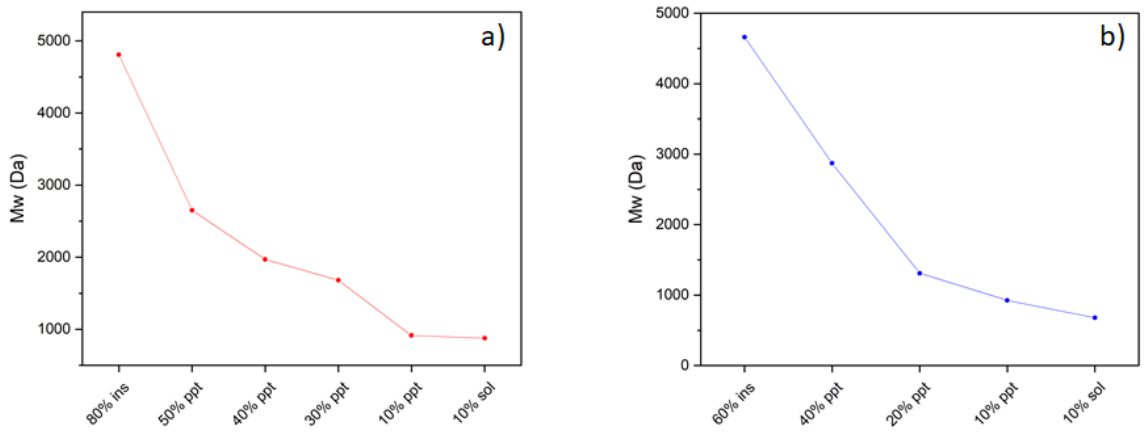


**Figure 32.** $M_w$ trend of selected lignin fractions obtained from (a) acetone and (b) ethanol-based refining processes (detector: RID).

**Table 14.** Weight average ($M_w$) and number average ($M_n$) molecular weight and polydispersity values of selected lignin fractions from acetone and ethanol-based refining processes.

| | | $M_w$ (Da) | | $M_n$ (Da) | | D | |
|---|---|---|---|---|---|---|---|
| | | Detector | | | | | |
| | Fraction name | RID | UV | RID | UV | RID | UV |
| | Starting Kraft lignin | 3790 | 3910 | 1150 | 1390 | 3.29 | 2.81 |
| Acetone | 60% ins | 4660 | 5500 | 721 | 1820 | 6.46 | 3.02 |
| | 40% ppt | 2870 | 2770 | 1470 | 1440 | 1.96 | 1.92 |
| | 20% ppt | 1310 | 1340 | 982 | 911 | 1.34 | 1.47 |
| | 10% ppt | 926 | 936 | 643 | 731 | 1.44 | 1.28 |
| | 10% sol | 677 | 706 | 522 | 531 | 1.30 | 1.33 |
| Ethanol | 80% ins | 4810 | 5590 | 1140 | 2160 | 4.20 | 2.58 |
| | 50% ppt | 2650 | 3220 | 846 | 1660 | 3.14 | 1.94 |
| | 40% ppt | 1970 | 2180 | 936 | 1200 | 2.11 | 1.82 |
| | 30% ppt | 1680 | 1390 | 1050 | 896 | 1.60 | 1.56 |
| | 10% ppt | 915 | 886 | 734 | 712 | 1.25 | 1.25 |
| | 10% sol | 876 | 688 | 580 | 551 | 1.51 | 1.25 |

The thermal behavior of the lignin fractions was then evaluated by DSC analysis. As plotted in Figure 33 and summarized in Table 15, the glass transition temperature ($T_g$) of all the lignins progressively decreased, starting from about 200°C of the two insoluble fractions to 117°C and 92°C of the soluble ones (from acetone and ethanol-based methods, respectively). This trend clearly reflects the above-mentioned decreasing $M_w$ of the fractions, since this increases molecular mobility.[64]

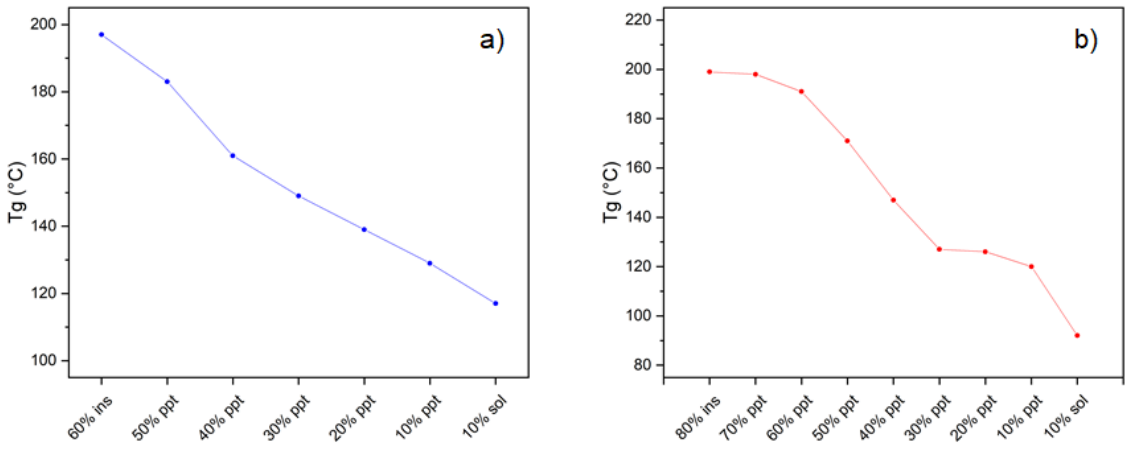


**Figure 33.** $T_g$ trend of the lignin fractions obtained from (a) acetone and (b) ethanol-based refining processes.

**Table 15.** $T_g$ values of the lignin fractions obtained from acetone and ethanol-based refining processes. *starting Kraft lignin $T_g$ = 168°C

| | Fraction name | $T_g$ (°C)* |
|---|---|---|
| Acetone | 60% ins | 197 |
| | 50% ppt | 183 |
| | 40% ppt | 161 |
| | 30% ppt | 149 |
| | 20% ppt | 139 |
| | 10% ppt | 129 |
| | 10% sol | 117 |
| Ethanol | 80% ins | 199 |
| | 70% ppt | 198 |
| | 60% ppt | 191 |
| | 50% ppt | 171 |
| | 40% ppt | 147 |
| | 30% ppt | 127 |
| | 20% ppt | 126 |
| | 10% ppt | 120 |
| | 10% sol | 92 |

In order to investigate the chemical structure of the lignin fractions, NMR experiments were carried out. In particular, the number of hydroxyl groups (OH) in aliphatic, phenolic and carboxylic acid moieties was determined by means of $^{31}$P-NMR after derivatizing the hydroxyls in the lignin samples with phosphorus-containing reagent (values are reported in Table 16). As plotted in Figure 34 for selected samples, lowering the molecular weight by means of fractionation led to lignin fractions with gradually increased hydroxyl groups. Indeed, aliphatic, phenolic and carboxylic OHs showed all an increasing trend, with the lowest $M_w$ fractions (10% ppt and 10% sol) having the higher OH value. The higher amounts of OHs indicate, in agreement with GPC results, that 10% ppt and 10% sol consist of oligomers rather than longer polymer chains. Furthermore, this also might mean higher reactivity towards chemical modifications such as esterification of aliphatic and phenolic hydroxyls.[64,139]

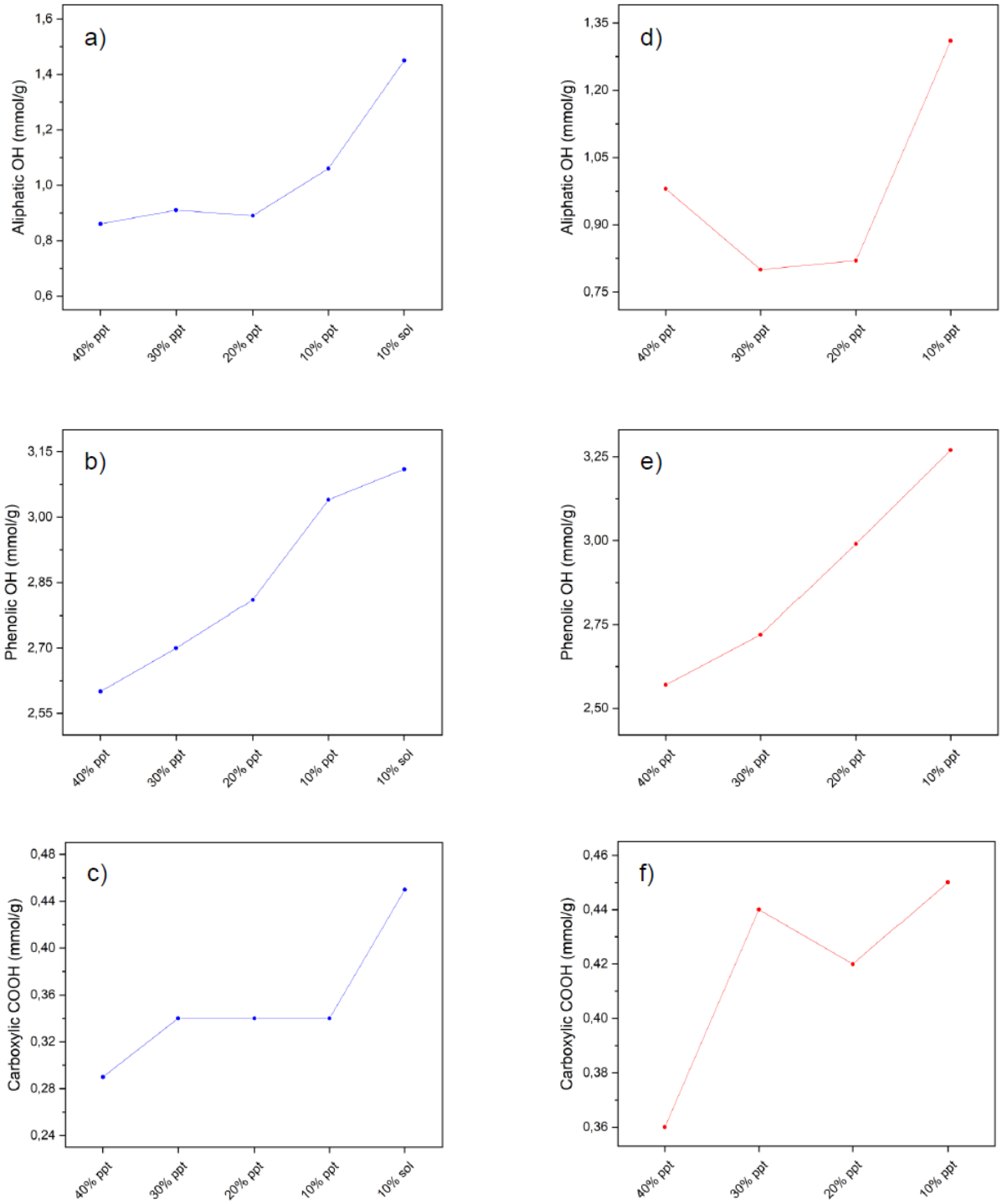


**Figure 34.** Emerging trend of aliphatic and phenolic hydroxyl groups and carboxylic acids in selected fractions from (a-c) acetone and (d-f) ethanol-based refining processes.

**Table 16.** Number of aliphatic and phenolic hydroxyl groups and carboxylic acids for selected lignin fractions from acetone and ethanol refining processes.

| | Fraction name | Aliphatic OHs (mmol/g) | Phenolic OHs (mmol/g) | Carboxylic acids (mmol/g) |
|---|---|---|---|---|
| | Starting Kraft lignin | 1.12 | 2.44 | 0.29 |
| Acetone | 40% ppt | 0.86 | 2.60 | 0.29 |
| | 30% ppt | 0.91 | 2.70 | 0.34 |
| | 20% ppt | 0.89 | 2.81 | 0.34 |
| | 10% ppt | 1.06 | 3.04 | 0.34 |
| | 10% sol | 1.45 | 3.11 | 0.45 |
| Ethanol | 40% ppt | 0.98 | 2.57 | 0.36 |
| | 30% ppt | 0.80 | 2.72 | 0.44 |
| | 20% ppt | 0.82 | 2.99 | 0.42 |
| | 10% ppt | 1.31 | 3.27 | 0.45 |

Considering the work schedule mentioned in the introduction and according to the data obtained, the focus was shifted to those fractions having a $M_w$ lower than 2000 Da and, consequently, lower $T_g$ and higher total OH number (aliphatic + phenolic hydroxyls). This choice was made because of their higher molecular mobility and potentially higher chemical reactivity towards esterification. However, as reported in Table 1, these fractions (from 30% ppt to 10% sol for both acetone and ethanol-based protocols) were obtained with moderate to low yields (1-6%). The refining processes were therefore repeated as described above but this time the fractionation was stopped when a solvent concentration of 30% was reached. At this point, the desired 30% sol fractions were recovered by evaporating the solutions at reduced

pressure and then characterized by means of GPC and DSC analyses. As reported in Table 17, the yield of both fractions is about 15%, the $M_w$ lower than 1000 Da and the dispersity about 1.40, meaning more homogeneous lignins than the starting Kraft. In addition, the lower $T_g$ values were consistent with the decreasing $M_w$. Unfortunately, due to some technical issues and lack of time, it has not been possible to perform $^{31}$P-NMR.

**Table 17.** Isolated yield, weight average molecular weight ($M_w$), dispersity (D) and glass transition temperature ($T_g$) of the 30% sol fractions obtained from acetone and ethanol-based refining processes. * Detector: RID

| | Fraction name | Yield (%) | $M_w$ (Da)* | D* | $T_g$ (°C) |
|---|---|---|---|---|---|
| | Starting Kraft lignin | - | 3790 | 3.29 | 168 |
| Acetone | 30% sol | 15 | 808 | 1.44 | 126 |
| Ethanol | 30% sol | 13 | 756 | 1.39 | 119 |

### 4.5.1.2. Sequential solvent extraction

On the other hand, sequential solvent extraction method[137] consists in four sequential extractions using easily recoverable, green, and sustainable solvents[140] such as ethyl acetate (EtOAc), ethanol (EtOH), methanol (MeOH) and acetone (Scheme 8).

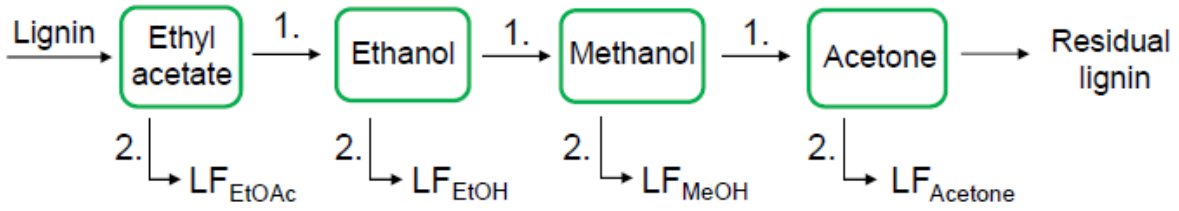


**Scheme 8.** Schematic description of the sequential solvent extraction refining approach (1. Filtration of the insoluble lignin fraction for subsequent extraction; 2. Solvent evaporation to get the soluble lignin fraction; LF= lignin soluble fraction).

As reported in Table 18, $LF_{EtOAc}$ produced a moderate yield (6%), $LF_{MeOH}$ and $LF_{Acetone}$ intermediate ones (14% and 20%, respectively) while $LF_{EtOH}$ the highest

(34%). The insoluble residue recovered at the end of the process presented a 25% yield.

**Table 18.** Isolated yields of the fraction obtained from the sequential solvent extraction refining process.

| Fraction name | Yield (%) |
|---|---|
| $LF_{EtOAc}$ | 6 |
| $LF_{EtOH}$ | 35 |
| $LF_{MeOH}$ | 14 |
| $LF_{Acetone}$ | 20 |
| insoluble residue | 25 |

Since lignin refining is mainly performed to obtain homogeneous fractions with controlled structure, molecular size and narrow distribution,[64,136,138,139] GPC analysis was carried out to control these properties. The weight average ($M_w$) and number average ($M_n$) molecular weight and polydispersity (D) values of all the extracted fractions are reported in detail in Table 19. As also clearly shown in Figure 35 for $M_w$, the above-mentioned sequence of extraction led to lignin fractions with gradually increasing molecular weight. In particular, $LF_{EtOAc}$ represents the lowest $M_w$ fraction (about 1100 Da), while $LF_{Acetone}$ the largest one (about 6900 Da). In between, $LF_{EtOH}$ and $LF_{MeOH}$ (about 1700 and 3400 Da, respectively). Regarding the polydispersity, $LF_{EtOAc}$ D value is the lowest (about 1.50) while the one of the remaining 3 fractions ranges around 2.00. Importantly, all the D values are lower than the one of the starting unfractionated Kraft lignin, thus meaning more homogeneous samples.

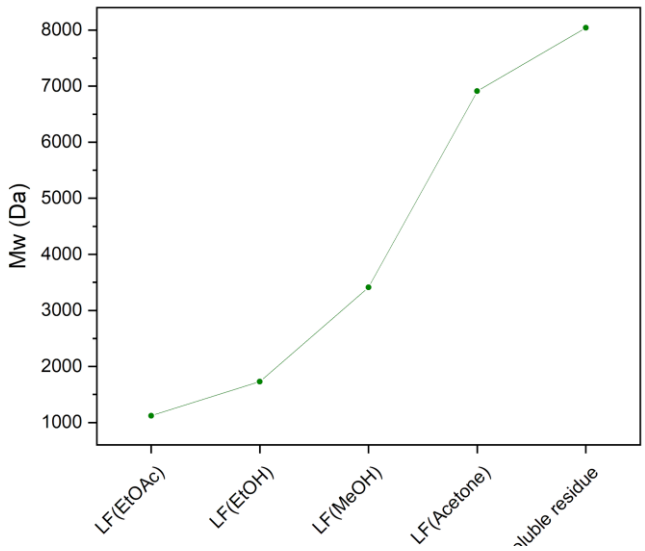


**Figure 35.** $M_w$ trend of the lignin fractions obtained from the sequential solvent extraction refining process (detector: RID).

**Table 19.** Weight average ($M_w$) and number average ($M_n$) molecular weight and polydispersity values of the lignin fractions obtained from the sequential solvent extraction refining process.

| | $M_w$ (Da) | | $M_n$ (Da) | | D | |
|---|---|---|---|---|---|---|
| | Detector | | | | | |
| Fraction name | RID | UV | RID | UV | RID | UV |
| Starting Kraft lignin | 3790 | 3910 | 1150 | 1390 | 3.29 | 2.81 |
| $LF_{EtOAc}$ | 1120 | 1220 | 740 | 774 | 1.52 | 1.58 |
| $LF_{EtOH}$ | 1730 | 1890 | 811 | 970 | 2.14 | 1.95 |
| $LF_{MeOH}$ | 3410 | 3150 | 1520 | 1490 | 2.25 | 2.11 |
| $LF_{Acetone}$ | 6910 | 6920 | 3460 | 3610 | 2.00 | 1.91 |
| insoluble residue | 8040 | 8360 | 5000 | 5080 | 1.61 | 1.64 |

The thermal behavior of the extracted lignin fractions was then evaluated by DSC analysis. As plotted in Figure 36 and summarized in Table 20, $T_g$ values of the

lignins progressively increased, starting from about 100°C of $LF_{EtOAc}$ to 212°C of $LF_{Acetone}$. This trend reflects increasing $M_w$ of the fractions, since this lowers molecular mobility.[64]

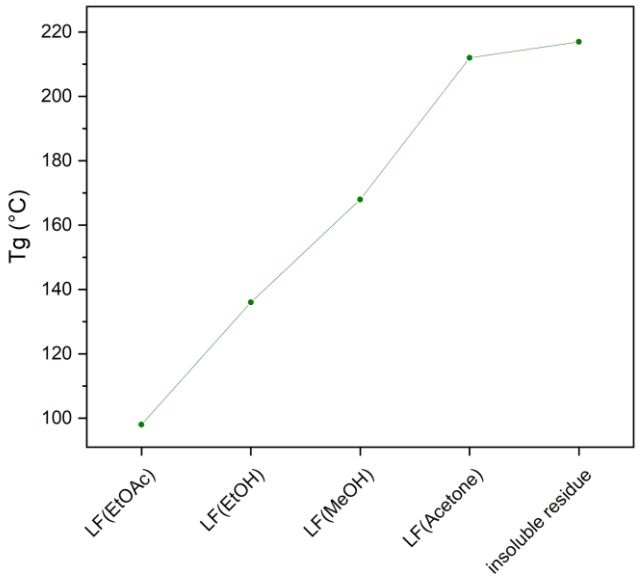


**Figure 36.** $T_g$ trend of the lignin fractions obtained from sequential solvent extraction refining processes.

**Table 20.** $T_g$ values of the lignin fractions obtained from sequential solvent extraction refining processes. *starting Kraft lignin $T_g$ = 168°C

| Fraction name | $T_g$ (°C)* |
|---|---|
| $LF_{EtOAc}$ | 98 |
| $LF_{EtOH}$ | 136 |
| $LF_{MeOH}$ | 168 |
| $LF_{Acetone}$ | 212 |
| insoluble residue | 217 |

Taking the $M_w$ of the fractions (Table 19) and the DSC results (Table 20) into account, the focus was shifted towards $LF_{EtOAc}$ and $LF_{EtOH}$. These fractions, weighing less than 2000 Da with a D value, respectively, of about 1.50 and 2, were considered

more suitable for next applications. Indeed, a lower $M_w$ together with a lower $T_g$ mean higher molecular mobility and, consequently, potential higher reactivity during chemical modifications.[64] In order to determine the structure and, particularly, the hydroxyl functionalities of the two selected soluble fractions, $^{31}$P-NMR experiments were carried out. As reported in Table 21, the amount of carboxylic acids decreased with increasing $M_w$, whereas the number of aliphatic alcohols increased. Even in this case, the higher amount of phenolic OHs for both $LF_{EtOAc}$ and $LF_{EtOH}$ compared to the unfractionated Kraft lignin agreed with GPC results, indicating the presence of oligomers rather than longer polymer chains.[139]

**Table 21.** Number of aliphatic and phenolic hydroxyl groups and carboxylic acids in EtOAc and EtOH soluble fractions from the sequential solvent extraction refining process.

| Fraction name | Aliphatic OHs (mmol/g) | Phenolic OHs (mmol/g) | Carboxylic acids (mmol/g) |
|---|---|---|---|
| Starting Kraft lignin | 1.12 | 2.44 | 0.29 |
| $LF_{EtOAc}$ | 1.12 | 5.16 | 0.74 |
| $LF_{EtOH}$ | 2.47 | 4.42 | 0.57 |

Therefore, to overcome lignin chemical complexity and inherent heterogeneity often constraining its use, both water-induced precipitation and sequential solvent extraction refining methods were adopted. Different lignin fractions were obtained and then characterized by means of GPC, DSC and $^{31}$P-NMR analyses. The refining processes turned out to be easily tunable, leading to fractions with well-defined structures with higher potential in different applications. In particular, the fractions with low molecular weight, low polydispersity and high amount of hydroxyl groups were selected for next uses.

### 4.5.2. Preliminary chemical modifications

The lignin fraction selected for preliminary chemical modifications was $LF_{EtOH}$ mainly due to its wider availability (higher yield) if compared to the other obtained fractions. In particular, acetylation and butyrylation reactions were tested. The choice of esterifying both aliphatic and phenolic OHs with linear apolar carbon chains was specially made to hinder lignin aggregation.[141] This phenomenon, caused by strong attractive interactions among lignin polar OH groups as well as π-stacking of the aromatic rings, is indeed the main responsible for bad compatibility with polymers.[142,143] Therefore, turning OHs into esters with apolar side chains may break up some of these forces.[144] Schematic descriptions of the acetylation and butyrylation protocols are shown in Scheme 9 and Scheme 10.

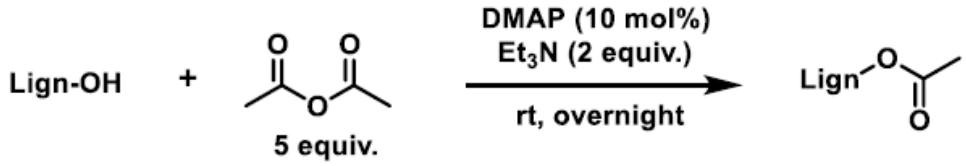


**Scheme 9.** Reaction conditions for the acetylation of $LF_{EtOH}$.

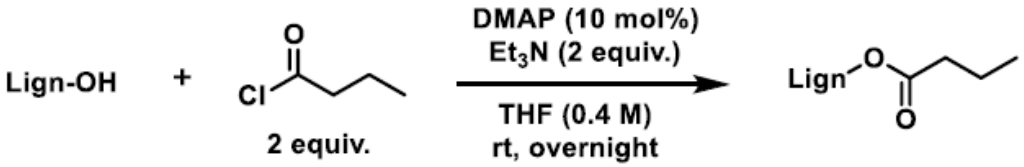


**Scheme 10.** Reaction conditions for the butyrylation of $LF_{EtOH}$.

In order to confirm the chemical structure of the products, infrared spectroscopy (FT-IR) experiments were carried out. The spectra of the starting $LF_{EtOH}$ (black) and of the acetylated (red) and butyrylated (blue) products are compared in Figure 37. As expected, the wide absorption peak centered at about 3400 $cm^{-1}$ (O-H stretching vibration) totally disappeared due to the reaction with both acetic anhydride (red spectrum) and butyryl chloride (blue spectrum). Moreover, the new characteristic peaks at 1760 $cm^{-1}$ (ester C=O stretching) clearly indicated that the two esterification reactions took place.

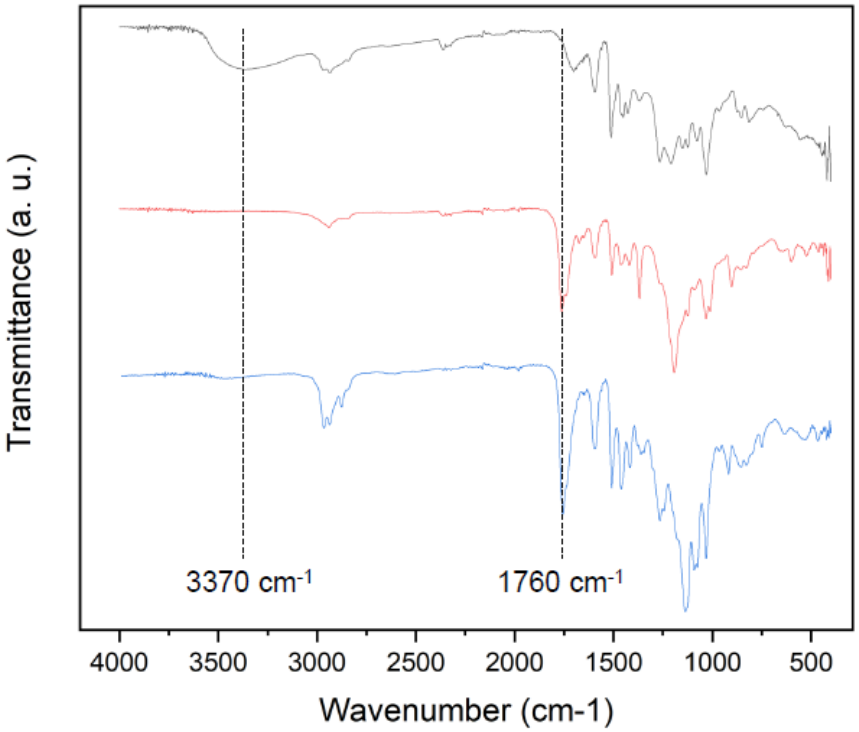


**Figure 37.** FTIR spectra of starting $LF_{ETOH}$ (black) and corresponding acetylated (red) and butyrylated (blue) products. The dashed lines indicate the wave number of the characteristic absorption peaks, which appear and/or disappear during the synthesis of the target compounds.

The two acylated products were then thermally characterized by means of DSC analysis. As shown in Figure 38 and reported in Table 22, the $T_g$ decreased from 136°C of the starting $LF_{ETOH}$ to 114°C and 79°C of the acetylated and butyrylated compounds, respectively. This expected trend reflects the smaller amount of attractive interactions among lignin polar OHs due to their replacement with apolar aliphatic moieties. Indeed, these new groups act as internal plasticizers, breaking up interactions between the chains and thus increasing molecular mobility.[141] In addition, the longer the carbon segment, the higher the plasticizing effect (lower $T_g$).

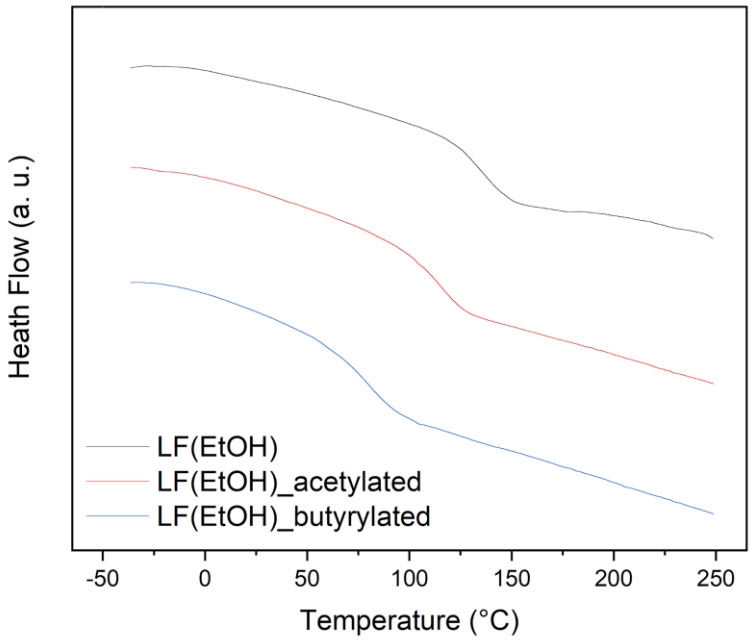


**Figure 38.** DSC thermograms of ethanol soluble fraction ($LF_{EtOH}$) and corresponding acetylated and butyrylated products. The decrease in the $T_g$ is clearly visible.

**Table 22.** $T_g$ values of acetylated and butyrylated products. * Starting $LF_{EtOH}$ $T_g$ = 136°C

| Sample | $T_g$ (°C)* |
|---|---|
| Acetylated | 114 |
| Butyrylated | 79 |

### 4.5.3. PVA-lignin blends

Due to easy availability of polyvinyl alcohol (PVA) in the lab, the use of this polymer was taken into account. As already mentioned in the introduction, PVA is one of the most important synthetic polymers in industry. It has a low cost and, importantly, it is nontoxic and biodegradable. In addition, it has good mechanical and film-forming properties.[87] It is a fully water-soluble polymer and therefore the first challenge was represented by blending this highly hydrophilic polymer with hydrophobic Kraft lignin. To the best of our knowledge, well-fractionated Kraft lignin/PVA systems have not been reported in literature, indicating the need for further investigations into this

topic. Considering PVA chemical structure, blending might succeed by taking advantage of its -OH groups, which could act as hydrogen-bonding sites for the many hydroxyl, carbonyl and carboxyl moieties present in lignin and therefore promote compatibility.[145,146]

### 4.5.4. Preliminary compatibility evaluation

In order to evaluate the compatibility between PVA and modified lignins, thin films with different lignin content were prepared by solvent casting method. As visible in Figure 39, first attempts to blend esterified lignins with PVA failed. Probably, the aliphatic carbon chains introduced by means of chemical modifications caused a significant increase in lignin hydrophobicity[141,147] making miscibility with PVA worse. Indeed, lignin was not spread homogeneously within the polymer matrix, but segregated in the form of solid particles.[146]

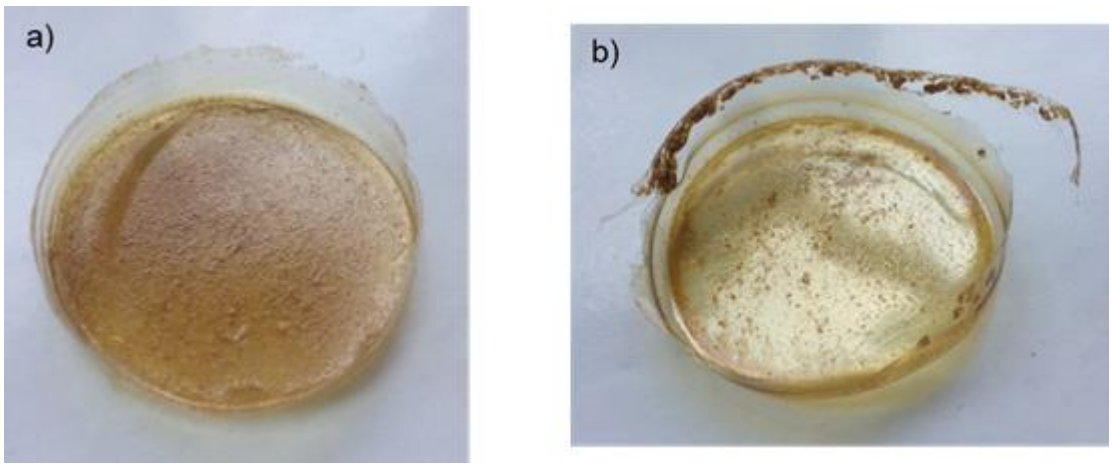


**Figure 39.** PVA thin films containing 10 phr of (a) acetylated and (b) butyrylated $LF_{EtOH}$. Bad miscibility between polymer and additive can be seen.

Therefore, tests with esterified lignin fractions were temporarily set aside while instead unmodified lignin fractions started drawing increasing attention. Indeed, the low $M_w$ lignins richer in total OH and carboxylic acid numbers obtained from the previously described refining approaches might represent a viable alternative due to their higher polarity and, consequently, potentially better miscibility with PVA through the establishment of strong H-bond networks.[148] Following the same solvent casting procedure, acetone 30%sol, ethanol 30%sol, $LF_{EtOAc}$ and $LF_{EtOH}$ unmodified fractions were blended with PVA at content of 1, 3, 5, 10 phr. As depicted in Figure 40, compatibility between these fractions and PVA improved, resulting, especially at low

additive contents, in transparent brownish films. However, at 10 phr concentration, some darker areas came out, thus meaning less effective distribution throughout the polymer due to stronger lignin-lignin self-interactions rather than polymer-lignin ones.[146] Probably, 10 phr represent the limit concentration for these kinds of systems.

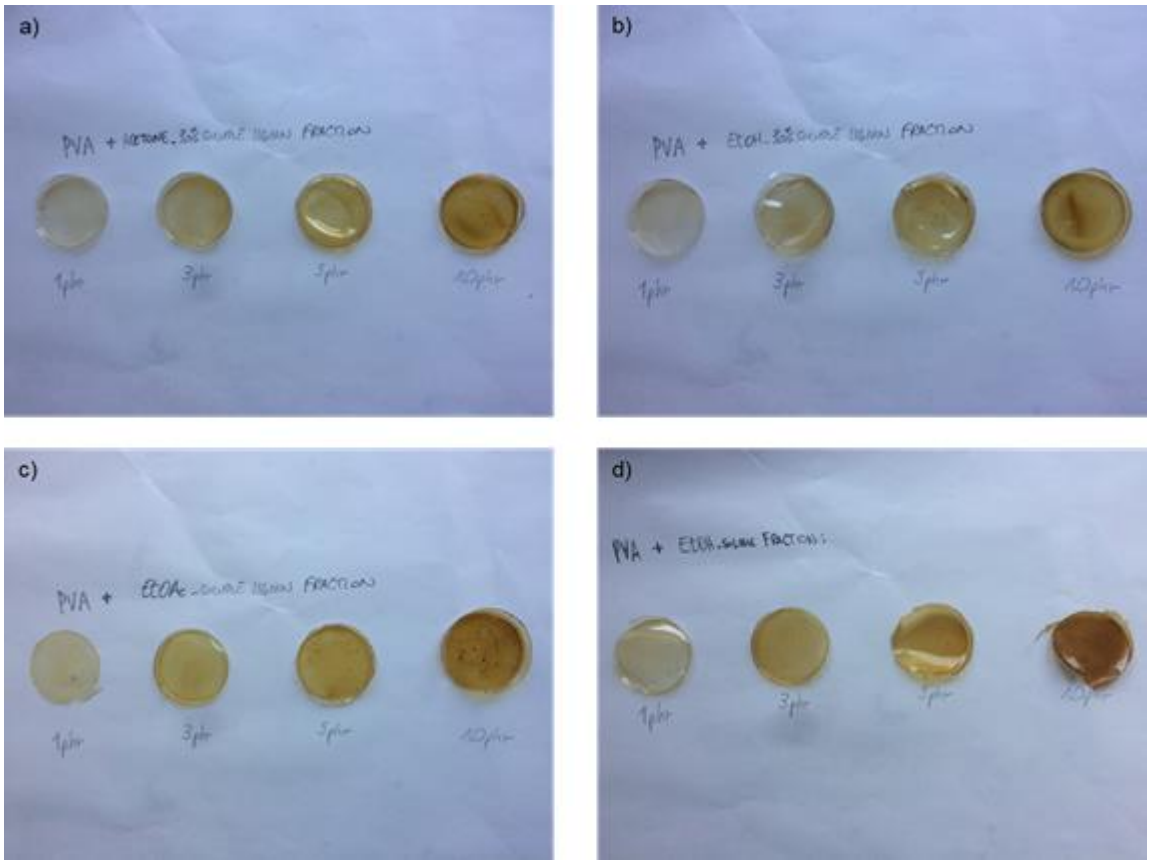


**Figure 40.** PVA thin films containing, respectively, 1, 3, 5 and 10 phr of (a) acetone 30% sol, (b) ethanol 30% sol, (c) $LF_{EtOAc}$ and (d) $LF_{EtOH}$ unmodified lignin fractions.

DSC analysis was first performed on the so-obtained materials (except for PVA/$LF_{EtOH}$ films due to technical issues) in order to evaluate any effect on PVA $T_g$ and/or melting behavior. As reported in Table 23, lignin additives had no significant influence over the $T_g$ as well as on the melting temperature ($T_m$) of the neat polymer. However, DSC thermograms gave an important indication of compatibility between the two phases, because no double $T_g$ was seen. Indeed, if lignin and PVA had been completely immiscible, the $T_g$ of each single component would have been detected.

**Table 23.** $T_g$ and $T_m$ values of neat PVA and of PVA containing 1, 3, 5 and 10 phr of acetone 30% sol, ethanol 30% sol and $LF_{EtOAc}$ lignin fractions.

| Sample | Additive content (phr) | $T_g$ (°C) | $T_m$ (°C) |
|---|---|---|---|
| PVA_neat | 0 | 76 | 223 |
| PVA_acetone 30% sol | 1 | 80 | 225 |
| | 3 | 81 | 227 |
| | 5 | 81 | 228 |
| | 10 | 83 | 228 |
| PVA_ethanol 30% sol | 1 | 73 | 225 |
| | 3 | 78 | 228 |
| | 5 | 81 | 229 |
| | 10 | 84 | 229 |
| PVA_$LF_{EtOAc}$ | 1 | 70 | 223 |
| | 3 | 73 | 226 |
| | 5 | 80 | 226 |
| | 10 | 84 | 227 |

### 4.5.5. Future works

In order to properly assess compatibility, morphology studies by means of SEM microscopy should be carried out. In addition, DMA measurements should be performed to evaluate the effect of lignin on the viscoelastic properties of PVA. After that, it would be necessary to evaluate the UV absorption of these PVA/lignin systems with a UV-VIS spectrometer. Indeed, if lignin activity as UV-blocker was

proved, promising applications of these PVA/lignin composites as eco-friendly biodegradable UV-shielding materials would arise.

## 4.6. Glycerol-levulinic acid-based plasticizer

The use of biopolymers is not enough by itself to solve all the issues related to traditional plastics (fossil sources depletion, greenhouse gas emissions, waste management, environmental pollution and health hazard). Indeed, since all polymers are almost always a formulation of many ingredients, also the nature of the additives play a crucial role. For instance, considering the whole life cycle of a material, they may either migrate or leach out of the polymer matrix during use as well as after disposal, resulting in environmental spills with possible adverse effect on soil, groundwater and human beings. That is why there is the strong need to develop sustainable, eco-friendly and safe additives starting from renewable resources. These new compounds should ensure at least the same effectiveness and long-lasting performances of commercially available ones but without any hazardous effect. As already shown in the introduction, biobased chemical platforms such as levulinic acid and glycerol represent a valuable starting point to build up a new class of plasticizers. Therefore, in order to fully exploit the high chemical versatility of both levulinic acid and glycerol, they were combined together through the development of a selective and potentially scalable route.

### 4.6.1. Optimization of the reaction conditions

Although glycerol has been widely studied and converted in many different value added products,[46,70] the esterification of glycerol in acidic conditions still suffer from some drawbacks. As already explained for ketal-ester derivatives, also direct condensation of levulinic acid with glycerol leads to a mixture of products in a non-selective manner particularly difficult to control.[58,59] In particular, it is possible to have at once mono-, di- and triesters as well as dioxanes and dioxolanes acetal rings or even a combination of all. This happens because protic acid catalysts promote both esterification and acetalization. So, at first, the optimization of the esterification reaction between glycerol and levulinic acid to give the corresponding triester was carried out. All the observations and considerations made before about Fischer esterification, its reversibility and its milder reaction conditions compared to common alternative esterification methods (Steglich,[96] Yamaguchi,[97] Mitsunobu,[98] acylation by acyl chlorides and anhydrides) are still valid. Therefore, in order to push the

equilibrium of the reaction toward the products,[99] the excess of levulinic acid was studied at first. PTSA (10 mol% with respect to glycerol) was selected as the catalyst due to its good solubility in both glycerol and levulinic acid. These reagents are indeed liquid and miscible with each other, so no solvent was added. Then, in order to allow the water formed during the reaction to evaporate, a temperature of 90°C was set for 24 h (Scheme 11).

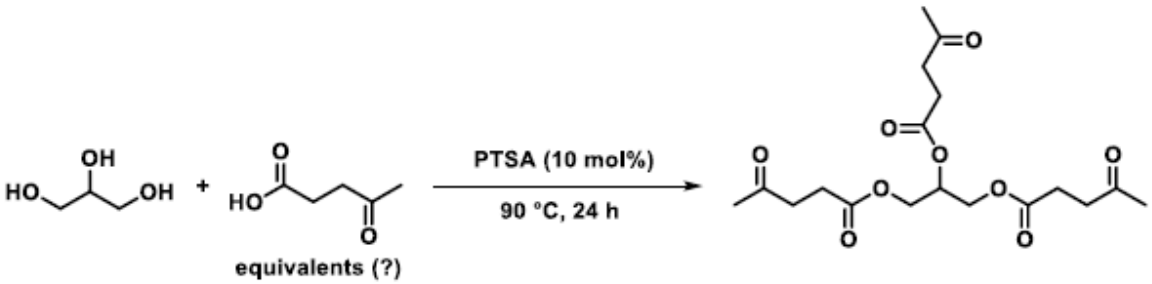


**Scheme 11.** Optimization of the esterification between glycerol and levulinic acid: equivalents screening.

As summarized in Table 24, slight excess of levulinic acid led to a mixture of products with low selectivity in the target triester (entry 1). By increasing the equivalents of the reactant, the process became more selective, giving the product at higher yields (entries 2 and 3).

**Table 24.** Optimization of the esterification between glycerol and levulinic acid: equivalents screening.

| Entry | Equivalents of Levulinic Acid* | Isolated yield (%) |
|---|---|---|
| 1 | 1.3 | not determined |
| 2 | 3 | 15 |
| 3 | 5 | 30 |

* with regard to each hydroxyl group of glycerol

However, the yield was still too low to proceed further. Since a brownish color of the crude mixture was noticed at the end of all the experiments, we thought that probably the reaction time was too long, leading to a partial degradation of the product. Therefore, the reaction time was reduced to 6 h (Scheme 12). The reaction afforded the desired triester in 38% yield, still quite low though.

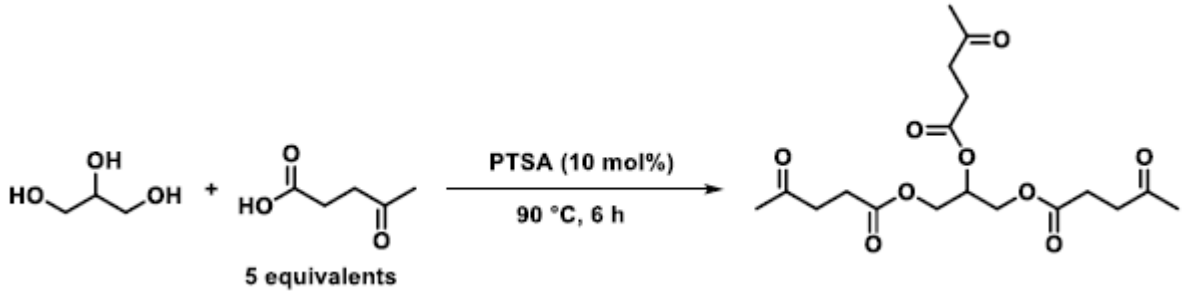


**Scheme 12.** Optimization of the esterification between glycerol and levulinic acid: reaction time decreased from 24 to 6 h.

At this point, in order to increase the yield, one of the remaining attempts to make was to increase the temperature of the reaction (Scheme 13). Different temperatures were therefore screened (Table 25). The maximum yield was obtained at 110°C (60%, entry 1), while higher temperatures led to lower yields (25 and 21%, entries 2 and 3, respectively).

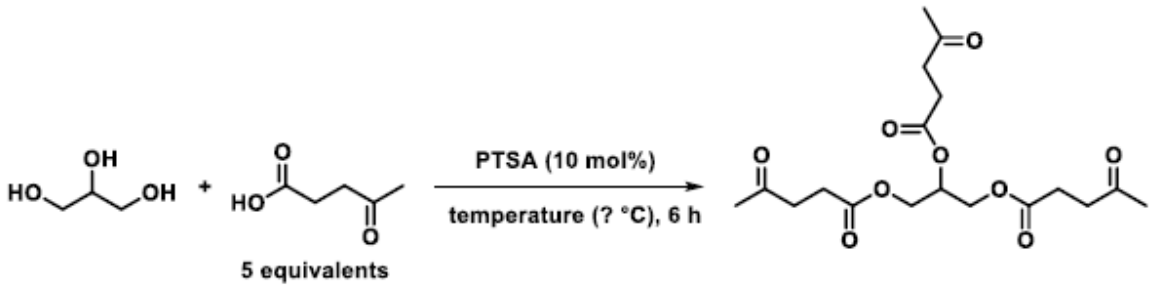


**Scheme 13.** Optimization of the esterification between glycerol and levulinic acid: temperature screening.

**Table 25.** Optimization of the esterification between glycerol and levulinic acid: temperature screening.

| Entry | Temperature (°C) | Isolated yield (%) |
|---|---|---|
| 1 | 110 | 60 |
| 2 | 130 | 25 |
| 3 | 150 | 21 |

Besides being a solvent-free process with no harsh reaction conditions (vacuum, inert atmosphere, high temperature, corrosive catalyst, unsafe reagents) and no sophisticated equipment involved (distillation apparatus, water-cooled reflux condenser, double/triple necks flask, vacuum glassware), the work-up is very easy and no further purifications of the product are necessary. In particular, work-up

includes quenching with an aqueous base to deactivate the catalyst, extraction with diethyl ether and simple washing steps with an aqueous base solution to get rid of the unreacted excess of levulinic acid. Importantly, these characteristics potentially make the whole process industrially scalable.

### 4.6.2. Characterization of glycerol-trilevulinate

In order to confirm the chemical structure of the product, $^{1}$H-NMR experiments were carried out (Figure 41). The multiplet centered at about 5.24 ppm was assigned to the single central proton of the glycerol segment (A), while the two double doublets centered at 4.27 and 4.17 ppm were assigned to the methylene protons of the same segment (B). These signals, all in the ester region above 4 ppm, prove that esterification of glycerol took place. Due to the symmetry of the molecule, the remaining levulinic protons (C, D, and E) are equivalent, each giving a single signal for all. In particular, multiplets centered at about 2.75 and 2.59 ppm were assigned to α-ketone (more deshielded and therefore at lower fields) and α-ester (more shielded and therefore at higher fields) methylene protons (D and C, respectively). The singlet at 2.18 ppm was finally assigned to the methyl protons (E).

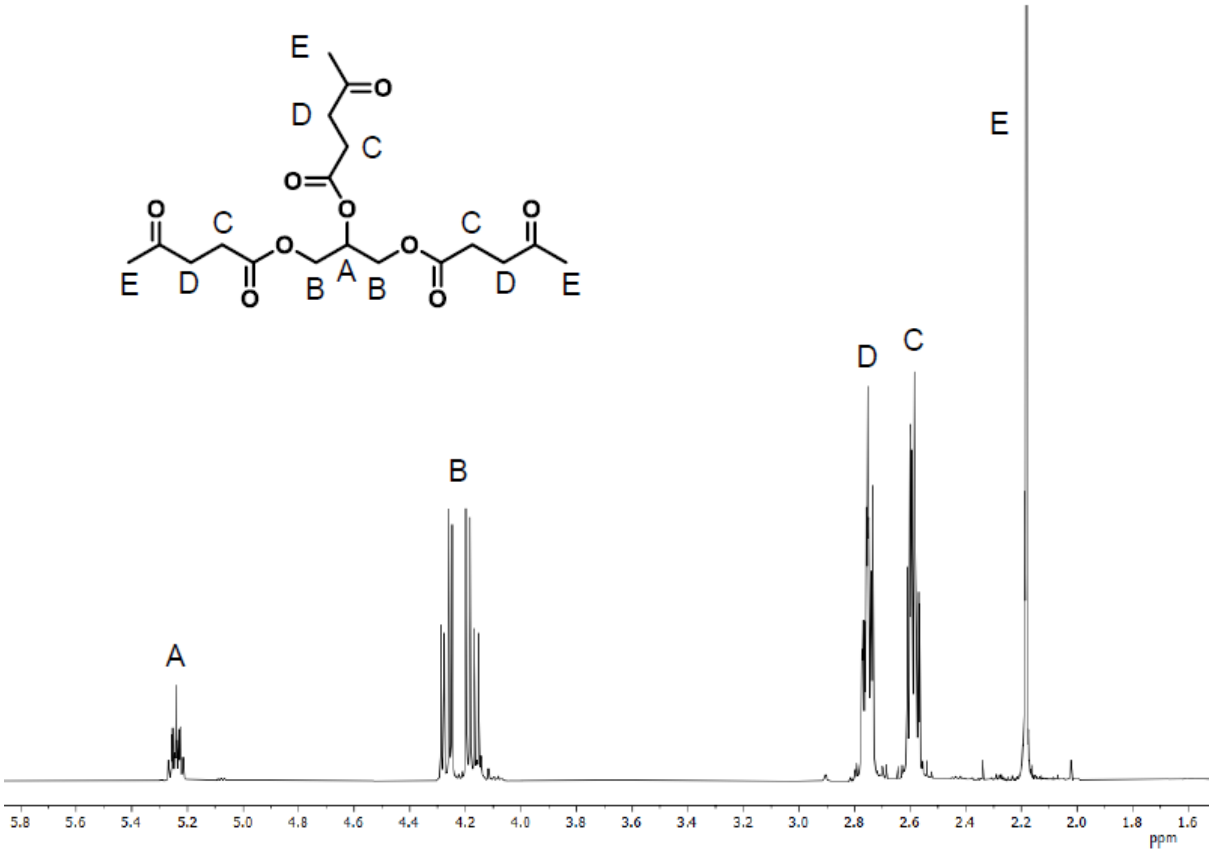


**Figure 41.** $^{1}$H-NMR spectrum of glycerol-trilevulinate with corresponding proton assignments.

### 4.6.3. Preliminary evaluation of the plasticizing effectiveness on PVC

This glycerol-trilevulinate, before any further chemical modification (for instance, acetalization of the three ketone moieties), was tested itself as a plasticizer. So, PVC was selected as the model polymer matrix in order to carry out some preliminary evaluations. Homogeneous plasticized PVC thin films were therefore prepared by solvent casting, with additive contents of 10 and 20 phr. A neat PVC film was also prepared for comparison reasons.

Since the plasticizing effect is indicated by the decrease in the glass transition temperature ($T_g$) of the material, DSC analyses were performed on both neat and plasticized PVC films. The resulting $T_g$ values are summarized in Figure 42 as a function of the additive content. Generally, a decrease of the $T_g$ can be observed compared to neat PVC, directly proportional to the additive content. In particular, $T_g$ shifted from 73°C to 38°C at an additive concentration of 10 phr and to 27°C at 20 phr. This preliminary indication clearly suggests that the proposed glycerol-trilevulinate has a great potential plasticizing effectiveness already at this stage.

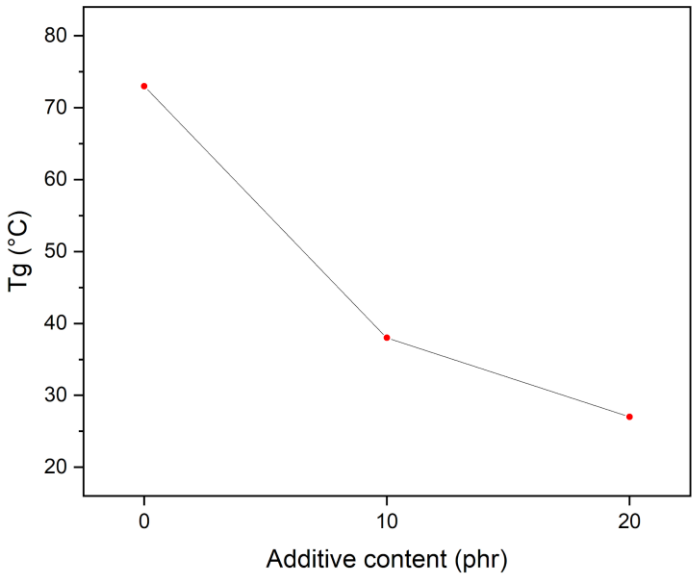


**Figure 42.** $T_g$ values of neat and plasticized PVC films as a function of the additive content.

### 4.6.4. Future works

The performance of glycerol-trilevulinate as PVC plasticizer will be further evaluated by means of morphological, thermal and mechanical analyses. After that, the plasticizing effectiveness of our molecule will be investigated in different polymer matrices, including both traditional and natural polymers. The goal is to create a kind of database of plastics in which this biobased and easily obtainable plasticizer can be used. Every formulation will be then properly characterized.

# 5. CONCLUSIONS

This work evolved from the observation that the recent rapid growth and spread of biopolymers in plastic industry as well as in material science is not properly combined with the development of a new generation of dedicated additives. In particular, plasticizers are an increasingly significant part of the global market of additives and, as the field of plastics continues to grow and innovate, so does the plasticizer industry. However, most of the commercially available plasticizers are not suitable for the aforementioned biopolymers, mainly because of environmental issues. The development of novel plasticizers able to meet sustainability and circular economy is therefore the main goal of current research on this topic. In addition, serious health hazards posed by some traditional plasticizers make research on greener and safer alternatives extremely important as well. With this in mind, a new class of biobased asymmetric ketal-diester derivatives was successfully prepared thanks to a selective protecting-group-free route designed, developed and optimized starting from levulinic acid, a promising renewable chemical platform. This synthesis allowed us not only to easily overcome chemoselectivity issues related to the bifunctional nature of levulinic acid, but also to introduce different side chains in our molecules. As a result, five fully biobased plasticizers were obtained. They were then added to PVC as the model polymer in order to evaluate the influence of chemical structure on their plasticizing effectiveness. Morphological, thermal and mechanical data showed a strong correlation between the structural features of the additives (polarity, molecular weight, geometry) and the final properties of the material. In particular, isobutyric and benzylic segments led to the higher decrease of the $T_g$ of PVC, bringing it even under room temperature. Indeed, the steric hindrance and the possibility to freely rotate of these moieties allowed to be more effective in breaking up PVC chain-chain dipolar interactions. On the other hand, as regards the mechanical properties, a correlation between DSC thermograms and *E′* values was observed, with additives bearing linear aliphatic side-chains giving the broadest $T_{g,DSC}$ ranges as well as the lowest modulus. In addition, all the ketal-ester derivatives improved the thermal stability of PVC, especially moving dehydrochlorination at higher temperatures thanks to the acetal ring, which can react with hydrochloric acid preventing the latter from catalyzing the degradation of the matrix. Our plasticizers also showed remarkably low extraction values when

aggressive leaching tests in hexane were performed, while no significant aqueous extraction occurred. The best additives herein proposed were then compared in terms of $T_g$ reduction with commercially available phthalates (DDP, DEHP), aliphatic Hexamoll® DINCH**,** citrate (ATBC) and adipate (DHEA). Very positive results were observed, with our biobased plasticizers behaving as well as and, in some cases, even better than these well-known commercial plasticizers. More importantly, they showed comparable performances also at lower concentrations, thereby proving the actual plasticizing effectiveness of the synthesized ketal-diester derivatives.

The same ketal-diesters of levulinic acid were then added to bacterial PHB and new fully biobased plasticized formulations were therefore obtained. Despite the highly crystalline nature of PHB, morphological observations proved miscibility between the components with no phase separation. This condition of homogeneity was also confirmed by thermal analysis, which showed the influence of the proposed plasticizers in both the amorphous and the crystalline phases of the material. Indeed, due to an increase in chain mobility, a decrease in both $T_g$ and $T_m$ was detected for all the compositions. Increased mobility also allowed the macromolecules to rearrange in new ordered configurations, resulting in a further nucleation and therefore in higher degrees of crystallinity. Despite this last aspect, the overall plasticizing effect led to an enhanced flexibility, with a decrease in the storage modulus *E′*. Last but not least, leaching tests performed in both water and hexane resulted in remarkably low plasticizer losses.

In order to overcome lignin extremely heterogeneous chemical structure and high polydispersity, which have been limiting its huge potential as renewable resource of aromatic building blocks, two refining approaches were adopted. In particular, aqueous solvent precipitation and sequential solvent extraction were found to be very easily tunable processes, which afforded us to isolate readily usable lignin fractions with tailored properties. Chromatographic, thermal and spectroscopic data showed indeed interesting linear trends, giving us the opportunity to select the proper lignin fraction depending on the desired molar mass, dispersity and amount of hydroxyl groups. Low molecular weight lignins were selected as suitable for the next stage, due to their higher molecular mobility (lower $T_g$) and amount of reactive hydroxyl groups. Acetylation and butyrylation reactions were then successfully

performed on the ethanol soluble fraction in order to improve to some extent compatibility with polymers by preventing lignin aggregation. Successively, these esterified products were blended with PVA, whose numerous hydroxyl groups are able to help miscibility by acting as hydrogen-bonding sites for lignin functionalities. Preliminary blending tests showed however partial phase separation. However, when selected unmodified lignin fractions were used, promising results in terms of compatibility were achieved. Indeed, thermograms presented only one $T_g$ value for each formulation, suggesting no phase separation.

A solvent-free synthetic procedure involving biobased glycerol and levulinic acid was also developed. Notwithstanding the multiple functional groups of both these reagents, only the desired glycerol-trilevulinate was selectively obtained. Importantly, the mild reaction conditions, the absence of the solvent, the essential setup required, the very easy work-up together with the lack of further time-consuming purifications such as column chromatography make the developed route industrially scalable. Additionally, preliminary blending with PVC showed the high plasticizing potential of this triester, which significantly lowered the $T_g$ of the material.

# 6. APPENDIX

## 6.1. Potential renewable origins of the carboxylic acids and diols used

Levulinic acid from cellulose;[55] 1,3-propanediol and ethylene from lignocellulose;[68] myristic acid from plant species of the genus *Myristica*;[149] stearic acid from triglycerides and vegetable oils;[150] isovaleric acid from the root of plant species of *Valeriana officinalis*;[151] phenylacetic acid has been found to be an active plant hormone produced within plants;[152] benzoic acid from flowers of *Petunia hybrida* plants.[153]

## 6.2. Yields, $^1$H-NMR and FT-IR assignments of the intermediates 2a-e

*2-hydroxyethyl tetradecanoate,* ***2a****, [$CH_3(CH_2)_{10}CH_2CH_2C(=O)OCH_2CH_2OH$]* The compound was obtained as a white solid (95% yield). $^1$H-NMR ($CDCl_3$, 400 MHz) δ = 4.24-4.19 (m, 2H, OC$H_2$$CH_2$OH), 3.87-3.79 (m, 2H, $OCH_2CH_2$OH), 2.35 (t, J = 7.6 Hz, 2H, $CH_2CH_2$C(=O)O), 1.87 (t, J = 5.5 Hz, 1H, $CH_2OH$), 1.69-1.58 (m, 2H, $CH_2CH_2$C(=O)O), 1.37-1.18 (m, 20H, $CH_3(CH_2)_{10}$), 0.88 (t, J = 6.6 Hz, 3H, $CH_3(CH_2)_{10}$) ppm. ATR/FT-IR n = 3390, 3315 (alcohol O-H stretch); 2916, 2849 ($sp^3$ C-H stretch); 1733 (C=O stretch) $cm^{-1}$.

*2-hydroxyethyl stearate,* ***2b****, [$CH_3(CH_2)_{14}CH_2CH_2C(=O)OCH_2CH_2OH$]* Following the general procedure but at a reaction temperature of 90°C, the compound was obtained as a white solid (80% yield). $^1$H-NMR ($CDCl_3$, 400 MHz) δ = 4.24-4.19 (m, 2H, OC$H_2$$CH_2$OH), 3.86-3.80 (m, 2H, $OCH_2CH_2$OH), 2.35 (t, J = 7.7 Hz, 2H, $CH_2CH_2$C(=O)O), 1.86 (t, J = 6.0 Hz, 1H, $CH_2OH$), 1.70-1.58 (m, 2H, $CH_2CH_2$C(=O)O), 1.37-1.19 (m, 28H, $CH_3(CH_2)_{14}$), 0.88 (t, J = 6.8 Hz, 3H, $CH_3(CH_2)_{14}$) ppm. ATR/FT-IR n = 3389, 3314 (alcohol O-H stretch); 2916-2849 ($sp^3$ C-H stretch); 1733 (C=O stretch) $cm^{-1}$.

*2-hydroxyethyl 3-methylbutanoate,* ***2c****, [$(CH_3)_2CHCH_2C(=O)OCH_2CH_2OH$]* The compound was obtained as a colourless oil (85% yield). $^1$H-NMR ($CDCl_3$, 400 MHz) δ = 4.24-4.20 (m, 2H, OC$H_2$$CH_2$OH), 3.86-3.80 (m, 2H, $OCH_2CH_2$OH), 2.24 (d, J =

7.1 Hz, 2H, $(CH_3)_2CHCH_2$), 2.18-2.06 (m, 1H, $(CH_3)_2CHCH_2$), 2.0 (t, J = 6.0 Hz, 1H, $CH_2OH$), 0.97 (d, J = 6.6 Hz, 6H, $(CH_3)_2CH$) ppm. ATR/FT-IR n = 3340 (alcohol O-H stretch); 2960-2875 ($sp^3$ C-H stretch); 1733 (C=O stretch) $cm^{-1}$.

*2-hydroxyethyl benzoate,* ***2d****, [$C_6H_5C(=O)OCH_2CH_2OH$]* The compound was obtained as a colourless oil (89% yield). $^1$H-NMR ($CDCl_3$, 400 MHz) δ = 8.09-8.04 (m, 2H, *ortho*), 7.61-7.54 (m, 1H, *para*), 7.49-7.41 (m, 2H, *meta*), 4.49-4.44 (m, 2H, $OCH_2CH_2OH$), 3.99-3.93 (m, 2H, $OCH_2CH_2OH$), 2.18 (t, J = 6.0 Hz, 1H, $CH_2OH$) ppm. ATR/FT-IR n = 3421 (alcohol O-H stretch); 3067 ($sp^2$ C-H stretch); 2950, 2879 ($sp^3$ C-H stretch); 1715 (C=O stretch); 1601, 1584, 1451 (aromatic C=C stretch); 707, 687, 675 (aromatic $sp^2$ C-H bend) $cm^{-1}$.

*2-hydroxyethyl 2-phenylacetate,* ***2e****, [$C_6H_5CH_2C(=O)OCH_2CH_2OH$]* The compound was obtained as a colourless oil (86% yield). $^1$H-NMR ($CDCl_3$, 400 MHz) δ = 7.36-7.27 (m, 5H, $C_6H_5$), 4.25-4.22 (m, 2H, $OCH_2CH_2OH$), 3.84-3.79 (m, 2H, $OCH_2CH_2OH$), 3.68 (s, 2H, $(C_6H_5)CH_2C(=O)O$), 1.81 (t, J = 6.0 Hz, 1H, $CH_2OH$) ppm. ATR/FT-IR n = 3430 (alcohol O-H stretch); 3033 ($sp^2$ C-H stretch); 2952, 2925 ($sp^3$ C-H stretch); 1729 (C=O stretch); 1603, 1583, 1455 (aromatic C=C stretch); 723, 708, 696 (aromatic $sp^2$ C-H bend) $cm^{-1}$.

## 6.3. Yields, $^1$H-NMR and FT-IR assignments of the intermediates 3a-e

*2-((4-oxopentanoyl)oxy)ethyl tetradecanoate,* ***3a****, [$CH_3(CH_2)_{10}CH_2CH_2C(=O)OCH_2CH_2O(O=)CCH_2CH_2C(=O)CH_3$]* The compound was obtained as a yellowish-white solid (75% yield). $^1$H-NMR ($CDCl_3$, 400 MHz) δ = 4.27 (s, 4H, $OCH_2CH_2O$), 2.76 (t, J = 6.3 Hz, 2H, $CH_2CH_2C(=O)CH_3$), 2.60 (t, J = 6.8 Hz, 2H, $CH_2CH_2C(=O)CH_3$), 2.32 (t, J = 7.2 Hz, 2H, $CH_2CH_2C(=O)O$), 2.19 (s, 3H, $CH_2C(=O)CH_3$), 1.67-1.59 (m, 2H, $CH_2CH_2C(=O)O$), 1.37-1.19 (m, 20H, $CH_3(CH_2)_{10}$), 0.88 (t, J = 7.0 Hz, 3H, $CH_3(CH_2)_{10}$) ppm. ATR/FT-IR n = 2917, 2849 ($sp^3$ C-H stretch); 1731, 1713 (C=O stretch); 1473, 1463, 1385, 1371 ($sp^3$ C-H bend) $cm^{-1}$.

*2-((4-oxopentanoyl)oxy)ethyl stearate,* ***3b****,* *[$CH_3(CH_2)_{14}CH_2CH_2C(=O)OCH_2CH_2O(O=)CCH_2CH_2C(=O)CH_3$]* The compound was obtained as a yellowish-white solid (91% yield). $^1$H-NMR ($CDCl_3$, 400 MHz) δ = 4.27 (s, 4H, OC*$H_2$*C*$H_2$*O), 2.76 (t, J = 6.5 Hz, 2H, $CH_2CH_2$C(=O)$CH_3$), 2.60 (t, J = 6.7 Hz, 2H, C*$H_2$*$CH_2$C(=O)$CH_3$), 2.32 (t, J = 7.5 Hz, 2H, $CH_2CH_2$C(=O)O), 2.19 (s, 3H, $CH_2$C(=O)C*$H_3$*), 1.67-1.57 (m, 2H, C*$H_2$*$CH_2$C(=O)O), 1.36-1.20 (m, 28H, $CH_3$(C*$H_2$*)$_{14}$), 0.88 (t, J = 6.9 Hz, 3H, C*$H_3$*$(CH_2)_{14}$) ppm. ATR/FT-IR n = 2917, 2849 (sp$^3$ C-H stretch); 1730, 1713 (C=O stretch); 1473, 1463, 1385, 1371 (sp$^3$ C-H bend) cm$^{-1}$.

*2-((3-methylbutanoyl)oxy)ethyl 4-oxopentanoate,* ***3c****,* *[$(CH_3)_2CHCH_2C(=O)OCH_2CH_2O(O=)CCH_2CH_2C(=O)CH_3$]* The compound was obtained as a yellowish oil (95% yield). $^1$H-NMR ($CDCl_3$, 400 MHz) δ = 4.27 (s, 4H, OC*$H_2$*C*$H_2$*O), 2.76 (t, J = 6.6 Hz, 2H, $CH_2$C*$H_2$*C(=O)$CH_3$), 2.60 (t, J = 6.6 Hz, 2H, C*$H_2$*$CH_2$C(=O)$CH_3$), 2.22 (d, J = 6.9 Hz, 2H, $(CH_3)_2$CHC*$H_2$*), 2.19 (s, 3H, $CH_2$C(=O)C*$H_3$*), 2.16-2.04 (m, 1H, $(CH_3)_2$C*H*$CH_2$), 0.97 (d, J = 6.6 Hz, 6H, (C*$H_3$*)$_2$CH) ppm. ATR/FT-IR n = 2961, 2875 (sp$^3$ C-H stretch); 1733, 1717 (C=O stretch) cm$^{-1}$.

*2-((4-oxopentanoyl)oxy)ethyl benzoate,* ***3d****,* *[$C_6H_5C(=O)OCH_2CH_2O(O=)CCH_2CH_2C(=O)CH_3$]* The compound was obtained as a colourless oil (98% yield). $^1$H-NMR ($CDCl_3$, 400 MHz) δ = 8.09-8.02 (m, 2H, *ortho*), 7.61-7.55 (m, 1H, *para*), 7.49-7.42 (m, 2H, *meta*), 4.54-4.51 (m, 2H, OC*$H_2$*$CH_2$O), 4.44-4.41 (m, 2H, $OCH_2$C*$H_2$*O), 2.76 (t, J= 6.5 Hz, 2H, $CH_2$C*$H_2$*C(=O)$CH_3$), 2.62 (t, J= 6.8 Hz, 2H, C*$H_2$*$CH_2$C(=O)$CH_3$) 2.17 (s, 3H, $CH_2$C(=O)C*$H_3$*) ppm. ATR/FT-IR n = 2961, 2915 (sp$^3$ C-H stretch); 1713 (C=O stretch); 1601, 1584 (aromatic C=C stretch); 711, 688, 675 (aromatic sp$^2$ C-H bend) cm$^{-1}$.

*2-(2-phenylacetoxy)ethyl 4-oxopentanoate,* ***3e****,* *[$C_6H_5CH_2C(=O)OCH_2CH_2O(O=)CCH_2CH_2C(=O)CH_3$]* The compound was obtained as a colourless oil (96% yield). $^1$H-NMR ($CDCl_3$, 400 MHz) δ = 7.37-7.21 (m, 5H, overlapped with $CHCl_3$ signal, C$_6$*$H_5$*), 4.32-4.26 (m, 4H, OC*$H_2$*C*$H_2$*O), 3.66 (s, 2H, $C_6H_5$C*$H_2$*C(=O)O), 2.72 (t, J = 6.7 Hz, 2H, $CH_2$C*$H_2$*C(=O)$CH_3$), 2.56 (t, J = 6.5 Hz, 2H, C*$H_2$*$CH_2$C(=O)$CH_3$), 2.18 (s, 3H, $CH_2$C(=O)C*$H_3$*) ppm. ATR/FT-IR n = 2961, 2916 (sp$^3$ C-H stretch); 1729, 1717 (C=O stretch); 1601 (aromatic C=C stretch); 724, 708, 697 (aromatic sp$^2$ C-H bend) cm$^{-1}$.

## 6.4. Yields, $^{1}$H- and $^{13}$C-NMR and FT-IR assignments of the final products (4a-e)

*2-((3-(2-methyl-1,3-dioxan-2-yl)propanoyl)oxy)ethyl tetradecanoate,* ***4a****,* *[$CH_3(CH_2)_{10}CH_2CH_2C(=O)OCH_2CH_2O(O=)CCH_2CH_2C(-OCH_2CHH'CH_2O-)CH_3$]* The compound was obtained as a colorless oil (55% yield). $^{1}$H-NMR ($CDCl_3$, 400 MHz) δ = 4.27 (s, 4H, $OCH_2CH_2O$), 3.97-3.81 (m, 4H, $C(-OCH_2CHH'CH_2O-)$), 2.49 (t, J = 7.9 Hz, 2H, $O(O=)CCH_2CH_2$), 2.32 (t, J = 7.5 Hz, 2H, $CH_2CH_2C(=O)O$), 2.03 (t, J = 7.9 Hz, 2H, $O(O=)CCH_2CH_2$), 1.86-1.74 (m, 1H, $C(-OCH_2CHH'CH_2O-)$), 1.67-1.58 (m, 2H, $CH_2CH_2C(=O)O$), 1.56-1.49 (m, 1H, $C(-OCH_2CHH'CH_2O-)$), 1.40 (s, 3H, $C(-OCH_2CHH'CH_2O-)CH_3$), 1.34-1.21 (m, 20H, $CH_3(CH_2)_{10}$), 0.88 (t, J = 6.8 Hz, 3H, $CH_3(CH_2)_{10}$) ppm. $^{13}$C-NMR ($CDCl_3$, 150 MHz δ = 173.83 ($O(O=)CCH_2CH_2$), 173.77 ($CH_2CH_2C(=O)O$), 98.1 ($C(-OCH_2CHH'CH_2O-)$), 62.2 ($OCH_2CH_2O$), 62.1 ($OCH_2CH_2O$), 59.9 ($C(-OCH_2CHH'CH_2O-)$), 34.3 ($CH_2CH_2C(=O)O$), 34.1 ($O(O=)CCH_2CH_2$), 32.0 ($CH_3(CH_2)_{10}$), 29.8 ($CH_3(CH_2)_{10}$), 29.78 ($CH_3(CH_2)_{10}$), 29.75 ($CH_3(CH_2)_{10}$), 29.6 ($CH_3(CH_2)_{10}$), 29.5 ($CH_3(CH_2)_{10}$), 29.4 ($CH_3(CH_2)_{10}$), 29.3 ($CH_3(CH_2)_{10}$), 28.5 ($O(O=)CCH_2CH_2$), 25.5 ($C(-OCH_2CHH'CH_2O-)$), 25.0 ($CH_2CH_2C(=O)O$), 22.8 ($CH_3(CH_2)_{10}$), 20.6 ($C(-OCH_2CHH'CH_2O-)CH_3$), 14.2 ($CH_3(CH_2)_{10}$) ppm. ATR/FT-IR n = 2923, 2854 ($sp^3$ C-H stretch); 1738 (C=O stretch); 1115, 1092, 1056, 968 (acetal C-O) $cm^{-1}$.

*2-((3-(2-methyl-1,3-dioxan-2-yl)propanoyl)oxy)ethyl stearate,* ***4b****,* *[$CH_3(CH_2)_{14}CH_2CH_2C(=O)OCH_2CH_2O(O=)CCH_2CH_2C(-OCH_2CHH'CH_2O-)CH_3$]* The compound was obtained as a colorless oil (60% yield). $^{1}$H-NMR ($CDCl_3$, 400 MHz) δ = 4.27 (s, 4H, $OCH_2CH_2O$), 3.98-3.81 (m, 4H, $C(-OCH_2CHH'CH_2O-)$), 2.48 (t, J = 8.0 Hz, 2H, $O(O=)CCH_2CH_2$), 2.32 (t, J = 7.5 Hz, 2H, $CH_2CH_2C(=O)O$), 2.03 (t, J = 7.8 Hz, 2H, $O(O=)CCH_2CH_2$), 1.86-1.74 (m, 1H, $C(-OCH_2CHH'CH_2O-)$), 1.67-1.59 (m, 2H, $CH_2CH_2C(=O)O$), 1.56-1.49 (m, 1H, $C(-OCH_2CHH'CH_2O-)$), 1.40 (s, 3H, $C(-OCH_2CHH'CH_2O-)CH_3$), 1.34-1.22 (m, 28H, $CH_3(CH_2)_{14}$), 0.88 (t, J = 6.8 Hz, 3H, $CH_3(CH_2)_{14}$) ppm. $^{13}$C-NMR ($CDCl_3$, 150 MHz) δ = 173.82 ($O(O=)CCH_2CH_2$), 173.76 ($CH_2CH_2C(=O)O$), 98.3 ($C(-OCH_2CHH'CH_2O-)$), 62.2 ($OCH_2CH_2O$), 62.1 ($OCH_2CH_2O$), 59.9 ($C(-OCH_2CHH'CH_2O-)$), 34.3 ($CH_2CH_2C(=O)O$), 34.1 ($O(O=)CCH_2CH_2$), 32.1 ($CH_3(CH_2)_{14}$), 29.83 ($CH_3(CH_2)_{14}$), 29.82 ($CH_3(CH_2)_{14}$), 29.79 ($CH_3(CH_2)_{14}$), 29.75 ($CH_3(CH_2)_{14}$), 29.6 ($CH_3(CH_2)_{14}$), 29.5 ($CH_3(CH_2)_{14}$), 29.4 ($CH_3(CH_2)_{14}$), 29.3 ($CH_3(CH_2)_{14}$), 28.5 ($O(O=)CCH_2CH_2$),

25.5 (C(-OCH$_2$*C*HH'CH$_2$O-)), 25.0 (*C*H$_2$CH$_2$C(=O)O), 22.8 (CH$_3$(*C*H$_2$)$_{14}$), 20.6 (C(-OCH$_2$CHH'CH$_2$O-)*C*H$_3$), 14.2 (*C*H$_3$(CH$_2$)$_{14}$) ppm. ATR/FT-IR n = 2917, 2850 (sp$^3$ C-H stretch); 1737 (C=O stretch); 1116, 1091, 1056, 967 (acetal C-O) cm$^{-1}$.

*2-((3-(2-methyl-1,3-dioxan-2-yl)propanoyl)oxy)ethyl 3-methylbutanoate,* ***4c****, [(CH$_3$)$_2$CHCH$_2$C(=O)OCH$_2$CH$_2$O(O=)CCH$_2$CH$_2$C(-OCH$_2$CHH'CH$_2$O-)CH$_3$]* The compound was obtained as a colorless oil (50% yield). $^1$H-NMR (CDCl$_3$, 400 MHz) δ = 4.27 (s, 4H, OC*H$_2$*C*H$_2$*O), 3.97-3.81 (m, 4H, C(-OC*H$_2$*CHH'C*H$_2$*O-)), 2.48 (t, J = 7.8 Hz, 2H, O(O=)CC*H$_2$*CH$_2$), 2.22 (d, J = 7.1 Hz, 2H, (CH$_3$)$_2$CHC*H$_2$*), 2.16-2.06 (m, 1H, (CH$_3$)$_2$C*H*CH$_2$), 2.03 (t, J = 7.7 Hz, 2H, O(O=)CCH$_2$C*H$_2$*), 1.86-1.74 (m, 1H, C(-OCH$_2$C*H*H'CH$_2$O-)), 1.58-1.49 (m, 1H, C(-OCH$_2$CH*H'*CH$_2$O-)), 1.40 (s, 3H, C(-OCH$_2$CHH'CH$_2$O-)C*H$_3$*), 0.96 (d, J = 6.7 Hz, 6H, (C*H$_3$*)$_2$CH) ppm. $^{13}$C-NMR (CDCl$_3$, 150 MHz) δ = 173.8 (O(O=)*C*CH$_2$CH$_2$), 173.0 ((CH$_3$)$_2$CHCH$_2$*C*(=O)O), 98.1 (*C*(-OCH$_2$CHH'CH$_2$O-)), 62.2 (O*C*H$_2$CH$_2$O), 62.0 (OCH$_2$*C*H$_2$O), 59.9 (C(-O*C*H$_2$CHH'*C*H$_2$O-)), 43.3 ((CH$_3$)$_2$CH*C*H$_2$C(=O)O), 34.0 (O(O=)CCH$_2$*C*H$_2$), 28.4 (O(O=)C*C*H$_2$CH$_2$), 25.8 (C(-OCH$_2$*C*HH'CH$_2$O-)), 25.5 ((CH$_3$)$_2$*C*HCH$_2$C(=O)O), 22.5 ((*C*H$_3$)$_2$CHCH$_2$C(=O)O), 20.6 (C(-OCH$_2$CHH'CH$_2$O-)*C*H$_3$) ppm. ATR/FT-IR n = 2959, 2871 (sp$^3$ C-H stretch); 1735 (C=O stretch); 1116, 1090, 1056, 968 (acetal C-O) cm$^{-1}$.

*2-((3-(2-methyl-1,3-dioxan-2-yl)propanoyl)oxy)ethyl benzoate,* ***4d****, [C$_6$H$_5$C(=O)OCH$_2$CH$_2$O(O=)CCH$_2$CH$_2$C(-OCH$_2$CHH'CH$_2$O-)CH$_3$]* The compound was obtained as a colorless oil (50% yield). $^1$H-NMR (CDCl$_3$, 400 MHz) δ = 8.05 (d, J = 8.3, 2H, *ortho*), 7.57 (t, J = 7.4 Hz, 1H, *para*), 7.45 (t, J = 7.9 Hz, 2H, *meta*), 4.56-4.49 (m, 2H, OC*H$_2$*CH$_2$O), 4.45-4.39 (m, 2H, OCH$_2$C*H$_2$*O), 3.95-3.78 (m, 4H, C(-OC*H$_2$*CHH'C*H$_2$*O-)), 2.50 (t, J= 7.6 Hz, 2H, O(O=)CC*H$_2$*CH$_2$), 2.03 (t, J= 7.8 Hz, 2H, O(O=)CCH$_2$C*H$_2$*), 1.83-1.70 (m, 1H, C(-OCH$_2$C*H*H'CH$_2$O-)), 1.55-1.45 (m, 1H, C(-OCH$_2$CH*H'*CH$_2$O-)), 1.38 (s, 3H, C(-OCH$_2$CHH'CH$_2$O-)C*H$_3$*) ppm. $^{13}$C-NMR (CDCl$_3$, 150 MHz) δ =173.9 (O(O=)*C*CH$_2$CH$_2$), 166.5 (C$_6$H$_5$*C*(=O)O), 133.3 (*para* carbon), 130.0 (quaternary aromatic carbon), 129.8 (*ortho* carbons), 128.5 (*meta* carbon), 98.3 (*C*(-OCH$_2$CHH'CH$_2$O-)), 62.9 (O*C*H$_2$CH$_2$O), 62.2 (OCH$_2$*C*H$_2$O), 59.9 (C(-O*C*H$_2$CHH'*C*H$_2$O-)), 34.1 (O(O=)CCH$_2$*C*H$_2$), 28.5 (O(O=)C*C*H$_2$CH$_2$), 25.5 (C(-OCH$_2$*C*HH'CH$_2$O-)), 20.6 (C(-OCH$_2$CHH'CH$_2$O-)*C*H$_3$) ppm. ATR/FT-IR n = 2954,

2869 ($sp^3$ C-H stretch); 1717 (C=O stretch); 1602, 1585 (aromatic C=C stretch); 1095, 964 (acetal C-O); 711, 687, 674 (aromatic $sp^2$ C-H bend) $cm^{-1}$.

*2-(2-phenylacetoxy)ethyl 3-(2-methyl-1,3-dioxan-2-yl)propanoate,* ***4e****, [$C_6H_5CH_2C(=O)OCH_2CH_2O(O=)CCH_2CH_2C(-OCH_2CHH'CH_2O-)CH_3$]* The compound was obtained as a colorless oil (50% yield). $^1$H-NMR ($CDCl_3$, 400 MHz) δ = 7.36-7.26 (m, 5H, $C_6H_5$), 4.32-4.25 (m, 4H, $OCH_2CH_2O$), 3.97-3.81 (m, 4H, $C(-OCH_2CHH'CH_2O-)$), 3.65 (s, 2H, $C_6H_5CH_2C(=O)O$), 2.46 (t, J = 7.8 Hz, 2H, $O(O=)CCH_2CH_2$), 2.01 (t, J = 8.0 Hz, 2H, $O(O=)CCH_2CH_2$), 1.86-1.74 (m, 1H, $C(-OCH_2CHH'CH_2O-)$), 1.58-1.49 (m, 1H, $C(-OCH_2CHH'CH_2O-)$), 1.40 (s, 3H, $C(-OCH_2CHH'CH_2O-)CH_3$) ppm. $^{13}$C-NMR ($CDCl_3$, 150 MHz) δ = 173.8 ($O(O=)CCH_2CH_2$), 171.5 ($C_6H_5CH_2C(=O)O$), 133.9 (quaternary aromatic carbon), 129.4 (*para* carbon), 128.7 (*ortho* carbons), 127.3 (*meta* carbons), 98.3 ($C(-OCH_2CHH'CH_2O-)$), 62.7 ($OCH_2CH_2O$), 62.0 ($OCH_2CH_2O$), 59.9 ($C(-OCH_2CHH'CH_2O-)$), 41.3 ($C_6H_5CH_2C(=O)O$), 34.0 ($O(O=)CCH_2CH_2$), 28.4 ($O(O=)CCH_2CH_2$), 25.5 ($C(-OCH_2CHH'CH_2O-)$), 20.6 ($C(-OCH_2CHH'CH_2O-)CH_3$) ppm. ATR/FT-IR n = 2957, 2871 ($sp^3$ C-H stretch); 1733 (C=O stretch); 1602 (aromatic C=C stretch); 1144, 1050, 964 (acetal C-O); 725, 707, 697 (aromatic $sp^2$ C-H bend) $cm^{-1}$.

## 6.5. 2D-NMR characterization of the ketal-diesters 4a-e

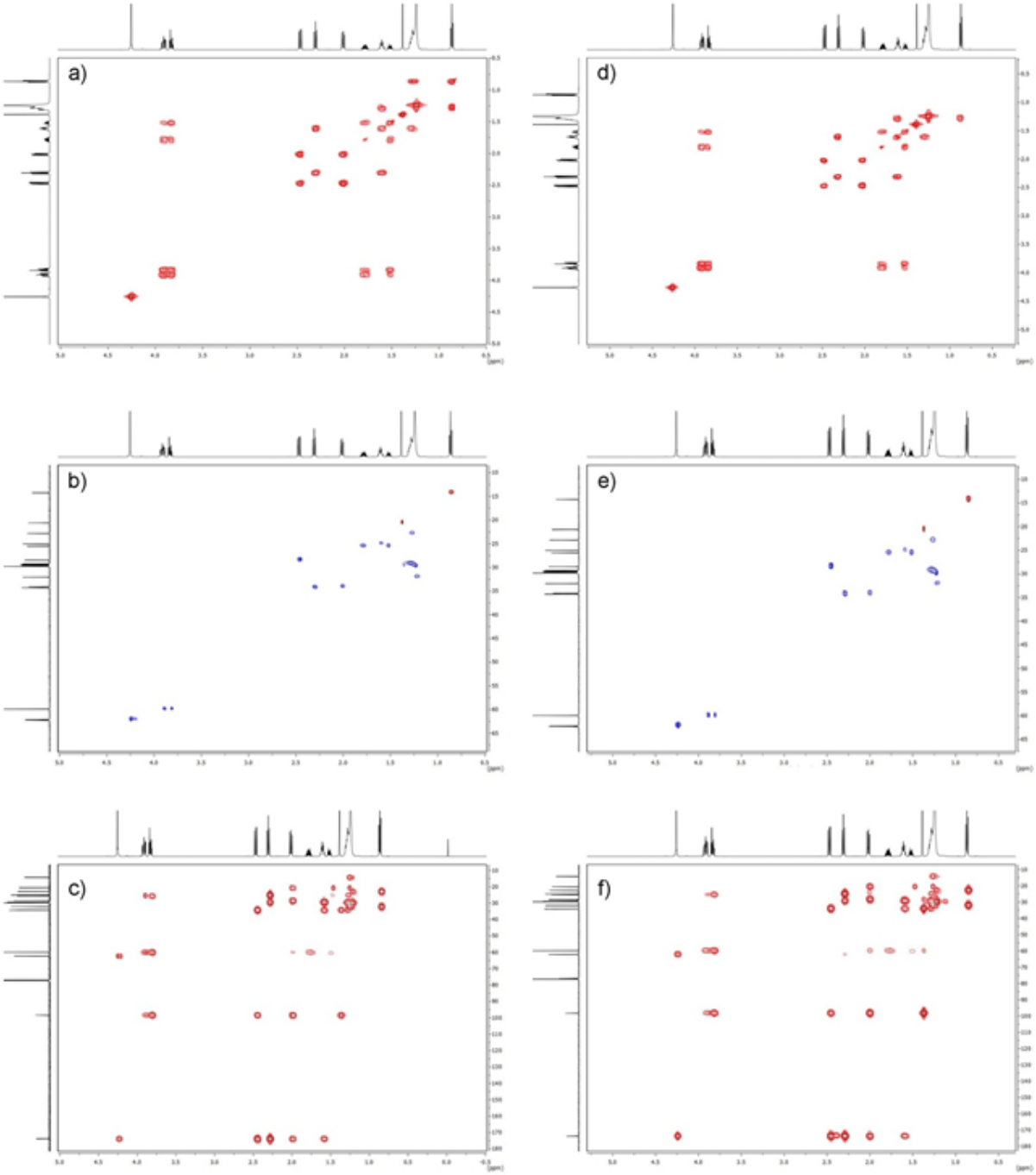


**Figure 43.** $^{1}$H-$^{1}$H COSY, $^{1}$H-$^{13}$C HSQC and $^{1}$H-$^{13}$C HMBC spectra of additives (a-c) **4a** and (d-f) **4b**. [Residual solvent signals: $CHCl_3$, 7.26 ppm for $^{1}$H-NMR and $CHCl_3$, 77.16 ppm for $^{13}$C-NMR].

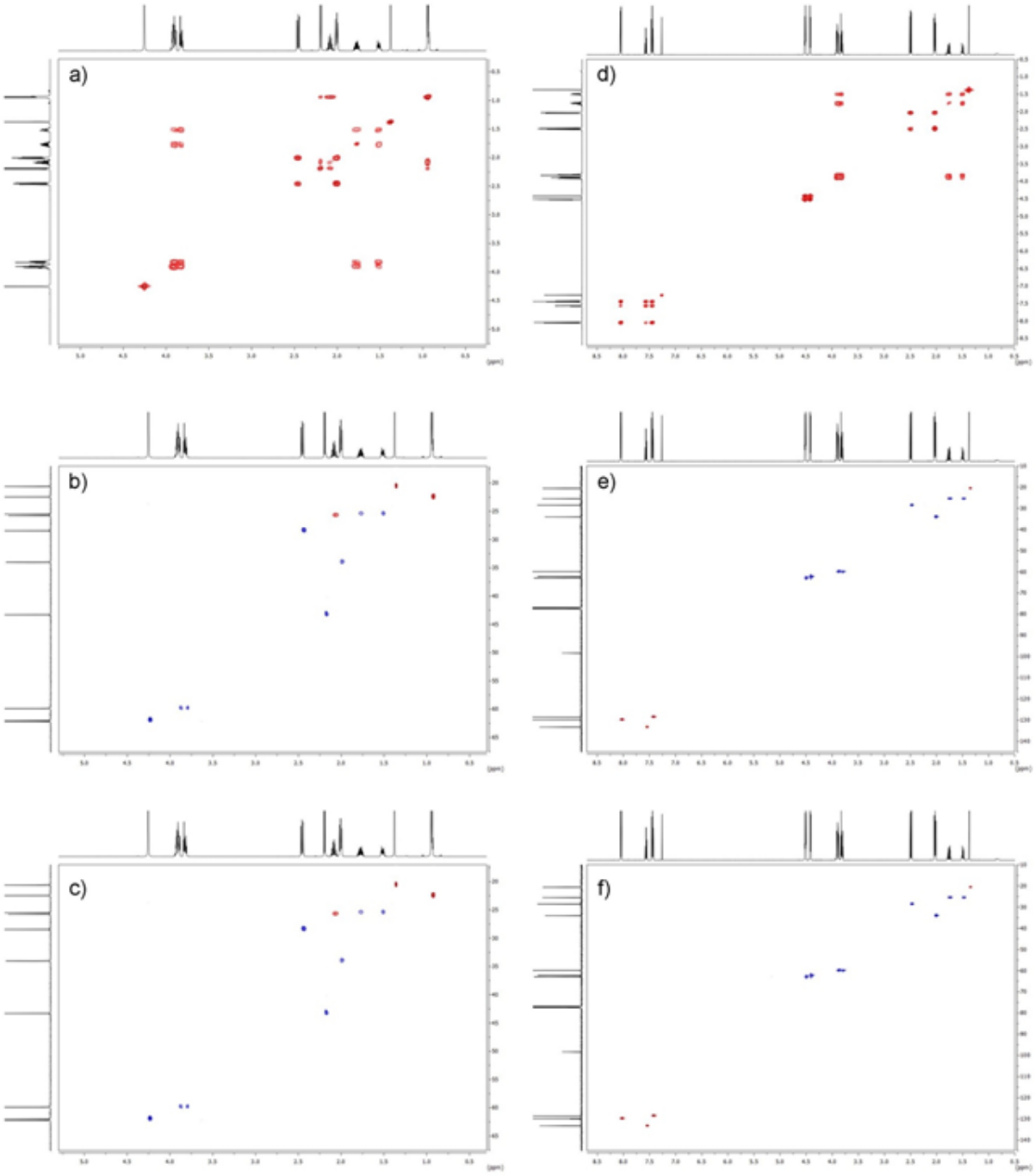


**Figure 44.** $^{1}$H-$^{1}$H COSY, $^{1}$H-$^{13}$C HSQC and $^{1}$H-$^{13}$C HMBC spectra of additives (a-c) **4c** and (d-f) **4d**. [Residual solvent signals: $CHCl_3$, 7.26 ppm for $^{1}$H-NMR and $CHCl_3$, 77.16 ppm for $^{13}$C-NMR].

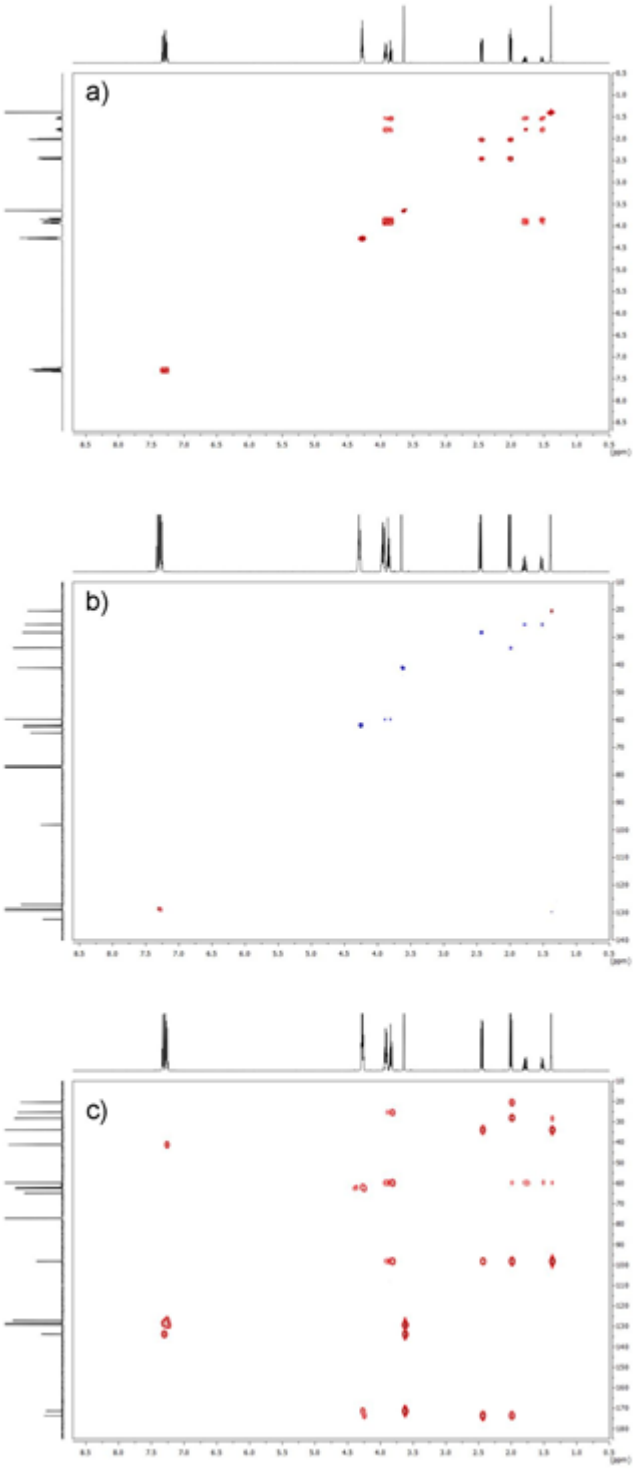


**Figure 45.** $^{1}$H-$^{1}$H COSY, $^{1}$H-$^{13}$C HSQC and $^{1}$H-$^{13}$C HMBC spectra of additive (a-c) **4e**. [Residual solvent signals: $CHCl_3$, 7.26 ppm for $^{1}$H-NMR and $CHCl_3$, 77.16 ppm for $^{13}$C-NMR].

# 7. REFERENCES


(1) Smith, P. B.; Payne, G. F. The Emergence of Renewable and Sustainable Polymers. In *Renewable and Sustainable Polymers*; Payne, G. F., Smith, P. B., Eds.; American Chemical Society: Washington, DC, 2011; Vol. 1063, pp 1–10.

(2) Chen, G. Q.; Patel, M. K. Plastics Derived from Biological Sources: Present and Future: A Technical and Environmental Review. *Chem. Rev.* **2012**, *112* (4), 2082–2099.

(3) Ravenstijn, J. Bioplastics in the Consumer Electronics Industry. *Ind. Biotechnol.* **2010**, 252.

(4) Harmon, J. P.; Otter, R. Green Chemistry and the Search for New Plasticizers. *ACS Sustain. Chem. Eng.* **2018**, *6*, 2078–2085.

(5) Hahladakis, J. N.; Velis, C. A.; Weber, R.; Iacovidou, E.; Purnell, P. An Overview of Chemical Additives Present in Plastics: Migration, Release, Fate and Environmental Impact during Their Use, Disposal and Recycling. *J. Hazard. Mater.* **2018**, *344*, 179–199.

(6) Yates, M. R.; Barlow, C. Y. Life Cycle Assessments of Biodegradable, Commercial Biopolymers - A Critical Review. *Resour. Conserv. Recycl.* **2013**, *78*, 54–66.

(7) Hopewell, J.; Dvorak, R.; Kosior, E. Plastics Recycling: Challenges and Opportunities. *Philos. Trans. R. Soc. B Biol. Sci.* **2009**, *364* (1526), 2115–2126.

(8) Babu, R. P.; O'Connor, K.; Seeram, R. Current Progress on Bio-Based Polymers and Their Future Trends. *Prog. Biomater.* **2013**, *2* (8), 1–16.

(9) Song, J. H.; Murphy, R. J.; Narayan, R.; Davies, G. B. H. Biodegradable and Compostable Alternatives to Conventional Plastics. *Philos. Trans. R. Soc. B Biol. Sci.* **2009**, *364* (1526), 2127–2139.

(10) Niaounakis, M. Introduction. In *Biopolymers: Processing and Products*; Niaounakis, M., Ed.; William Andrew Publishing, 2015; pp 1–77.

(11) Niaounakis, M. Blending. In *Biopolymers: Processing and Products*; Niaounakis, M., Ed.; William Andrew Publishing, 2015; pp 117–185.

(12) C. J. Bart, J. *Additives in Polymers: Industrial Analysis and Applications*; John Wiley & Sons Ltd, Ed.; John Wiley & Sons Ltd: The Atrium, Southern Gate,

Chichester, West Sussex PO19 8SQ, England, 2005.

(13) Murphy, J. Types of Additive and the Main Technical Trends. In *Additives for Plastics Handbook*; Murphy, J., Ed.; Elsevier Science Publishers LTD, 2001; pp 5–11.

(14) Niaounakis, M. Compounding and Additives. In *Biopolymers: Processing and Products*; Niaounakis, M., Ed.; William Andrew Publishing, 2015; pp 215–262.

(15) Erythropel, H. C.; Maric, M.; Cooper, D. G. Designing Green Plasticizers: Influence of Molecular Geometry on Biodegradation and Plasticization Properties. *Chemosphere* **2012**, *86*, 759–766.

(16) Stepek, J.; Daoust, H. *Additives for Plastic*; Springer Science+Business Media, LLC: New York, 1983; Vol. 53.

(17) Murphy, J. Modifying Processing Characteristics: Plasticizers. In *Additives for Plastics Handbook*; Murphy, J., Ed.; Elsevier Science Publishers LTD, 2001; pp 169–175.

(18) Vieira, M. G. A.; Da Silva, M. A.; Dos Santos, L. O.; Beppu, M. M. Natural-Based Plasticizers and Biopolymer Films: A Review. *Eur. Polym. J.* **2011**, *47* (3), 254–263.

(19) Rahman, M.; Brazel, C. S. The Plasticizer Market: An Assessment of Traditional Plasticizers and Research Trends to Meet New Challenges. *Prog. Polym. Sci.* **2004**, *29* (12), 1223–1248.

(20) Marcilla, A.; Beltran, M. Mechanisms of Plasticizers Action. In *Handbook of Plasticizers*; Wypych, G., Ed.; William Andrew Publishing: Norwich, NY, USA, 2012; pp 119–133.

(21) Daniels, P. H. A Brief Overview of Theories of PVC Plasticization and Methods Used to Evaluate PVC-Plasticizer Interaction. *J. Vinyl Addit. Technol.* **2009**, *15* (4), 219–223.

(22) Senichev, V. Y.; Tereshatov, V. V. Theories of Compatibility. In *Handbook of Plasticizers*; Wypych, G., Ed.; William Andrew Publishing: Norwich, NY, USA, 2012; pp 135–164.

(23) Mauritz, K. A.; Storey, R. F.; Wilson, B. S. Efficiency of Plasticization of PVC Higher-Order Di-Alkyl Phthalates and Survey of Mathematical Models for Prediction of Polymer/Diluent Blend Tg's. *J. Vinyl Technol.* **1990**, *12* (3), 165–173.

(24) Kirkpatrick, A. Some Relations Between Molecular Structure and Plasticizing

Effect. *J. Appl. Phys.* **1940**, *11* (4), 255–261.

(25) Aiken, W.; Alfrey, T. J.; Janssen, A.; Mark, H. Creep Behavior of Plasticized Vinylite VY NW*. *J. Polym. Sci.* **1947**, *2* (2), 178–198.

(26) Sinisi, A.; Degli Esposti, M.; Toselli, M.; Morselli, D.; Fabbri, P. Biobased Ketal–Diester Additives Derived from Levulinic Acid: Synthesis and Effect on the Thermal Stability and Thermo-Mechanical Properties of Poly(Vinyl Chloride). *ACS Sustain. Chem. Eng.* **2019**, *7* (16), 13920–13931.

(27) Erythropel, H. C.; Shipley, S.; Börmann, A.; Nicell, J. A.; Maric, M.; Leask, R. L. Designing Green Plasticizers: Influence of Molecule Geometry and Alkyl Chain Length on the Plasticizing Effectiveness of Diester Plasticizers in PVC Blends. *Polymer (Guildf).* **2016**, *89*, 18–27.

(28) Wypych, G. Plasticizer Types. In *Handbook of Plasticizers*; Wypych, G., Ed.; William Andrew Publishing: Norwich, NY, USA, 2012; pp 7–83.

(29) Krauskopf, L. G.; Godwin, A. Plasticizers. In *PVC Handbook*; Daniels, C. A., Wilkes, C. E., Summers, J. W., Eds.; Hanser Publications: Cincinnati, OH, USA, 2005; pp 173–193.

(30) Cadogan, D. F.; Howick, C. J. Plasticizers. In *Ullmann's Encyclopedia of Industrial Chemistry*; Wiley-VCH Verlag GmbH & Co. KGaA: Weinheim, 2012; pp 599–618.

(31) Feige, J. N.; Gelman, L.; Rossi, D.; Zoete, V.; Métivier, R.; Tudor, C.; Anghel, S. I.; Grosdidier, A.; Lathion, C.; Engelborghs, Y.; et al. The Endocrine Disruptor Monoethyl-Hexyl-Phthalate Is a Selective Peroxisome Proliferator-Activated Receptor γ Modulator That Promotes Adipogenesis. *J. Biol. Chem.* **2007**, *282* (26), 19152–19166.

(32) Larsen, S. T. Health and Safety Issues With Plasticizers and Plasticized Materials. In *Handbook of Plasticizers*; Wypych, G., Ed.; William Andrew Publishing, 2012; pp 581–640.

(33) United States Congress. *PUBLIC LAW 110–314—AUG. 14, 2008, CONSUMER PRODUCT SAFETY IMPROVEMENT ACT*; 2008.

(34) Minister of Supply and Services Canada. PRIORITY SUBSTANCES LIST ASSESSMENT REPORT: BIS (2-ETHYLHEXYL) PHTHALATE. 1994.

(35) European Parliament. Directive 2005/84/EC Of The European Parliament And The Council. *Official Journal of the European Union*. 2005, pp 40–43.

(36) Yuan, J.; Cheng, B. A Strategy for Nonmigrating Highly Plasticized PVC. *Sci.*

*Rep.* **2017**, *7*, 1–6.

(37) Jia, P.; Zhang, M.; Hu, L.; Song, F.; Feng, G.; Zhou, Y. A Strategy for Nonmigrating Plasticized PVC Modified with Mannich Base of Waste Cooking Oil Methyl Ester. *Sci. Rep.* **2018**, *8*, 1–8.

(38) Lindström, A.; Hakkarainen, M. Migration Resistant Polymeric Plasticizer for Poly(Vinyl Chloride). *J. Appl. Polym. Sci.* **2007**.

(39) Lakeev, S. N.; Maydanova, I. O.; Mullakhmetov, R. F.; Davydova, O. V. Ester Plasticizers for Polyvinyl Chloride. *Russ. J. Appl. Chem.* **2016**, *89* (1), 1–15.

(40) Hosney, H.; Nadiem, B.; Ashour, I.; Mustafa, I.; El-Shibiny, A. Epoxidized Vegetable Oil and Bio-Based Materials as PVC Plasticizer. *Journal of Applied Polymer Science*. 2018.

(41) Lee, S.; Park, M. S.; Shin, J.; Kim, Y.-W. Effect of the Individual and Combined Use of Cardanol-Based Plasticizers and Epoxidized Soybean Oil on the Properties of PVC. *Polym. Degrad. Stab.* **2018**, *147*, 1–11.

(42) Feng, G.; Hu, L.; Ma, Y.; Jia, P.; Hu, Y.; Zhang, M.; Liu, C.; Zhou, Y. An Efficient Bio-Based Plasticizer for Poly (Vinyl Chloride) from Waste Cooking Oil and Citric Acid: Synthesis and Evaluation in PVC Films. *J. Clean. Prod.* **2018**, *189*, 334–343.

(43) Erythropel, H. C.; Brown, T.; Maric, M.; Nicell, J. A.; Cooper, D. G.; Leask, R. L. Designing Greener Plasticizers: Effects of Alkyl Chain Length and Branching on the Biodegradation of Maleate Based Plasticizers. *Chemosphere* **2015**, *134*, 106–112.

(44) Jamarani, R.; Erythropel, H. C.; Nicell, J. A.; Leask, R. L.; Marić, M. How Green Is Your Plasticizer? *Polymers*. 2018.

(45) Erythropel, H. C.; Dodd, P.; Leask, R. L.; Maric, M.; Cooper, D. G. Designing Green Plasticizers: Influence of Alkyl Chain Length on Biodegradation and Plasticization Properties of Succinate Based Plasticizers. *Chemosphere* **2013**, *91*, 358–365.

(46) Isikgor, F. H.; Becer, C. R. Lignocellulosic Biomass: A Sustainable Platform for the Production of Bio-Based Chemicals and Polymers. *Polym. Chem.* **2015**, *6* (25), 4497–4559.

(47) Zhou, C. H.; Xia, X.; Lin, C. X.; Tong, D. S.; Beltramini, J. Catalytic Conversion of Lignocellulosic Biomass to Fine Chemicals and Fuels. *Chem. Soc. Rev.* **2011**, *40* (11), 5588–5617.

(48) Ten, E.; Vermerris, W. Functionalized Polymers from Lignocellulosic Biomass: State of the Art. *Polymers (Basel).* **2013**, *5* (2), 600–642.

(49) Ragauskas, A. J.; Williams, C. K.; Davison, B. H.; Britovsek, G.; Cairney, J.; Eckert, C. A.; Frederick, W. J.; Hallett, J. P.; Leak, D. J.; Liotta, C. L.; et al. The Path Forward for Biofuels and Biomaterials. *Science (80-. ).* **2006**, *311* (5760), 484–489.

(50) Sun, Y.; Cheng, J. Hydrolysis of Lignocellulosic Materials for Ethanol Production: A Review. *Bioresour. Technol.* **2002**, *83* (1), 1–11.

(51) Werpy, T.; Petersen, G. *Top Value Added Chemicals from Biomass: Volume 1 - Results of Screening for Potential Candidates from Sugars and Synthesis Gas*; 2004.

(52) Bozell, J. J.; Moens, L.; Elliott, D. C.; Wang, Y.; Neuenscwander, G. G.; Fitzpatrick, S. W.; Bilski, R. J.; Jarnefeld, J. L. Production of Levulinic Acid and Use as a Platform Chemical for Derived Products. *Resour. Conserv. Recycl.* **2000**, *28*, 227–239.

(53) Yan, K.; Jarvis, C.; Gu, J.; Yan, Y. Production and Catalytic Transformation of Levulinic Acid: A Platform for Speciality Chemicals and Fuels. *Renew. Sustain. Energy Rev.* **2015**, *51*, 986–997.

(54) Pileidis, F. D.; Titirici, M.-M. Levulinic Acid Biorefineries: New Challenges for Efficient Utilization of Biomass. *ChemSusChem* **2016**, *9*, 562–582.

(55) Hayes, D. J.; Fitzpatrick, S.; Hayes, M. H. B.; Ross, J. R. H. The Biofine Process - Production of Levulinic Acid, Furfural, and Formic Acid from Lignocellulosic Feedstocks. *Biorefineries-Industrial Process. Prod. Status Quo Futur. Dir.* **2008**, *1*, 139–164.

(56) Freitas, F. A.; Licursi, D.; Lachter, E. R.; Raspolli Galletti, A. M.; Antonetti, C.; Brito, T. C.; Nascimento, R. S. V. Heterogeneous Catalysis for the Ketalisation of Ethyl Levulinate with 1,2-Dodecanediol : Opening the Way to a New Class of Bio-Degradable Surfactants. *Catal. Commun.* **2016**, *73*, 84–87.

(57) Xuan, W.; Hakkarainen, M.; Odelius, K. Levulinic Acid as a Versatile Building Block for Plasticizer Design. *ACS Sustain. Chem. Eng.* **2019**, *7*, 12552–12562.

(58) Mullen, B. D.; Badarinarayana, V.; Santos-Martinez, M.; Selifonov, S. Catalytic Selectivity of Ketalization versus Transesterification. *Top. Catal.* **2010**, *53*, 1235–1240.

(59) Amarasekara, A. S.; Hawkins, S. A. Synthesis of Levulinic Acid-Glycerol Ketal-

Ester Oligomers and Structural Characterization Using NMR Spectroscopy. *Eur. Polym. J.* **2011**, *47*, 2451–2457.

(60) Amarasekara, A. S.; Animashaun, M. A. Acid Catalyzed Competitive Esterification and Ketalization of Levulinic Acid with 1,2 and 1,3-Diols: The Effect of Heterogeneous and Homogeneous Catalysts. *Catal. Letters* **2016**, *146*, 1819–1824.

(61) Upton, B. M.; Kasko, A. M. Strategies for the Conversion of Lignin to High-Value Polymeric Materials: Review and Perspective. *Chemical Reviews*. 2016.

(62) Tuck, C. O.; Pérez, E.; Horváth, I. T.; Sheldon, R. A.; Poliakoff, M. Valorization of Biomass: Deriving More Value from Waste. *Science (80-. ).* **2012**, *337* (6095), 695–699.

(63) Kai, D.; Tan, M. J.; Chee, P. L.; Chua, Y. K.; Yap, Y. L.; Loh, X. J. Towards Lignin-Based Functional Materials in a Sustainable World. *Green Chemistry*. 2016, pp 1175–1200.

(64) Gioia, C.; Lo Re, G.; Lawoko, M.; Berglund, L. Tunable Thermosetting Epoxies Based on Fractionated and Well-Characterized Lignins. *J. Am. Chem. Soc.* **2018**, *140* (11), 4054–4061.

(65) Stewart, D. Lignin as a Base Material for Materials Applications: Chemistry, Application and Economics. *Ind. Crops Prod.* **2008**, *27* (2), 202–207.

(66) Lora, J. Industrial Commercial Lignins: Sources, Properties and Applications. In *Monomers, Polymers and Composites*; Belgacem, M. N., Gandini, A., Eds.; Elsevier: New York, 2008; pp 225–241.

(67) Tomani, P. The Lignoboost Process. *Cellul. Chem. Technol.* **2010**, *44* (1–3), 53–58.

(68) Beine, A. K.; Hausoul, P. J. C.; Palkovits, R. Production of Ethylene and Propylene Glycol from Lignocellulose. In *Chemicals and Fuels from Bio-Based Building Blocks*; John Wiley & Sons, Incorporated, 2016; pp 245–270.

(69) Mallesham, B.; Govinda Rao, B.; Reddy, B. M. Production of Biofuel Additives by Esterification and Acetalization of Bioglycerol. *Comptes Rendus Chim.* **2016**.

(70) Talebian-Kiakalaieh, A.; Amin, N. A. S.; Najaafi, N.; Tarighi, S. A Review on the Catalytic Acetalization of Bio-Renewable Glycerol to Fuel Additives. *Front. Chem.* **2018**, *6* (NOV), 1–25.

(71) Cespi, D.; Passarini, F.; Mastragostino, G.; Vassura, I.; Larocca, S.; Iaconi, A.;

Chieregato, A.; Dubois, J. L.; Cavani, F. Glycerol as Feedstock in the Synthesis of Chemicals: A Life Cycle Analysis for Acrolein Production. *Green Chem.* **2015**, *17* (1), 343–355.

(72) Ciacci, L.; Passarini, F.; Vassura, I. The European PVC Cycle: In-Use Stock and Flows. *Resour. Conserv. Recycl.* **2017**, *123*, 108–116.

(73) Chiellini, F.; Ferri, M.; Morelli, A.; Dipaola, L.; Latini, G. Perspectives on Alternatives to Phthalate Plasticized Poly(Vinyl Chloride) in Medical Devices Applications. *Prog. Polym. Sci.* **2013**, *38* (7), 1067–1088.

(74) Hakkarainen, M. New PVC Materials for Medical Applications - The Release Profile of PVC/Polycaprolactone-Polycarbonate Aged in Aqueous Environments. *Polym. Degrad. Stab.* **2003**, *80* (3), 451–458.

(75) Titow, W. V. *PVC PLASTICS Properties, Processing, and Applications*; W. V. Titov, Ed.; Elsevier Science Publishers LTD: Barking, Essex IG11 8JU, England, 1990.

(76) Groover, M. P. *Fundamentals of Modern Manufacturing: Materials, Processes and Systems*; John Wiley & Sons, Inc.: Hoboken, New Jersey, USA, 2010.

(77) Chodak, I. Polyhydroxyalkanoates: Origin, Properties and Applications. In *Monomers, Polymers and Composites from Renewable Resources*; Belgacem, M. N., Gandini, A., Eds.; Elsevier: New York, 2008; pp 451–478.

(78) Hazer, B.; Steinbüchel, A. Increased Diversification of Polyhydroxyalkanoates by Modification Reactions for Industrial and Medical Applications. *Appl. Microbiol. Biotechnol.* **2007**, *74* (1), 1–12.

(79) Sharma, P. K.; Munir, R. I.; Blunt, W.; Dartiailh, C.; Cheng, J.; Charles, T. C.; Levin, D. B. Synthesis and Physical Properties of Polyhydroxyalkanoate Polymers with Different Monomer Compositions by Recombinant Pseudomonas Putida LS46 Expressing a Novel PHA SYNTHASE (PhaC116) Enzyme. *Appl. Sci.* **2017**, *7* (3).

(80) Nomura, C. T.; Tanaka, T.; Gan, Z.; Kuwabara, K.; Abe, H.; Takase, K.; Taguchi, K.; Doi, Y. Effective Enhancement of Short-Chain-Length - Medium-Chain-Length Polyhydroxyalkanoate Copolymer Production by Coexpression of Genetically Engineered 3-Ketoacyl-Acyl-Carrier-Protein Synthase III (FabH) and Polyhydroxyalkanoate Synthesis Genes. *Biomacromolecules* **2004**, *5* (4), 1457–1464.

(81) Numata, K.; Abe, H.; Iwata, T. Biodegradability of Poly(Hydroxyalkanoate)

Materials. *Materials (Basel).* **2009**, *2* (3), 1104–1126.

(82) Lemoigne, M. Lemoigne, 1925.Pdf. *Ann. Inst. Pasteur* **1925**, *39*, 144.

(83) Lemoigne, M. Produits de Dehydration et de Polymerisation de l'acide β-Oxobutyrique. *Bull. Soc. Chim. Biol.* **1926**, *8*, 770–782.

(84) Bugnicourt, E.; Cinelli, P.; Lazzeri, A.; Alvarez, V. Polyhydroxyalkanoate (PHA): Review of Synthesis, Characteristics, Processing and Potential Applications in Packaging. *Express Polym. Lett.* **2014**, *8* (11), 791–808.

(85) Weihua, K.; He, Y.; Asakawa, N.; Inoue, Y. Effect of Lignin Particles as a Nucleating Agent on Crystallization of Poly(3-Hydroxybutyrate). *J. Appl. Polym. Sci.* **2004**, *94* (6), 2466–2474.

(86) Kopinke, F. D.; Remmler, M.; Mackenzie, K. Thermal Decomposition of Biodegradable Polyesters - I: Poly(β-Hydroxybutyric Acid). *Polym. Degrad. Stab.* **1996**, *52* (1), 25–38.

(87) Goodship, V.; Jacobs, D. *Polyvinyl Alcohol: Materials, Processing and Applications*; Smithers Rapra Technology: Shawbury, Shrewsbury, Shropshire, SY4 4NR, United Kingdom, 2008.

(88) Huiyu, B. Preparation, Structure, Properties, and Interactions of the PVA/Cellulose Composites. In *Handbook of Composites from Renewable Materials*; Thakur, V. K., Thakur, M. K., Kessler, M. R., Eds.; Scrivener Publishing LLC, 2017; Vol. 7, pp 275–297.

(89) Qiu, K.; Netravali, A. N. *Polyvinyl Alcohol Based Biodegradable Polymer Nanocomposites*; 2015.

(90) Taghizadeh, M. T.; Yeganeh, N.; Rezaei, M. Kinetic Analysis of the Complex Process of Poly(Vinyl Alcohol) Pyrolysis Using a New Coupled Peak Deconvolution Method. *J. Therm. Anal. Calorim.* **2014**, *118* (3), 1733–1746.

(91) Chen, H.; Li, R.; Xu, X.; Zhao, P.; Wong, D. S. H.; Chen, X.; Chen, S.; Yan, X. Citrate-Based Fluorophores in Polymeric Matrix by Easy and Green in Situ Synthesis for Full-Band UV Shielding and Emissive Transparent Display. *J. Mater. Sci.* **2019**, *54* (2), 1236–1247.

(92) ASTM International. D1239-14 Resistance of Plastic Films to Extraction by Chemicals. 2014, pp 1–3.

(93) Panaitescu, D. M.; Nicolae, C. A.; Frone, A. N.; Chiulan, I.; Stanescu, P. O.; Draghici, C.; Iorga, M.; Mihailescu, M. Plasticized Poly(3-Hydroxybutyrate) with Improved Melt Processing and Balanced Properties. *J. Appl. Polym. Sci.* **2017**,

*134* (19), 1–14.

(94) Constant, S.; Wienk, H. L. J.; Frissen, A. E.; Peinder, P. De; Boelens, R.; Van Es, D. S.; Grisel, R. J. H.; Weckhuysen, B. M.; Huijgen, W. J. J.; Gosselink, R. J. A.; et al. New Insights into the Structure and Composition of Technical Lignins: A Comparative Characterisation Study. *Green Chem.* **2016**, *18* (9), 2651–2665.

(95) Fischer, E.; Speier, A. Darstellung Der Ester. *Ber. Dtsch. Chem. Ges.* **1895**, 3252–3258.

(96) Neises, B.; Steglich, W. Simple Method for the Esterification of Carboxylic Acids. *Angew. Chemie - Int. Ed.* **1978**, *17*, 522–524.

(97) Inanaga, J.; Hirata, K.; Saeki, H.; Katsuki, T.; Yamaguchi, M. A Rapid Esterification by Means of Mixed Anhydride and Its Application to Large-Ring Lactonization. *Bull. Chem. Soc. Jpn.* **1979**, *52* (7), 1989–1991.

(98) Mitsunobu, O.; Yamada, M. Preparation of Esters of Phosphoric Acid via Quaternary Phosphonium Salts. *J. Org. Chem.* **1965**, *30* (4), 1071–1073.

(99) Münster, A. The Le Chatelier-Braun Principle. In *Classical Thermodynamics*; Münster, A., Ed.; Wiley–Interscience: London, 1970; pp 173–174.

(100) Greene, T. W.; Wuts, P. G. M. *Protective Groups in Organic Synthesis*, Third Edit.; John Wiley & Sons Ltd: New York, 1999.

(101) Galbiati, E.; Zoppo, M. Del; Tieghi, G.; Zerbi, G. Dipole-Dipole Interactions in Simple Esters and in Liquid-Crystal Polyesters. *Polymer (Guildf).* **1993**, *34* (9), 1806–1810.

(102) Li, W.; Qin, J.; Wang, S.; Han, D.; Xiao, M.; Meng, Y. Macrodiols Derived from CO2-Based Polycarbonate as an Environmentally Friendly and Sustainable PVC Plasticizer: Effect of Hydrogen-Bond Formation. *ACS Sustain. Chem. Eng.* **2018**, *6*, 8476–8484.

(103) Aakeröy, C. B.; Evans, T. A.; Seddon, K. R.; Pálinkó, I. The C-H---Cl Hydrogen Bond : Does It Exist ? *New J. Chem.* **1999**, *23* (2), 145–152.

(104) Steiner, T. Unrolling the Hydrogen Bond Properties of C-H···O Interactions. *Chem. Commun.* **1997**, No. 8, 727–734.

(105) Steiner, T. Donor and Acceptor Strengths in C-H---O Hydrogen Bonds Quantified from Crystallographic Data of Small Solvent Molecules. *New J. Chem.* **1998**, *22* (10), 1099–1103.

(106) Daniels, P. H.; Cabrera, A. Plasticizer Compatibility Testing: Dynamic

Mechanical Analysis and Glass Transition Temperatures. *J. Vinyl Addit. Technol.* **2015**, *21* (1), 7–11.

(107) Kastner, J.; Cooper, D. G.; Marić, M.; Dodd, P.; Yargeau, V. Aqueous Leaching of Di-2-Ethylhexyl Phthalate and “Green” Plasticizers from Poly(Vinyl Chloride). *Sci. Total Environ.* **2012**, *432*, 357–364.

(108) Akhina, H.; Gopinathan Nair, M. R.; Kalarikkal, N.; Pramoda, K. P.; Hui Ru, T.; Kailas, L.; Thomas, S. Plasticized PVC Graphene Nanocomposites: Morphology, Mechanical, and Dynamic Mechanical Properties. *Polym. Eng. Sci.* **2018**, *58*, E104–E113.

(109) Persico, P.; Ambrogi, V.; Acierno, D.; Carfagna, C. Processability and Mechanical Properties of Commercial PVC Plastisols Containing Low-Environmental-Impact Plasticizers. *J. Vinyl Addit. Technol.* **2009**, *15* (3), 139–146.

(110) Hornat, C. C.; Yang, Y.; Urban, M. W. Quantitative Predictions of Shape-Memory Effects in Polymers. *Adv. Mater.* **2017**, *29* (7), 1603334.

(111) Jia, P.; Hu, L.; Shang, Q.; Wang, R.; Zhang, M.; Zhou, Y. Self-Plasticization of PVC Materials via Chemical Modification of Mannich Base of Cardanol Butyl Ether. *ACS Sustain. Chem. Eng.* **2017**, *5* (8), 6665–6673.

(112) Jordan, K. J.; Suib, S. L.; Koberstein, J. T. Determination of the Degradation Mechanism from the Kinetic Parameters of Dehydrochlorinated Poly(Vinyl Chloride) Decomposition. *J. Phys. Chem. B* **2001**, *105* (16), 3174–3181.

(113) Steiner, T. Donor and Acceptor Strengths in C-H···O Hydrogen Bonds Quantified from Crystallographic Data of Small Solvent Molecules. *New J. Chem.* **1998**, *22* (10), 1099–1103.

(114) Steiner, T. The Hydrogen Bond in the Solid State. *Angew. Chemie - Int. Ed.* **2002**, *41* (1), 48–76.

(115) Starnes Jr., W. H.; Ge, X. Mechanism of Autocatalysis in the Thermal Dehydrochlorination of Poly(Vinyl Chloride). *Macromolecules* **2004**, *37* (2), 352–359.

(116) Aouachria, K.; Massardier, V.; Benaniba, M. T.; Belhaneche-Bensemra, N. Evaluation of the Effects of Acetyl Tributyl Citrate as Bio-Based Plasticizer on the Physical, Thermal, and Dynamical Mechanical Properties of Poly(Vinyl Chloride)/Polymethyl Methacrylate Blends. *J. Vinyl Addit. Technol.* **2018**, *25* (S1), E73–E82.

(117) Rahim, A.; Saha, P.; Jha, K. K.; Sukumar, N.; Sarma, B. K. Reciprocal Carbonyl-Carbonyl Interactions in Small Molecules and Proteins. *Nat. Commun.* **2017**, *8* (1), 1–12.

(118) Singh, S. K.; Mishra, K. K.; Sharma, N.; Das, A. Direct Spectroscopic Evidence for an N→π* Interaction. *Angew. Chemie - Int. Ed.* **2016**, *55* (27), 7801–7805.

(119) Newberry, R. W.; Raines, R. T. N→π* Interactions in Poly(Lactic Acid) Suggest a Role in Protein Folding. *Chem. Commun.* **2013**, *49* (70), 7699–7701.

(120) El-Hadi, A.; Schnabel, R.; Straube, E.; Müller, G.; Henning, S. Correlation between Degree of Crystallinity, Morphology, Glass Temperature, Mechanical Properties and Biodegradation of Poly (3-Hydroxyalkanoate) PHAs and Their Blends. *Polym. Test.* **2002**, *21* (6), 665–674.

(121) Mekonnen, T.; Mussone, P.; Khalil, H.; Bressler, D. Progress in Bio-Based Plastics and Plasticizing Modifications. *J. Mater. Chem. A* **2013**, *1* (43), 13379–13398.

(122) Chaos, A.; Sangroniz, A.; Gonzalez, A.; Iriarte, M.; Sarasua, J. R.; del Río, J.; Etxeberria, A. Tributyl Citrate as an Effective Plasticizer for Biodegradable Polymers: Effect of Plasticizer on Free Volume and Transport and Mechanical Properties. *Polym. Int.* **2019**, *68* (1), 125–133.

(123) Ziaee, Z.; Supaphol, P. Non-Isothermal Melt- and Cold-Crystallization Kinetics of Poly(3-Hydroxybutyrate). *Polym. Test.* **2006**, *25* (6), 807–818.

(124) Kurusu, R. S.; Siliki, C. A.; David, É.; Demarquette, N. R.; Gauthier, C.; Chenal, J. M. Incorporation of Plasticizers in Sugarcane-Based Poly(3-Hydroxybutyrate)(PHB): Changes in Microstructure and Properties through Ageing and Annealing. *Ind. Crops Prod.* **2015**, *72*, 166–174.

(125) Di Lorenzo, M. L.; Gazzano, M.; Righetti, M. C. The Role of the Rigid Amorphous Fraction on Cold Crystallization of Poly(3-Hydroxybutyrate). *Macromolecules* **2012**, *45* (14), 5684–5691.

(126) de Koning, G. J. M.; Scheeren, A. H. C.; Lemstra, P. J.; Peeters, M.; Reynaers, H. Crystallization Phenomena in Bacterial Poly[(R)-3-Hydroxybutyrate]: 3. Toughening via Texture Changes. *Polymer (Guildf).* **1994**, *35* (21), 4598–4605.

(127) Gunaratne, L. M. W. K.; Shanks, R. A. Multiple Melting Behaviour of Poly(3-Hydroxybutyrate-Co-Hydroxyvalerate) Using Step-Scan DSC. *Eur. Polym. J.*

**2005**, *41* (12), 2980–2988.

(128) Anbukarasu, P.; Sauvageau, D.; Elias, A. Tuning the Properties of Polyhydroxybutyrate Films Using Acetic Acid via Solvent Casting. *Sci. Rep.* **2015**, *5*, 1–14.

(129) Menčík, P.; Přikryl, R.; Stehnová, I.; Melčová, V.; Kontárová, S.; Figalla, S.; Alexy, P.; Bočkaj, J. Effect of Selected Commercial Plasticizers on Mechanical, Thermal, and Morphological Properties of Poly(3-Hydroxybutyrate)/Poly(Lactic Acid)/Plasticizer Biodegradable Blends for Three-Dimensional (3D) Print. *Materials (Basel).* **2018**, *11* (10).

(130) Choi, J. S.; Park, W. H. Effect of Biodegradable Plasticizers on Thermal and Mechanical Properties of Poly(3-Hydroxybutyrate). *Polym. Test.* **2004**, *23*, 455–460.

(131) Billingham, N. C.; Henman, T. J.; Holmes, P. A. Degradation and Stabilisation of Polyesters of Biological and Synthetic Origin. In *Developments in Polymer Degradation—7*; Grassie, N., Ed.; Springer, Dordrecht, 1987; pp 81–121.

(132) Ali, I.; Jamil, N. Polyhydroxyalkanoates: Current Applications in the Medical Field. *Front. Biol. (Beijing).* **2016**, *11* (1), 19–27.

(133) Bonartsev, A. P.; Bonartseva, G. A.; Reshetov, I. V.; Kirpichnikov, M. P.; Shaitan, K. V. Application of Polyhydroxyalkanoates in Medicine and the Biological Activity of Natural Poly(3-Hydroxybutyrate). *Acta Naturae* **2019**, *11* (2), 4–16.

(134) Rodriguez-Contreras, A. Recent Advances in the Use of Polyhydroyalkanoates in Biomedicine. *Bioengineering* **2019**, *6* (3), 1–14.

(135) Li, Z.; Yang, J.; Loh, X. J. Polyhydroxyalkanoates: Opening Doors for a Sustainable Future. *NPG Asia Materials*. 2016.

(136) Jääskeläinen, A. S.; Liitiä, T.; Mikkelson, A.; Tamminen, T. Aqueous Organic Solvent Fractionation as Means to Improve Lignin Homogeneity and Purity. *Ind. Crops Prod.* **2017**, *103*, 51–58.

(137) Duval, A.; Vilaplana, F.; Crestini, C.; Lawoko, M. Solvent Screening for the Fractionation of Industrial Kraft Lignin. *Holzforschung* **2015**, *70* (1), 11–20.

(138) Francuskiewicz, F. *Polymer Fractionation*, 1st ed.; Springer-Verlag Berlin Heidelberg: Berlin, 1994.

(139) Jawerth, M.; Johansson, M.; Lundmark, S.; Gioia, C.; Lawoko, M. Renewable Thiol-Ene Thermosets Based on Refined and Selectively Allylated Industrial

Lignin. *ACS Sustain. Chem. Eng.* **2017**, *5*, 10918−10925.

(140) Prat, D.; Wells, A.; Hayler, J.; Sneddon, H.; McElroy, C. R.; Abou-Shehada, S.; Dunn, P. J. CHEM21 Selection Guide of Classical- and Less Classical-Solvents. *Green Chem.* **2015**, *17* (10), 4848.

(141) Luo, S.; Cao, J.; McDonald, A. G. Esterification of Industrial Lignin and Its Effect on the Resulting Poly(3-Hydroxybutyrate-Co-3-Hydroxyvalerate) or Polypropylene Blends. *Ind. Crops Prod.* **2017**, *97*, 281–291.

(142) Kim, Y.; Suhr, J.; Seo, H.-W.; Sun, H.; Kim, S.; Park, I.-K.; Kim, S.-H.; Lee, Y.; Kim, K.-J.; Nam, J.-D. All Biomass and UV Protective Composite Composed of Compatibilized Lignin and Poly (Lactic-Acid). *Sci. Rep.* **2017**, *7* (1).

(143) Deng, Y.; Feng, X.; Zhou, M.; Qian, Y.; Yu, H.; Qiu, X. Investigation of Aggregation and Assembly of Alkali Lignin Using Iodine as a Probe. *Biomacromolecules* **2011**, *12* (4), 1116–1125.

(144) Thielemans, W.; Wool, R. P. Lignin Esters for Use in Unsaturated Thermosets: Lignin Modification and Solubility Modeling. *Biomacromolecules* **2005**, *6* (4), 1895–1905.

(145) Ko, H. U.; Zhai, L.; Park, J. H.; Lee, J. Y.; Kim, D.; Kim, J. Poly(Vinyl Alcohol)–Lignin Blended Resin for Cellulose-Based Composites. *J. Appl. Polym. Sci.* **2018**, *135* (34).

(146) Pregi, E.; Kun, D.; Vu, V.; Pukánszky, B. Structure Evolution in Poly(Ethylene-Co-Vinyl Alcohol)/Lignin Blends: Effect of Interactions and Composition. *Eur. Polym. J.* **2019**, *111*, 74–81.

(147) Gordobil, O.; Delucis, R.; Egüés, I.; Labidi, J. Kraft Lignin as Filler in PLA to Improve Ductility and Thermal Properties. *Ind. Crops Prod.* **2015**, *72*, 46–53.

(148) Romhányi, V.; Kun, D.; Pukánszky, B. Correlations among Miscibility, Structure, and Properties in Thermoplastic Polymer/Lignin Blends. *ACS Sustain. Chem. Eng.* **2018**, *6* (11), 14323–14331.

(149) Playfair Ph.D., L. XX. On a New Fat Acid in the Butter of Nutmegs. *London, Edinburgh, Dublin Philos. Mag. J. Sci.* **1841**, *18* (115), 102–113.

(150) Beare-Rogers, J.; Dieffenbacher, A.; Holm, J. V. Lexicon of Lipid Nutrition (IUPAC Technical Report). *Pure Appl. Chem.* **2001**, *73* (4), 685–744.

(151) Eadie, M. J. Could Valerian Have Been the First Anticonvulsant? *Epilepsia* **2004**, *45* (11), 1338–1343.

(152) Wightman, F.; Lighty, D. L. Identification of Phenylacetic Acid as a Natural

Auxin in the Shoots of Higher Plants. *Physiol. Plant.* **1982**, *55*, 17–24.

(153) Van Moerkercke, A.; Schauvinhold, I.; Pichersky, E.; Haring, M. A.; Schuurink, R. C. A Plant Thiolase Involved in Benzoic Acid Biosynthesis and Volatile Benzenoid Production. *Plant J.* **2009**, *60*, 292–302.